SCUOLA DI SCIENZE

Dipartimento di Chimica Industriale"Toso Montanari"

Corso di Laurea Magistrale in

Chimica Industriale

Classe LM-71 - Scienze e Tecnologie della Chimica Industriale

Catalytic decomposition of formic acid using supported metal nanoparticles

Tesi di laurea sperimentale

CANDIDATO
Ludovica Bocelli

RELATORE
Chiar.mo Prof. Stefania Albonetti

CORRELATORE
Dr. Nikolaos Dimitratos

Anno Accademico 2015-2016

Keywords

Formic acid decomposition

Supported metal nanoparticles

Colloidal methods

Abstract

Upgrade of hydrogen to valuable fuel is a central topic in modern research due to its high availability and low price. For the difficulties in hydrogen storage, different pathways are still under investigation. A promising way is in the liquid-phase chemical hydrogen storage materials, because they can lead to greener transformation processes with the on line development of hydrogen for fuel cells. The aim of my work was the optimization of catalysts for the decomposition of formic acid made by sol immobilisation method (a typical colloidal method). Formic acid was selected because of the following features: it is a versatile renewable reagent for green synthesis studies. The first aim of my research was the synthesis and optimisation of Pd nanoparticles by sol-immobilisation to achieve better catalytic performances and investigate the effect of particle size, oxidation state, role of stabiliser and nature of the support. Palladium was chosen because it is a well-known active metal for the catalytic decomposition of formic acid. Noble metal nanoparticles of palladium were immobilized on carbon charcoal and on titania.

In the second part the catalytic performance of the "homemade" catalyst Pd/C to a commercial Pd/C and the effect of different monometallic and bimetallic systems (Au_xPd_y) in the catalytic formic acid decomposition was investigated.

The training period for the production of this work was carried out at the University of Cardiff with Dr. N. Dimitratos group.

Contents

Objective

The research in sustainable chemical synthesis creates large interested in the scientific world, due to environment issues. Nowadays satisfying the world demand of energy is not an easy challenge. The continue request of energy is cause due to the consumption of primary not renewable resources, which are going to finish. The bet of the researchers is to find renewable reagents for new green processes.

In the field of fuels it is of interest the development of methods to produce hydrogen, which can be available as green fuel. The studies on catalytic decomposition of formic acid validated that chemical as possible source of hydrogen. So new studies to improve and optimize the reaction conditions are conducted.

The general aim of the described experiments in this thesis was the synthesis of supported noble metal nanoparticles and their catalytic applications in the decomposition of formic acid. The reaction was performed in batch conditions and followed by HPLC analysis.

The sol immobilization method was chosen to synthesize the catalysts. The synthesized catalysts were then tested in the reaction of formic acid decomposition and their synthetic features were optimized to try to obtain the best catalytic performances. The aim was to elucidate the role of Pd particle size, oxidation state, role of stabiliser and nature of support for the aforementioned reaction.

Introduction

The world's energy consumption is everyday increasing, owing to the rising standards of living and the growing population. In order to satisfy the global demand the energy generation capacity is necessarily increasing as well. Furthermore problems about fossil fuels and pollution due to their combustion can't be ignored. It is clearly in contrast with the current environmental protection policies, which seek to limit these emissions. For this purpose the search for more secure, diversified and sustainable chemical processes are being investigated. The exploration of new strategies and then the utilisation of a sustainable energy supply are one of the greatest challenges to be addressed in this century.

Nowadays the attention on hydrogen is growing, because both it is globally accepted as candidate for clean energy due to the fact that the only by-product of its reaction with oxygen is water[1] in fuel cells and it should be used as alternative energy vector to connect energy sources to different end uses to hydrogen fuel cell vehicles to portable electronics[2], in all stationary power, transportation, industrial and residential sectors. However, despite the potential use of hydrogen, its widespread utilization is currently limited by the capacity limitations of hydrogen storage technologies and by the safety issues related with its storage and transportation under mild conditions. New methods of storage can be classified as physisorption materials and chemical release systems. Recently, formic acid, a major product formed during biomass processing, has been studied as a safe and convenient hydrogen storage material due to its high volumetric hydrogen content (4.4%), liquid state at room temperature, high stability, environmental benignity, nontoxicity and the fact that produces mainly gaseous products (H_2/CO_2) by decomposition.

During the internship at the Cardiff University, we have conducted studies on the tuning and direction of experiments for the decomposition of formic acid, with the aim of assessing the technical feasibility of the proposed process and optimizing the operating parameters of the involved catalyst.

Chapter 1: Hydrogen

1.1 Hydrogen economy and production methods

The hydrogen is the most abundant compound in the world. It has many good characteristics which made it very attractive such as:

- it is source for clean energy
- it is the lightest fuel
- richest in energy for unit mass and can be converted directly to electric, mechanic and thermal energy as possible to see in Table 1[3].

Table 1 Heat of combustion of different materials

Fuel	Energy (MJ/g)
H_2	0.14
Petroleum	0.04
Paraffin	0.04
Wood	0.02
$C_{(graphite)}$	0.03
Castor oil	0.04

In nature H_2 is combined with others elements, this means that is an energy vehicle, but not a primary source such as natural gas or petrol, thus it should be product with alternative routes which have to guarantee low pressure and high purity at low cost to be competitive. Others critical issues are the development of lower cost H_2 delivery and H_2 storage, they must be solved before considering hydrogen economically viable. H_2 supply is depended from many factors level of demand, resources availability, geographic issues and progress on hydrogen technologies. Typically hydrogen is used in ammonia process, petroleum refining, and metal refining, in the future it will be used hopefully as energy carrier[4] (Fig.1), I.P.Jain in his report explored many application available for this molecule from hydrogen powered industries to all our domestic energy requirements[3].

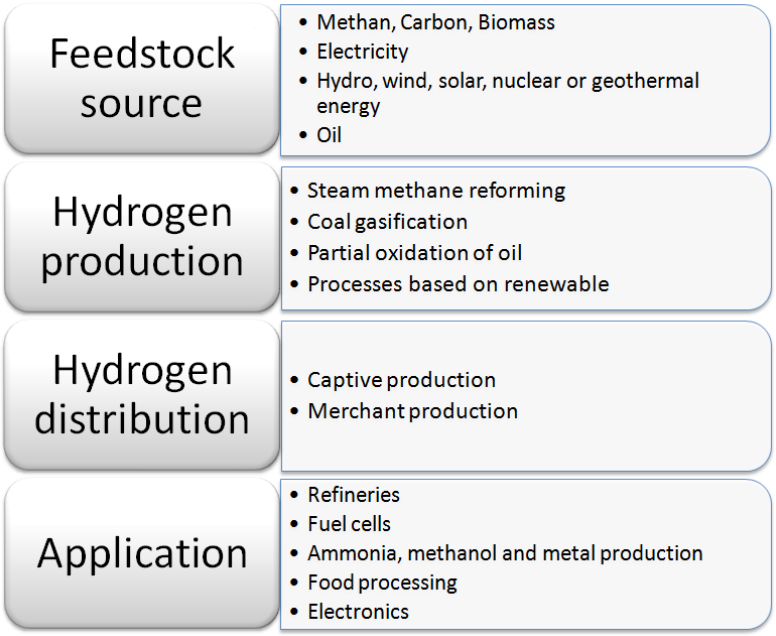

Fig. 1 Hydrogen an energy carrier linking multiple production methods and sources to various applications

Today hydrogen production could be classified based on the raw material used: carbon, natural gas and petroleum. The methane steam reforming is the most important method in H_2 production and it is accounted for more than one-third of the market share (around 55 million metric tons) in 2015 among other technologies of hydrogen production (partial oxidation, gasification, and electrolysis), because it allows to obtain richer blends on hydrogen content with a ratio H_2/CO of 3[5,6]. The reaction is showed below (eq.1):

$$CH_4 + H_2O \leftrightarrow CO + 3H_2 \quad \Delta H°=206 \text{ kJ/mol} \qquad \text{eq.1}$$

Associated with this kind of reaction there is the water gas shift reaction (eq.2):

$$CO + H_2O \leftrightarrow CO_2 + 3H_2 \quad \Delta H°=-41.1 \text{ kJ/ mol} \qquad \text{eq.2}$$

Where CO is converted in CO_2 and the content of hydrogen is increased[7].

In case of partial oxidation small petroleum fraction or methane react with a oxygen with development of heat. The process obtain a CO/H_2 ratio of 1.7-1.8 (eq.3)[8]:

$$CH_4 + ½\ O_2 \leftrightarrow CO + 2H_2 \quad \Delta H°=-35 \text{ kJ/mol} \qquad \text{eq.3}$$

Another pathway could be the methane auto-reforming (eq.4, eq.5, eq.6)[9]:

$$CH_4 + 3/2\ O_2 \leftrightarrow CO + 2H_2O \quad \Delta H°=-520 \text{ kJ/mol} \qquad \text{eq.4}$$

$$CH_4 + H_2O \leftrightarrow CO + 3H2 \quad \Delta H°=206 \text{ kJ/mol} \qquad \text{eq.5}$$

$$CO + H_2O \leftrightarrow CO_2 + 3H_2 \quad \Delta H°=-41.1 \text{ kJ/ mol} \qquad \text{eq.6}$$

Or the gasification of coal which products syn gas like in the previous process (eq.7)[10]:

$$C + 2H_2O \leftrightarrow CO_2 + 2H_2 \quad \Delta H° = 170 \text{ kJ/ mol} \qquad \text{eq.7}$$

The last traditional method that is important to know is the dry reforming (eq.8):

$$CO_2 + CH_4 \leftrightarrow CO + H_2 \quad \Delta H° = 247 \text{ kJ/ mol} \qquad \text{eq.8}$$

As the CO_2 is a component in the atmosphere this reaction could help to decrease its emission.

Others possibility are the processes based on renewable which permit the use of industrial wastes or agricultural scraps as start material. Some example of this process are the catalytic fermentation of bacteria, the biomass pyrolisis[11], the bio-production from wastes, photosynthetic production from alga[12] and the electrolysis of water. Electrolysis of water is the only one that has found a practical method, the H_2 is generated from the decomposition of water by electric current. Nevertheless, the energy consumption is the largest issues to be solved in this process too. Due to this hydrogen it is not economically available as source of energy from renewable and further scientific pursuits should be done.

1.2 Fuel cell

A feasible application of hydrogen is in the fuel cell to generate electric energy, these devices are able to convert chemical energy into the electric one using H_2 like fuel and air like combustive (Fig.2). The system of a fuel cell is very competitive, compared to a classical motor it does not need of a thermal cycle and there is not production of NO_x. The reactions developed in a fuel cell provide the reduction O_2 at the cathode (eq.9) and the oxidation of H_2 at the anode (eq.10)[13]:

$$O_2 + 4H^+ + 4e^- \rightarrow 2H_2O \qquad \text{eq.9}$$

$$2H_2 \rightarrow 4H^+ + 4e^- \qquad \text{eq.10}$$

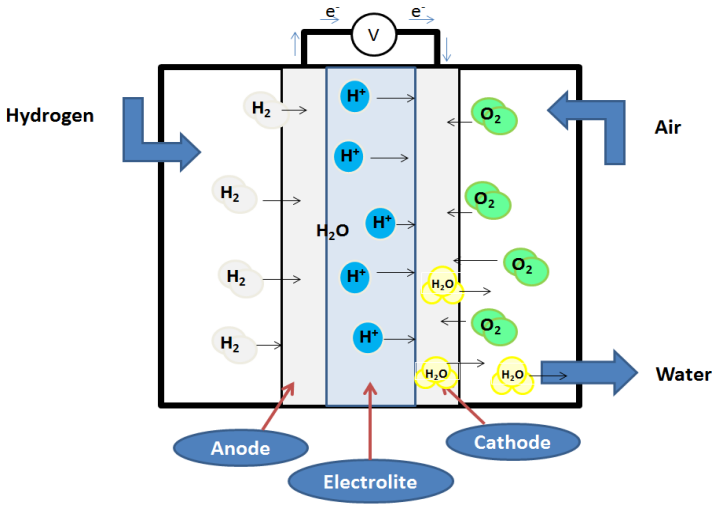

Fig. 2 Set up of a fuel cell

The fuel cells are classified on the type of the electrolyte used, modifying that the field of application changes, in the transportation sector the most used is the PEMFC (Proton Exchange Membrane Fuel Cell) where the electrolyte is a ion exchange membrane water-based. Nowadays a challenge is connected together a source of hydrogen directly to a PEMFC; since the catalyst used insight the fuel cell is platinum this is poisoned by CO, thus a process CO free must be developed to achieve the desired purpose[14,15].

1.3 Hydrogen transportation and storage

Nowadays petroleum fuels are still more competitive compared to hydrogen energy, because not only energetic consideration are made and the economic arguments have a huge relevance. From the production to the transfer of the hydrogen electric energy is required, so it is fundamental to estimate the cost-effective to operate a hydrogen economy. Until now the delivery cost of pure gaseous hydrogen is not comparable to other fuel, in the liquid form the costs would get off, but to liquefy this molecule the consumption of energy is very high. Against to this it is demonstrated that hydrogen is the greenest fuel[16].

The required costs for the H_2 storage are really huge (in 2005 it was ≈62 euro million/plant)[17], so one of the biggest challenge is to find efficient solutions. The problem of storage involves both stationary (*i.e.* plants) and dynamic systems (*i.e.* car and so on). In the first one it is not important the volume involved, instead in dynamic applications the volume and the weight of the tank can not be ignored, it should guarantee safety, reduced volumes, practicality and the necessary amount of automotive fuel.

Two approaches are available for the storage of hydrogen either a physical method or a chemical method. The physical method provide to increase the hydrogen density keeping it under pressure and controlling the temperature, but strong tanks are required. There is also the possibility to storage the hydrogen as a liquid, in this case a temperature of -240°C is necessary, the issue is that 40% of energy generated must be used to liquefy the hydrogen and after other energy has to be used to keep it in the liquid state (≈20%). If hydrogen is stored like that there are problem of transportation, because safety conditions are not easy to maintain. There are also other physical method such as to adsorb the hydrogen on material with large surface area or to cryoadsorb it. Anyway any material was found to adsorb the gas at atmospheric pressure and room temperature, so there is not a practical application of these method[18].

In case of chemical storage precursor compound of hydrogen are studied (metal hydrates, methanol, methane, light hydrocarbons, carbon nanostructures, alanate, borohydride, amides, alcohol etc.)[19], they are able to produce H_2 by chemical reaction. In general a storage material should guarantee to release hydrogen in mild condition to be link with the fuel cell and the kinetics of the reaction should be fast. Many conventional bulk material were studied, but until now none demonstrate to have all the required characteristics to be a storage media.

To sum up in the flow chart in Fig.3 are depicted various hydrogen storage method:

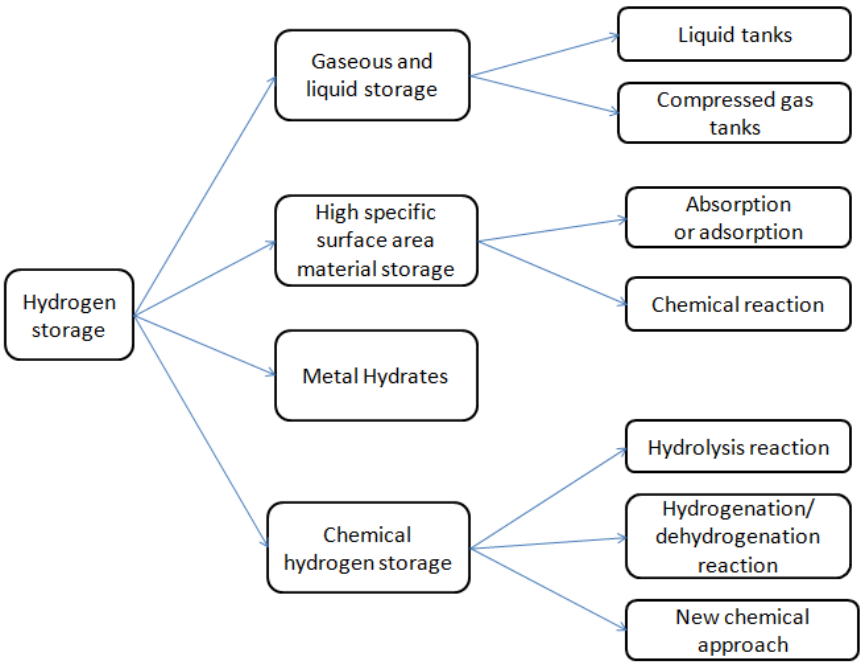

Fig. 3 Summary on different approaches for hydrogen storage

1.3.1 **Liquid-phase chemical hydrogen storage**

Mahendra *et al.*[20] and Jiang *et al.*[2] affirm that an appropriate media to store hydrogen should guarantee large amount of it to be economically convenient, in this context liquid-phase chemical hydrogen storage material assume an interesting role. The most promising are ammonia borane, hydrazine, hydrazine borane, aqueous sodium borohydride and formic acid, in which we will focus our attention (Table 2). The advantages in their use are:

- low potential risk;
- they can release hydrogen under mild conditions;
- low cost;
- they are easily transported;

Table 2 Physical characteristics of liquid-phase chemical storage

Liquid chemical storage	Physic state at room temperature	Density at room temperature (g/cm^{-3})	Hydrogen content (wt%)
Ammonia borane	Colourless solid	0.74	19.6
Hydrazine Monohydrate	Colourless liquid	1.02	8.0
Hydrazine borane	Colourless or white solid	0.78	15.4
Sodium bhorohydride	White solid	1.07	10.8
Formic acid	Colourless liquid	1.22	4.4

Ammonia borane

Ammonia borane (NH_3BH_3) is a compound with a high hydrogen content compared to its molecular weight (30.9 g mol^{-1}), which is higher than those for the other substances. NH_3BH_3 has many good properties that made it very interesting: it is nontoxic, stable and environmentally green, however as a by-product the formation of NH_3 is still a challenge to be solved. There are different processes to generate H_2 from NH_3BH_3 such as thermal decomposition, hydrolysis, methanolysis. Until now the hydrolysis process (eq.11) demonstrated the best hydrogen capacity up to 8.9 wt% of the starting material, besides it is able to proceed under ambient conditions in presence of suitable catalysts:

$$NH_3BH_3 + 2H_2O \rightarrow NH_4^+ + BO_2^- + 3H_2 \qquad \text{eq. 11}$$

Further studies should be expound on the reaction to be compatible with the practical applications.

Hydrazine

It is hydrogen dense and thus mainly attractive for portable and automotive applications. In the anhydrous form, H_2NNH_2 (>98%) is liquid at room temperature and it has a really high content of hydrogen 12.5%. It can decompose to hydrogen following two different pathways (eq. 12 and eq.13):

$$\text{Complete decomposition: } H_2NNH_2 \rightarrow N_2 + 3H_2 \quad \text{eq. 12}$$

$$\text{Incomplete decomposition: } 3H_2NNH_2 \rightarrow N_2 + NH_3 \quad \text{eq. 13}$$

The mechanism of these reaction can vary depending upon the catalysts used and the reaction conditions. The problem in the use of anhydrous hydrazine is its explosive nature in presence of metal catalysts surface, that limits it's safely apply. To solve this issue, hydrous hydrazine can be used (H_2NNH_2 *H_2O), but the hydrogen content decreases to 8 wt% from 12.5%. In the complete decomposition the by-product is nitrogen, which does not affect negatively the reaction and not need to be recycled. The challenge is to develop selective catalysts towards this pathway, in case of this hydrous hydrazine could be suitable as hydrogen storage material.

Hydrazine borane

$N_2H_4BH_3$ is quite stable in aqueous solution and its hydrogen storage capacity is 15.4%. Like the ammonia borane and hydrazine it is emerging as source of hydrogen, through chemical pathway such as thermolysis or hydrolysis[21] it can release the desired molecule. Nevertheless there is need of more selective catalysts towards hydrogen, thus researches should be made to improve the system. Using rhodium supported nanoparticles it was demonstrated to produce H_2 from the BH_3 hydrolysis, but the hydrazine group was not involve in the reaction, loosing 4/7 of its hydrogen. Bimetallic system, as NiPt or NiIr alloy, allows to lead at the same time the decomposition of the hydrazine part and the hydrolysis of BH_3 in aqueous solution[20].

Sodium bhorohydride

The most borohydride studied was $NaBH_4$, because it revealed an high hydrogen content of 10.8 wt%. It can produce H_2 by thermolysis or hydrolysis, but only the second process found an application (eq.14):

$$NaBH_4 + 2H_2O \rightarrow NaBO_2 + 4H_2 \quad \Delta H° = -210 \text{ kJ mol}^{-1} \qquad \text{eq.14}$$

The hydrogen obtained from this reaction is pure and humidified, but less than expected, an excess of water is used in the real condition, due to the problems of solubility of reagent and by-product, $NaBO_2$. The characteristics indicated favour its application in fuel cells; the reaction is thermodynamically favoured and very exothermic, due to this both homogeneous and heterogeneous catalysed pathway have been investigated[22]. It was found that the first method is suitable for continuous system, but not for the supply of hydrogen on demand, since it was difficult to suspend the reaction. In case of the heterogeneous catalysis both noble and non-noble metal catalysts were investigated on the $NaBH_4$ hydrolysis, finding really attractive the one based on nickel or cobalt[2].

At present, $NaBH_4$ has not economically sustainable and it can not be used as hydrogen chemical storage, because there is not available a cheap process to generate it in situ starting from the byproduct, although many processes are under investigation[20].

Formic acid

Formic acid, HCOOH, is the hydrogen chemical storage investigated in this study, because as mentioned before it has many good properties that made of its an attractive compound[23]. The study on the catalytic formic acid decomposition started with Sabatier *et all.* in 1912. Formic acid decomposition occurs by two different pathways: dehydrogenation (eq.15) and dehydration (eq.16)[24]. Selective dehydrogenation is indispensable for the production of ultrapure H_2 without undesirable dehydration, since toxic CO contamination produced by the latter pathway reduces the activity of Pt catalysts in fuel cell.

$$HCOOH \rightarrow CO_2 + H_2 \quad \Delta G = -48.4 \text{ kJmol}^{-1} \quad \text{eq.15}$$

$$HCOOH \rightarrow CO + H_2O \quad \Delta G = -28.5 \text{ kJmol}^{-1} \quad \text{eq.16}$$

The two reactions are linked by the water gas shift (WGS) reaction (Fig.4).

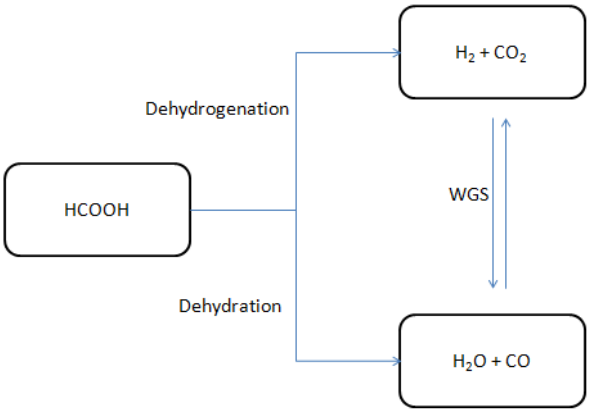

Fig. 4 Reaction pathways for the decomposition of formic acid

The by-product of dehydrogenation is CO_2, which can be recycled to produce formic acid, the catalytically reduction could close the cycle for the storage hydrogen system (Fig.5).

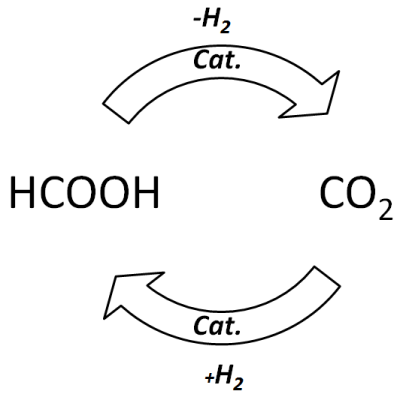

Fig. 5 Cycle for the hydrogen storage system

The decomposition pathway depends from the catalysts used, either homogeneous or heterogeneous catalysts can be used to decompose formic acid[25]. Some reports affirm improvement on both the decomposition of formic acid using homogeneous catalysts at ambient temperatures and on catalysts efficiency. At the present separating the catalysts from the reaction mixture is laborious, furthermore, the problems of severe reaction conditions, the huge amount of organic solvents/additives used and poor selectivity make this kind of processes available only for bench applications. For all these reasons it results more interesting to investigate on heterogeneous catalysts.

The first studies on the formic acid decomposition using Pd-Au alloy wires started in 1957[26]. One of the most studied monometallic catalyst is Pd/C. Initially it didn't find a

practical application, because it deactivated quickly. However, Wang *et al.* demonstrated a TOF of 228.3 h^{-1} at 30ºC after two hours using a solution of formic acid and sodium formate 1:9 respectively[27]. Previously Mori *et all.* found an higher TOF of 820 h^{-1} using: Pd, a weakly basic resin at 75ºC and a solution of formic acid and sodium formate 9:1 reaching a maximum rate of reaction of 2880 ml min^{-1} g^{-1} [28].

Besides gold based catalysts were tested on the reaction, it revealed different activity varying the support. Au/Al_2O_3 finely dispersed can promote the selective decomposition of formic acid at 80°C, at the same temperature Au/ZrO_2 had a TOF of 550h^{-1}, which reached 1593h^{-1} when Au was supported on ZrO_2-NCs at 50°C[29]. Bi *et al.* found that Au/TiO_2 demonstrated a TOF of 226h^{-1} and varying the support the particles size decreased increasing the reaction performances[30].

Also bimetallic nanoparticles provide a good catalytic activity and selectivity compared to the monometallic species, in the same work condition (HCOOH 1 M and 50°C) it was found that Pd/C had an initial TOF of 30h^{-1}, Au/C of 80h^{-1} and $Au_{41}Pd_{59}$/C of 230 h^{-1}. According to this Pd–Au and Pd–Ag alloys supported on carbon were explored. The critical issues with this materials is the detection of CO, in fact for the application in fuel cells the ppm level should stay below 15ppm.They overcame the poisoning and improved the reaction producing a high quality hydrogen from the decomposition of formic acid at low temperatures, continuing the studies the systems were improved, it was discovered that the activities of Pd–Au/C and Pd–Ag/C can be enhanced by co-deposition with CeO_2[31]. Since the good results other types of bimetallic systems were developed Ag-Pd alloy, Ag-Pd core-shell supported on carbon based resulting in a high TOF of 626 h^{-1}, but a drawback of CO generation due to the high temperature (90°C)[32]. Nevertheless using ML-101(a metal-organic framework) as support Ag-Pd alloy recorded a TOF of 848 h^{-1} at 80ºC and a whole selectivity for dehydrogenation pathway[33].

In the recent years strong improvements were carried on heterogeneous catalysis, but this is not enough, the application in fuel cell is correlated to other factors such as cost, catalyst deactivation, re-generation of by-products and control of the reaction kinetics. More studies are required to optimise the process; the research on the catalytic system will continue to finally apply it on portable devices.

Chapter 2: Metal nanoparticles

Starting from 21th century the research attention is moved from the micrometer size to the nanometer scale with the analysis of small agglomerates of atoms or molecules in the range of dimension between 1 and 100nm. New attractive properties of materials were discovered in this range. Compared to the atomic size and the bulk of materials, they show high surface/bulk atoms ratio and new features have been discovered as electron confinement and shape importance. According to this, working on the shapes and on the sizes of the same material is possible to vary its characteristics[34]. It is well known that metals have delocalised electrons on the surface in bulk systems which explain the thermal and electrical conductivity, instead when they assume nanometer size metal the electrons can move in more confined spaces, leading to completely different properties.

Recent advances in the liquid-phase synthesis of metal nanoparticles have improved the control in particle dimension and shape, providing more suitable catalysts for specific activities. The reaction's structure-sensitivity relationship is one of the most interesting aspects for the catalyst design in view of enhancement in the catalytic activity. This is linked to the activity of those nanosized technologies together with other aspects as surface relationships, intraparticle metal–metal bonding, strength of metal–support interaction, structure and atom packing geometry[35].

Characterisation of synthesised particles could carried out by spectroscopic and analytical techniques, so they can be classified in terms of dispersion on the support, size, defect, structure of the crystal, plasmonic band and oxidation state of the metal. Some of the techniques used are X-Ray photoelectron spectroscopy (XPS), X-Ray diffraction (XRD), transmission electron spectroscopy (TEM), scanning electron microscopy (SEM), ultraviolet-visible spectroscopy (UV-vis), dynamic light scattering (DLS)[36]. Furthermore the support features have to be analyzed, because they affect the activity and availability of immobilised metal nanoparticles. The most widely used techniques involve the BET theory and FT-IR analysis (CO-chemisorption)[37]. Characterization is done primarily in terms of accessibility of active sites, and even regarding particle dimension, morphology, textural properties (pore volumes and size, micro or mesopore capacity), chemical nature, surface functionality (groups, loading and acidity/basicity), and surface energy characteristics (hydrophobicity/hydrophilicity)[38,39,40].

The topic of nanoparticles has collected a huge number of publications in the last 30 years and the research efforts are expected to continue increasing as the benefits of the chemical properties achieved at the nano level become increasingly apparent for applications. A significant amount of research is devoted to enhance the synthetic step: the control of size, shape and dispersity of nanoparticles is key to selective and a better activity. Due to this, different techniques have been developed to enhance the interaction between nanoparticles and substrates or target molecules. New synthetic pathways have been found enhancing the activity of this research area, thus, increasing both the field of synthesis and of application has led to potentially great applications of those nanotechnology systems in everyday life.

The development of nanotechnologies push to enlarge the field of research, nanoparticles are been involved in medicine, sensor, chemistry. In medicine can be applied as delivery system, contrast agents and magnetic resonance imaging [MRI], in biochemistry and chemistry for chemical sensors (as electrochemical sensors and biosensors) and in heterogeneous catalysis (oxidations, hydrogenations and C-C coupling reactions, dehydrogenation)[41].

2.1 Synthesis and immobilization methods for metal nanoparticles

In the last 30 years many methods to synthesize nanoparticles have been investigated. The choice of the techniques influences the properties of the nanoparticles, therefore according to this, a good knowledge of the different processes is essential. It has been proved that modifying the method of the surface interactions between the metal and the support affects the physicochemical features as dispersion, size of the metal, surface area and pore diameter of the support. The different pathways can sum up in chemical methods (e.g. impregnation, electrochemical), physical way (as sonication, microwaves, UV, grinding), physichemical route (i.e. sonielectrochemical)[38].

They can be listed as: wetness impregnation, deposition-precipitation, sol immobilization, chemical vapour deposition, solid grinding and nanoparticle encapsulation.

In the impregnation method a solution of the metal precursor is added to a support and then it is dried and heat treated under air or H_2 for controlling the final morphology of

the supported nanoparticles. Two different pathways can be followed either incipient impregnation or wetness impregnation, they differ for the volume of initial solution contacted with the substrate, in the second one an excess of solution is used. The provided procedure for this technique is practical, thus is one of the more utilised in bench scale and industrial scale, the characteristics of the prepared particles are strictly linked to the drying and calcinations conditions phases, as well as to the support. The rate of heating, time, final temperature and atmosphere can determine the final morphology of the nanoparticles. The advantages of this technique are that the content of metal that is possible to support is higher compared to the other processes and there is no need of preformed nanoparticles[42]. The biggest disadvantage is that the synthesis of the particles is hardly to control, due to the thermal phase, where nucleation, growth happen and there is an elevate ion and metal mobility; the size particles obtained could be large and the presence of any ions of the metal precursor not reduced cannot be entirely negligible, because they could be the reason for a bad catalytic activity and a quickly deactivation of the catalyst[43].

Deposition-precipitation (DP) pathway is one of the first methods developed for the synthesis of gold nanoparticles, in this synthesis the metal precursor is precipitated in the hydroxide or carbonate form on the support by changing the pH of the solution and subsequently the solid is washed, dried and heat treated under air or H_2. Some advantages of this method are that it is possible to produce small nanoparticles based on the control of pH, a narrow size distribution of the particles and the support can be either acid or basic, the issues is that depending on the pH used the nominal metal loading could not correspond to the theoretical one: at low pH the metal loading can be increased, but larger nanoparticles are produced, at pH above 9 small nanoparticles are produced, but with loss of metal loading, as in the case of the use of NaOH in the synthesis[42]. This problem was solved by the use of urea in case of gold nanoparticles made by DP[44].

The last three techniques mentioned can be considered as particular types of impregnation. The metal chemical vapour deposition is efficient with every support and it provides the immobilisation of the metal through ligand exchange and new bonds among the precursor and the support. First the metal precursor (e.g. dimethyl-Au(III)-acetyl acetonate) it is vaporised in a vacuum system by heating and thus deposited on the support. After the deposition a heat treatment step occurs to burn the organic ligand presented in the metal precursor. Another method it is the solid grinding, the support

and the precursor (as metal oxides) are added together in a mortar or a ball milling and after grinding the powder is heat treated; it is a practical method available with many different supports. The last but not least is the sol immobilisation method, it is within impregnation the most employed in research, because is the simplest way to support metal nanoparticles and allows the possibility of tuning synthetic parameters. The sol immobilisation was used in this research, thus is treated in depth in the sequent paragraph.

2.1.1 **Sol immobilisation method**

In lab scale sol immobilisation method is largely utilised because is very versatile and it allows a tunable control of size of nanoparticles, shape, good dispersion and crystalline phase before embedding the nanoparticles in the support. Usually it does not need additional reduction treatments. The process includes reduction of the metal salt precursor in presence of a stabiliser (such as polymer, surfactant, polar molecules etc.) and the immobilisation of the sol on the supporting material. Many factors affect the kinetics of metal particles adsorption such as the IEP (Isoelectric Point), the stabiliser and the support, due to its morphology and specific surface, as well as it influences the dispersion of the particles[45]. To enforce the aqueous colloidal solution of the preformed particles against the aggregation three different methods are been developed based on stabilising the system:

- the use of surfactants (e.g. cetyltrimethylammonium bromide,i.e.CTAB) which increases the surface potential and/or the charge density;
- the use of macromolecules (e.g. dextrine, starch): they stick to the metal enhancing, with their hydrophilic or hydrophobic part, the interaction with the solvent and they decrease the Van der Waals forces;
- the steric effect: the steric stabiliser are polymers or other high molecular weight molecules with heteroatoms interacting with the nanoparticles. The most used are poly(N-vinyl-2-pyrrolidone) [PVP], poly(vinyl alcohol) [PVA], poly(acryl amide), poly(acrylic acid) and poly(ethyleneimine) with different protective values.

In some cases the stabilizer can act also as reducing agent. The stabiliser can be removed by thermal decomposition or solvent washing under mild conditions. The choice of the capping agent depends on the desired characteristics of the final product

and to the specific properties of the metal/substrate pair. The protective agents act on particle size and shape drivers and enhance the dispersion regardless of the support, in support of this changing the ligand different type of nanoparticle/ligand bond are formed such as covalent interactions which are stronger than electrostatic and consent a better stability of the solution, anyway they cannot be easily removed. On the other side electrostatic binding suffers more of the system perturbations (temperature, ionic strength, dilution) but facilitate the replacement with supports or other molecules[46] (Fig.6).

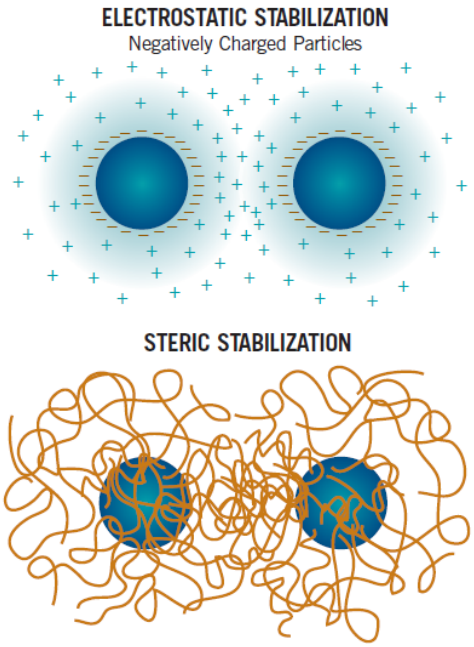

Fig. 6 Examples of the stabilization of the nanoparticles[47]

In the choice of the protective agent not only the interaction with the particles is important, but it has to pay attention also to the support chosen, for gold for example it is well known that a more functionalised support surface enhances the dispersion of the metal and decreases the nanoparticles aggregation[42].

The nanoparticles can be formed by different synthetic pathways too: thermal reduction, chemical reduction or oxidation, precipitation, sol-gel and galvanic exchange.

In case of chemical reduction the metal precursor is added into a solution of solvent and stabilizing agent under ambient conditions, it is necessary also the addition of a reducing agent to reach the zero oxidation state of the metal. The strength of the reducing agent is related to the type of precursor used: a stronger reducer (sodium borohydride or superhydride) is necessary more negative the reduction potential is.

Carboxylic acids or 1,2-alkanedyols can be preferred when there are no issues with the reduction conditions and eventually the growth of nanoparticles would be improved.

In this work sol immobilisation was chosen first to synthesise Pd monometallic catalysts with the purpose of optimising the synthetic step and obtaining the best features, then also gold and Au-Pd bimetallic catalysts were synthesised with the same procedure to compare their effect on the model reaction, the formic acid decomposition. A brief summary on the system involved is reported the next paragraphs.

2.1.2 **Palladium nanoparticles**

Palladium is a noble metal which has found many applications in catalysis from petroleum cracking to Heck reaction and Suzuki coupling[48], as well as in catalytic converter in the cars.

The formation of palladium nanoparticles during the sol immobilisation method provides a change in the colour of the metal precursor solution from brown to dark grey. Palladium doesn't have the surface plasmon resonance, but through UV-vis spectra it is possible to see the presence of a peak at 235 nm[24] (metal precuros peak), which disappear after the passage at zero oxidation state.

It is noteworthy that palladium shows activity towards formic acid decomposition as it is suggested in the previous paragraph, thus many researches have the aim of enhancing and make it available for a practical use.

2.1.3 **Gold nanoparticles**

Gold nanoparticles assumed a large interest in catalysis 30 years ago thanks to the work of Haruta[49] and Hutchings[50] on CO oxidation and ethylene hydrochlorination. Initially their applications found many obstacles, due to the difficulties on the synthesis step that lead to not reproducible catalytic activity. Many investigations helped to enlarge the knowledge on this compound on nanometer scale determining the particle morphology and the interaction between metal and support which are the main factors affecting the activity and the selectivity of the catalyst[42].

The formation of gold nanoparticles with sol method is visible to the naked eye by the colour change of the metal precursor solution from the yellow (Au^{3+}) to the ruby red

(Au^0). UV-vis spectra can be recorded by way of verification, in fact gold is characterised from the surface plasmon resonance (SPR) around 520 nm in the visible part. The SPR band allows the excitation of gold nanoparticles and the transferring of electrons in the surrounding environment with a quickly recombination of the electrons[41]. The nanoparticles dimension obtained with this technique is small and varies on the support used[42].The colloidal gold solution can be supported on different materials which deeply change the nanoparticles activity towards a selected reaction, Liu *et al.* have highlighted this in formic acid decomposition showing differences in the catalytic performances analysing Au supported on C, Al_2O_3, SiO_2, TiO_2, ZrO_2 and ZrO_2-NCs, finding the best activity for the last one[29].

2.1.4 **Bimetallic system: AuPd nanoparticles**

Since the promising results showed by bimetallic system in many reaction a lot of research was encouraged using these catalysts. In case of gold-based bimetallic nanoparticles, it was demonstrated that they play a benign role in the environmental catalysis; the first studies were carried on aerobic oxidation reactions. In this contest the AuPd nanoparticles showed to be very active towards the oxidation of alcohol to aldehyde in solvent free condition[51,52]. Some of the reaction more studied are in the case of benzyl alcohol oxidation[53,54], the glycerol oxidation[55], the direct production of hydrogen peroxide[53,56]. Some works have moved the attention also in the use of bimetallic catalysts in photocatalytic field[57,58], also the topic of the hydrogen production was touched using novel AuPd/TiO_2 catalysts[59,60].

Many techniques can be used to prepare bimetallic catalysts, the most interesting in lab scale are the impregnation and the sol-immobilisation routes[61].The structure of the bimetallic systems depends on the synthesis procedure, the post-treatments and the supporting material used. A way to control the structures is the sol immobilisation method: random alloy, Au core Pd shell (Au@Pd), Pd core Au shell (Pd@Au) can be obtained modifying the reduction sequences of the metal precursors[40,53,62]. In support of the formation of bimetallic particles the UV-Vis spectra can be observed, because it is peculiar: if the two metals precursor involved have the SPR band, the UV-Vis spectra shows only one SPR band with a maximum peak shifted in relation to the metal ratios, instead no band is showed when one of the metal precursor has not the SPR band as in the case of Au-Pd nanoparticles.

In the case of formic acid decomposition it is reported that alloys exhibit a higher activity, in particular Tesdree *et all.* found the AgPd alloy is more active that the monometallic particles, highlighting the synergic effect of the bimetallic compound. This is confirmed also AuPd nanoparticles, Metin *et al.*, suggest that using AuPd/C at 50°C improves the catalytic dehydrogenation of formic acid compared to Au/C and Pd/C as we reported in the chapter before.

Chapter 3: Summary and perspectives

Hydrogen is a green energy carrier and it could be produced from a variety of both renewable and non-renewable sources. Nowadays, non-renewable sources are mainly used for hydrogen production. Nevertheless for long term sustainable hydrogen generation it is fundamental that renewable energy sources such as solar, wind or biomass must primarily be used. In the field of transportation hydrogen has potential advantages over the conventional fuels including petroleum, diesel or natural gas. One of the most important application would in the fuel cells.

The challenge to can apply a sustainable hydrogen economy it is to find reversible and efficient storage of hydrogen. Many hydrogen sources based on both physical and chemical storage systems have been studied. Particularly chemical storage has attracted a lot of scientific reasearches as a solution to these restrictions or short-comings in current technology. These storage materials are small molecules with high hydrogen content, which are liquid under ambient conditions and are easily decomposed into carbon monoxide-free hydrogen over catalytic systems. Formic acid is one of the promising molecule for this.

Nevertheless the researchers' efforts the transition from bench scale to industrial application requires others deep investigations, in order to scale-up systems with relevant hydrogen output to supply fuel cells.

Chapter 4: Experimental Part

4.1 Introduction

This work is about the synthesis and the characterisation of supported nanoparticles supported either Carbon charcoal (Fischer Scientific) or Titania p-25 (Aeroxide). The catalysts were synthesised by using a colloidal method (or sol immobilisation method). The first aim of the synthesis was to improve the characteristics of the catalysts made by SOL-Immobilisation method. Then the catalyst with the best performance was compared with a commercial catalyst which is very active for the formic acid decomposition. Furthermore the catalytic performance of monometallic (Pd, Au) with respect to bimetallic (AuPd) supported nanoparticles was investigated for the aforementioned reaction. When the nanoparticles were prepared the active phase was deposited onto the chosen support (carbon and titania). The active phase was composed of a colloid suspension of metal nanoparticles made in aqueous solvent by reduction of the metal precursor (K_2PdCl_4 and/or $HAuCl_4$ H_2O) with sodium borohydride as reducing agent and polyvinyl alcohol (PVA) as stabilizer. The synthesis was carried out at room temperature and atmospheric pressure; the colloidal metal nanoparticles were immobilised onto the support and the powder was recovered by filtration, and finally the catalyst was dried in oven for 16 hours at 110 °C. Various techniques were used for the characterisation of the colloid suspensions and the supported nanoparticles such as:

- DLS (Dynamic Light Scattering) analyses were used to estimate the mean size and size distribution profile of colloidal metal nanoparticles;
- UV/vis spectroscopy tests were utilised to investigate the transition from metallic precursor to the metal nanoparticles, reduction of metal precursor and appearance of plasmon peak for the case of Au;
- Surface area both of the supports and of the supported catalysts are analysed by BET technique (Quantachrome Instruments);
- TEM (High Resolution Transmission Electron Microscopy) to valuate the dimension and the morphology of the particles and calculate mean particle size and particle size distribution;
- SEM (Scanning Electron Microscope) equipped with an energy-dispersive X-ray spectroscope (EDX) to examine the morphology and metal composition;

- XPS (X-Ray photoelectron spectroscopy) to study the surface content of the catalysts and calculate the oxidation state of metal;

The catalysts were examined for study of the catalytic decomposition of formic acid to hydrogen and carbon dioxide at mild conditions.

4.2 Chemicals

In Table 3 are recorded all the chemicals used :

Table 3 Chemicals

Formula	Name	Brand	Purity	Utilisation
HCOOH	Formic Acid	Sigma-Aldrich	95%	Reaction test
HCOOD	Formic Acid-d	Sigma-Aldrich	95%	Reaction test
DCOOH	Formic Acid	Sigma-Aldrich	95%	Reaction test
DCOOD	Formic Acid-d_2	Sigma-Aldrich	95%	Reaction test
$[C_2H_4O]_n$	Polyvinyl alcohol	Sigma-Aldrich	80%	Catalyst preparation
$NaBH_4$	Sodium borohydride	Sigma-Aldrich	≥99.99%	Catalyst preparation
$C_4H_6O_4$	Succinic acid	Sigma-Aldrich	≥99.0%	Calibration standard for HPLC
H_3PO_4	Phosphoric acid	Acros	ND	HPLC
H_2SO_4	Sulfuric acid	Sigma-Aldrich	≥98.0%	Catalyst preparation
$HAuCl_4 \cdot H_2O$	Hydrogen tetrachloroaurate [III] hydrate	Alfa Aesar	99.9%	Metal precursor
K_2PdCl_4	Potassium tetrachloropalladate [II]	Alfa Aesar	99.99%	Metal precursor
C	Carbon Charcoal, Wood	Fischer Scientific	ND	Catalyst preparation: support
TiO_2 (P25)	Titania	Aeroxide	ND	Catalyst preparation: support
Pd/C	Palladium on carbon	Sigma-Aldrich Code 20568010G	ND	Reaction test

4.3 Material catalyst performance

Different types of catalysts are been synthesised for this work such as:

- 1 wt.% Pd/C have been synthesised by SOL-Immobilisation technique using Potassium tetrachloropalladate (Alfa Aesar) and Carbon Charcoal Wood (Fischer Scientific) as supports, sulfuric acid 98% (Sigma Aldrich). One of the objective of the project was to study the effect of the stabiliser and of the reductant both on the colloid particle size and subsequently on their activity in the formic acid decomposition. When the synthesis parameters were optimised, a systematic study was carried out on the reaction with the best catalyst in comparison with the data obtained with the commercial catalysts 5 wt.% Pd/C (Sigma Aldrich). Moreover catalysts with different metal loading were investigated;
- 1 wt.% monometallic Pd/TiO_2, Au/TiO_2 and bimetallic $AuPd/TiO_2$ were synthesised by SOL-Immobilisation technique using Potassium tetrachloropalladate (Alfa Aesar), Hydrogen tetrachloroaurate [III] hydrate (Alfa Aesar) as metal precursor and Titania (P25) as support, sulfuric acid 98% (Sigma Aldrich). They were used to study the catalytic performance of different metals and metal composition (Au_xPd_y) in the formic acid decomposition.

The catalytic conversion of the formic acid decomposition was carried out using deionised water as reaction solvent.

4.4 Catalytic synthesis and characterisation

A colloid method was chosen to prepare both monometallic and bimetallic catalysts.
The first preformed monometallic Pd colloids were immobilised firstly on carbon, after on titania as the monometallic Au and bimetallic AuPd colloids. The technique of sol-immobilisation described has been presented in many reports[54,61]. The general protocol describes the addition of the desired chemicals (metal precursor, reducing agent and stabiliser) in a beaker with a aqueous solution under vigorous stirring (Fig. 7). First of all the metal precursor is diluted in water varying the concentration depending on the catalyst desired (i.e. for Pd 1 wt% the concentration is 2.3 E-07); the necessary amount of stabiliser is added and after 5 minutes the reductant is added to form a sol. After the colloid is supported on the support and dried in oven.

Fig. 7 Example of the preparation of the catalyst

4.4.1 Protocol for colloid suspension

Monometallic colloid suspension

- Fill a beaker with 400mL of distilled water for preparing 1 g of catalyst;
- Prepare firstly stock solutions of the metal precursor;
- Prepare a solution of both $NaBH_4$ and PVA in water: 0,1 M $NaBH_4$ (0.03783 g in 10 ml solution) and 1wt% PVA solution (0.1g in 10 ml solution). Use a volumetric flask. The $NaBH_4$ solution should be fresh and be used after 5 minutes otherwise $NaBH_4$ slowly decompose and the reducing power would be degraded;
- Add the desired amount of metal precursor to the solution;
- Add first the desired quantity of PVA (stirring 2-3 minutes) and $NaBH_4$ after to the aqueous solution in the beaker and start stirring;
- After 2-3 minutes there is change of colour. For gold red and for Pd grey-brown;
- Stir the solution for 30 minutes;

In Table 4 are recorded the ratio used among the chemicals in every synthesis.

Table 4 Table with the ratio among chemicals and metal

Sunspension	Pd wt%	Au wt%	PVA/M weight ratio	$NaBH_4$/M molar ratio
Pd-a	1	-	0	5
Pd-b	1	-	0,05	5
Pd-c	1	-	0,1	5
Pd-d	1	-	0,2	5
Pd-e	1	-	0,3	5
Pd-f	1	-	0,65	5
Pd-g	1	-	1,2	5
Pd-h	1	-	0,65	10
Pd-i	1	-	0,3	10
Au	-	1	0,3	10

Bimetallic colloid suspension

The protocol is similar to the monometallic one, except for the start when the stock solutions of the metal precursors (K_2PdCl_4, $HAuCl_4 \cdot H_2O$) are added together in the beaker with the desired ratio described in Table 5. The different steps can be summed up in the following procedure (Fig.8):

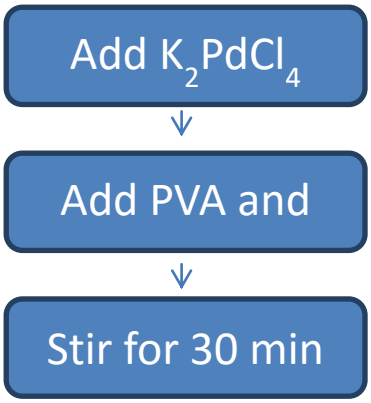

Fig. 8 Scheme of the procedure for bimetallic catalysts

In Table 5 are recorded the ratio used among the chemicals in every synthesis.

Table 5 Table with the ratio among chemicals and metals

Sunspension	%mol Au^{3+}	%mol Pd^{2+}	PVA/M weight ratio	$NaBH_4$/M molar ratio
Au_1Pd_1	50	50	0.3	10
Au_3Pd_1	75	25	0.3	10
Au_1Pd_3	25	75	0.3	10

Colloid suspension characterisation

The colloid suspension were characterised by DLS and UV-vis spectroscopy.

DLS: Dynamic Light Scattering

The instrument Zetasizer Nanoseries-ZS, Malvern Instruments LTD, was used for the study of the hydrodynamic diameter of the particles. The DLS is a technique for investigating the particles size in the sub-micron region and it is based on the Brownian motion and relates this to the particles size, because when the laser beam hits the particles a scattering phenomena happens. The range of detection is between 0.3nm to 10µm. The Brownian motion is a random movement of particles due to the bombardment by the solvent molecules that surround them[63]. The particles analysed are suspended in a liquid. The instrument measures the speed of diffusion of the

nanoparticles due to the Brownian motion, that it is correlated to the rate at which the intensity of the scattered light fluctuates when detected using a optical arrangement. The rate of the motion depends on the physical characteristic of the molecules: larger the particle, the slower the Brownian motion will be. The intensity of the scattered light has a fluctuation frequency depending from the dimension of the molecules too, so the size can be extrapolate from the analysis of the fluctuations of the intensity of the scattered light.

The red light of the laser has a wavelength of 633nm, it is scattered from the molecules in every direction, but it is measured only where the detector is set. This technique is not invasive. The fluctuations of the light are converted in electric signals and elaborated by a digital correlator.

The laser is attenuated from a lens, because if the light intensity were too high the detector would be saturated and there would be errors in the measurements.

The hydrodynamic diameter measured is the diameter of a sphere that consist of the coordination sphere and of al the species adsorbed on the surface. The diameter depends from many factors:

- the size of the particle “core”;
- the surface structure: any change to the surface of a particle that affects the diffusion speed will correspondingly change the apparent size of the particle;
- concentration and type of ions: they modify the electric double layer called the Debye length.

The sample concentration to have a reliable measure depends from the size of the molecules in suspension: for diameter less of 10nm the concentration should be ([conc] > 0.5 g/L), for diameter between 10nm and 100nm the concentration should be between ([conc] > 0.5 g/L) and wt% of 5 (for a density of 1g/cm^3) to avoid particle-particle interactions which change the speed and as consequence the measured diameter. Based on the concentration of the sample the instrument focuses the laser on the middle of the cuvette if it is low or in the insides if is high, so the multiple scattering is minimised (Fig.9).

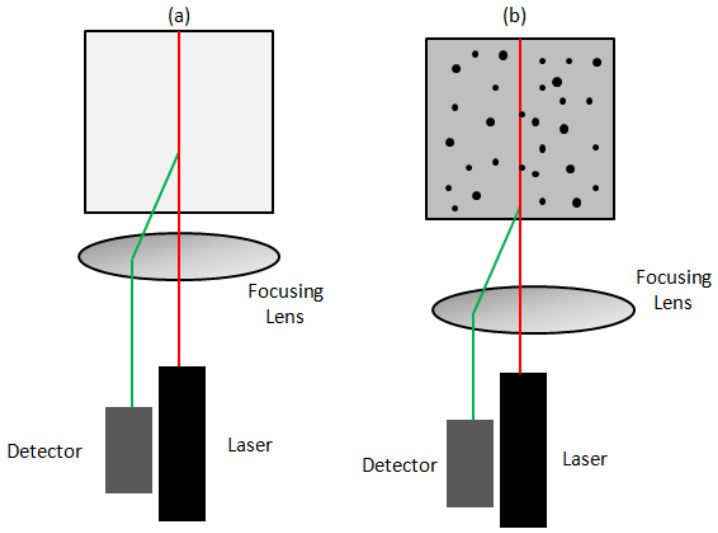

Fig. 9 Detector positions that are suggested for the analysis: (a) for low concentration; (b)for high concentration

In general the problem of the multiple scattering is avoided thank to the NIBS (Non Invasive Backscatter Detection). The multiple scattering happens when the light from one molecule is itself scattered from an other one, the effect is an underestimation of the dimension. With the detector at 173° the influence of the impurity, like dust, is reduced too.

With the DLS a statistic distribution of the dimension is obtained based on the scattering intensity. Besides it is possible to calculate from this other two distribution: one for the volume, one for the number.

In the end from the analysis is obtained a curve of distribution, a value for the average diameter, and an index of polydispersity (PDI) of the suspension. This index varies from 0 to 1: when the dispersity is less of 0.2 the suspension is considered monodisperse, from 0.2 to 0.5 it is more or less disperse, for bigger it is considered polydisperse.

Preparation of the sample

The solution of the sample was placed in a plastic cuvette. The software used to elaborate the data is Zetasizer Ver. 7.11, Malvern Instruments LTD. In Table 6 are reported the parameters used to study the sol for the different systems. For monometallic sample the refractive index is known, for the bimetallic system it was calculated as weighted average respect to the metal precursor content:

$$n_{Au_xPd_y} = \frac{n_{Au} * x + n_{Pd} * y}{x + y}$$

Where:

-$n_{Au_xPd_y}$ is the calculated refractive index for the bymetallic system;

-n_{Au} is the gold refractive index;

- x is the content in weight of Au;

-n_{Pd} is the palladium refractive index;

-y is the content in weight of Pd

Table 6 Refractive Index used for the DLS analysis of the different sol

Suspension	Refractive index
Pd	1.72
Au	0.27
Au_1Pd_1	0.99
Au_1Pd_3	1.36
Au_3Pd_1	0.64

UV-vis spectroscopy

UV/vis spectroscopic analyses were performed in a 1 cm^2 cuvette using *in-situ* AvaSoft UV-Vis Spectrometry (Fig.10).

Fig. 10 AvaSoft UV-Vis Spectrometry

The UV-visible technique refers to the absorption spectroscopy and it is based on the ability of a molecule to adsorb a photon of energy passing from the fundamental state to an excited state. In Fig.11 is showed the simplified scheme of a single beam UV-Vis spectrophotometer. It consists in the light sources in the range of UV-visible. a monochrometer made of two split separated by a diffraction grading. a sample cell holder; a detector device transforms the photons in electrical signal that is monitored by a computer.

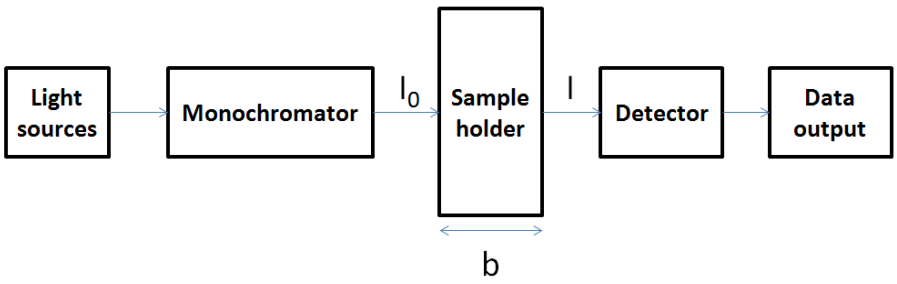

Fig. 11 Scheme of a single beam UV-vis spectrophotometer

This instrument allows to measure the intensity of light passing through the sample (I). and compares it to the intensity of light before it passes through the sample (I_0). The ratio is the transmittance and is usually expressed as a percentage (%T):

$$\%T = I/I_0$$

Usually instead of %T. the value is expressed as absorbance (A). this is based on the transmittance and it links the measurement to the concentration of the sample thank to the Lambert and Beer Law[64]:

$$A = -\log(\%T/100\%) = \epsilon\, b\, C$$

Where:

-ϵ is the molar attenuation coefficient

-b is the path length trough the sample

-C is the molar concentration of the analysed solution

The UV-visible spectrophotometer can also be configured to measure reflectance. In this case. the spectrophotometer measures the intensity of light reflected from a sample and compares it to the intensity of light reflected from a reference material. The ratio is called reflectance. and is usually expressed as a percentage (%R).

In this work this technique was usefull to characterise the colloid sol of the catalysts. so we could follow the reduction process by the colour change (Fig.12).

Fig. 12 Colloidal solution of palladium on the left and gold on the right

Preparation of the sample

The sol solution is placed in the quartz cuvette. then set in the holder and analysed.

4.4.2 **Protocol for supported catalysts**

The first part of the procedure provides of preparing the colloid suspension. as it is described above. When the colloid is ready. it is supported on the chosen support. The protocol is the same for monometallic and bimetallic catalysts. More in detail (Fig.13):

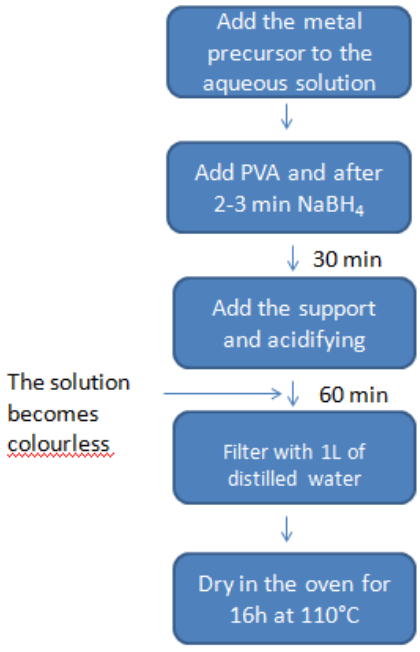

Fig. 13 Scheme for the catalyst preparation

n this thesis carbon and titania were studied as the chosen supports. In Table 7 are recorded all the catalysts investigated in this work.

Table 7 Homemade catalysts

Catalyst	Suspension	Support	%wt total metal	%mol Au	%mol Pd
Pd/C-a	Pd-a	C	1	-	100
Pd/C-b	Pd-b	C	1	-	100
Pd/C-c	Pd-c	C	1	-	100
Pd/C-d	Pd-d	C	1	-	100
Pd/C-e	Pd-e	C	1	-	100
Pd/C-f	Pd-f	C	1	-	100
Pd/C-g	Pd-g	C	1	-	100
Pd/C-h	Pd-h	C	1	-	100
0.2-Pd/C-e	Pd-e	C	0.2	-	100
0.5-Pd/C-e	Pd-e	C	0.5	-	100
0.7Pd/C-e	Pd-e	C	0.7	-	100
1.2-Pd/C-e	Pd-e	C	1.2	-	100
Pd/TiO_2-f	Pd-f	TiO_2	1	-	100
Pd/TiO_2-h	Pd-h	TiO_2	1	-	100
Pd/TiO_2-i	Pd-i	TiO_2	1	-	100
Au/ TiO_2	Au	TiO_2	1	100	-
Au_1Pd_3- TiO_2	Au_1Pd_3	TiO_2	1	25	75
Au_1Pd_1- TiO_2	Au_1Pd_1	TiO_2	1	50	50
Au_3Pd_1- TiO_2	Au_3Pd_1	TiO_2	1	75	25

Supported catalyst characterisation

The supported catalysts were characterised with different techniques such as: surface area analysis with BET theory. SEM-EDX. XPS. Some catalysts were investigated also with TEM.

Surface area analysis: N_2 Physisorption

The measure of the catalytic surface area is one of the main parameters. which characterised a material from the catalytic point of view. The unit used for the measure is m^2/g. The instrument used for the analysis is a Quantachrome Instruments. Nova2200e: Surface Area & Pore Size Analyser (Fig.14).

Fig. 14 Quantachrome instrument

This technique used the BET theory developed by Bunauer. Emmett and Teller; the area is measured determining the amount of gas adsorbed as molecular layer. The volume of physically adsorbed on the sample is estimated like difference of thermal conducibility of the gas before and after the adsorption. The gas used is nitrogen (N_2). The best conditions for adsorbing the N_2 on the solid surface is when the temperature of the liquid nitrogen is around 77K; thus the analysis of the specific surface area (S_{BET}) happens after the cooling of the sample with liquid nitrogen[65]. The model to calculate S_{BET} is:

$$\frac{\frac{p}{p_0}}{n(1-\frac{p}{p_0})} = \frac{1}{n_m C} + \frac{(C-1)p}{n_m C p_0}$$

P/P_0 range: 0.05-0.3

- p : Pressure.
- p_0 : Saturation pressure.
- n : number of moles adsorbed.
- n_m : number of moles adsorbed in the monolayer.
- C : BET constant. relative to the heat of absorption.

By plotting $\frac{\frac{p}{p_0}}{n(1-\frac{p}{p_0})}$ versus $\frac{p}{p_0}$ is obtained a linear relationship which the values of C and n_m can be calculated. From the value of n_m the specific area of the material is determined by the following equation:

$$S = n_m \cdot a_m \cdot N_a \cdot 10\exp(-21)$$

- S : apparent surface area (m^2/g).
- a_m : area occupied by one adsorbed molecule (m^2/molecule).
- N_a : Avogadro's number (molecules/mol).

Preparation of the sample

Prior to the determination of the specific surface area. all samples were outgassed under high vacuum. at 120°C for 3h with a Quantachrome degasser. 0.3g of powder were then placed in a cell with rod kept at 77K with liquid nitrogen and the analysis were carried out. The software used to elaborate the data is NovaWin.

SEM-EDX: Scanning Electron Microscope equipped with energy-dispersive X-ray spectroscope

The instrument used for SEM measures is a TM3030PLUS TABLETOP MICROSCOPE by Hitachi High Technologies Corporation Specification equipped with EDS System for Hitachi Tabletop Microscope TM3000 by Bruker (Fig.15).

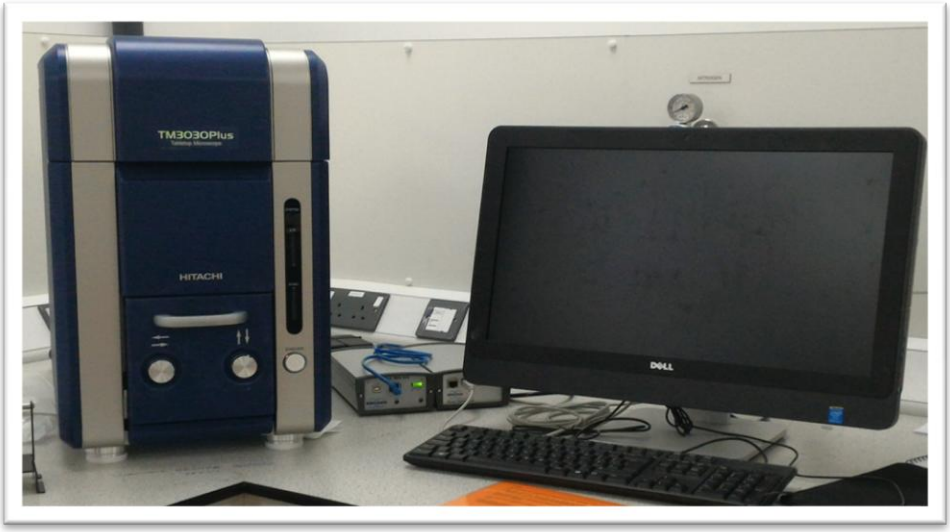

Fig. 15 SEM-EDX instrument

SEM is a non invasive analysis. The SEM uses a focused beam of high-energy electrons to generate a variety of signals at the surface of solid specimens. The signals allow to obtain information about the external morphology. chemical composition. and crystalline structure and orientation of materials making up the sample. Different types of signals arise from electron-sample interactions such as secondary electrons (that produce SEM images). backscattered electrons (BSE). diffracted backscattered electrons (EBSD that are used to determine crystal structures and orientations of minerals). photons (characteristic X-rays that are used for elemental analysis and continuum X-rays). visible light (cathodoluminescence–CL). and heat. For the SEM imaging sample the signals used are from the secondary electrons for showing morphology and topography on samples. Typically the source of electrons is a tungsten filament[66]. X-ray generation is produced by collisions of the incident electrons with electrons in discrete orbitals (shells) of atoms in the sample. Characteristic X-rays are produced for each element in a mineral that is "excited" by the electron beam. The SEM is also capable of performing analyses of selected point locations on the sample; this approach is especially useful in qualitatively or semi-quantitatively determining chemical compositions (using EDX).

Preparation of the sample

The powder is placed on a holder on a carbon adhesive layer. The sample surface should be the flattest possible to provide a clear image (Fig.16). The holder is set in the instrument under vacuum and then the analysis starts. because a gas atmosphere rapidly spreads and attenuates electron beams.

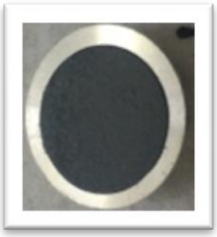

Fig. 16 Catalyst sample for SEM-EDX analysis

XPS: X-ray photoelectron spectroscopy

XPS is a technique for surface analysis for solid samples. The surface content of the catalysts was investigated using a Thermo k-Alpha^{+} Spectrometer (Fig.17).

Fig. 17 Thermo k-Alpha^{+} Spectrometer

This method is based on the photoelectric effect and it uses photons of a specific energy to excite the electronic state of atoms below the surface. The electrons emitted by the surface are then recorded by a detector. The spectra obtained is mirror of the electronic structure for atoms at the solid surface. because the resonance peaks are characteristic for the bound state of the electrons on the surface. The primary peaks arise from the ejected electron from the surface. Although the X-rays can cross the sample in depth. only the ejected electron from layers not deeper than 10nm can contribute to the energy spectra. The XPS analyses is quantitative: the intensity of a peak corresponds to the number of atom in a specific oxidation state. In the spectra there is an x axis for the binding energy E_B and an y axis for intensity I.

The kinetics energy is calculated from[67.68]:

$$E_K = h\nu - (E_B + \varphi)$$

where:

- E_K is the kinetic energy;
- hν is energy of the photon;
- E_B is the binding energy;
- φ is the spectrometer work function

The intensity is calculated as:

$$I = N\,\sigma\,\lambda\,K$$

where:

- I = intensity of photoelectron peak “p” for element “i”
- N = average atomic concentration of element “i” in the surface under analysis
- σ = photoelectron cross-section (Scofield factor) for element “i” as expressed by peak “p”
- λ = inelastic mean free path of a photoelectron from element “i” as expressed by peak “p”
- K = all other factors related to quantitative detection of a signal (assumed to remain constant during experiment)

Looking the energy spectra is possible to collect many information such as:

- the elemental and chemical composition of the surface from the peak position;
- how much material there is on the surface from the intensity of the peaks;
- FWHM (Full Width Half Maximum) that is useful to know the chemical state changes and the physical influences;
- broadening of a peak may indicate: a change in the number of chemical bonds contributing to a peak shape. a change in the sample condition (x-ray damage) and/or differential charging of the surface (localised differences in the charge-state of the surface)

Preparation of the sample

A few milligrams of the supported catalyst were placed in a hole of the holder. An holder can contain nine samples. The surface of the sample should be flat.

TEM: Trasmission Rlectron Microscopy

Particle size distributions were studied by means of transmission electron microscopy (TEM) using a JEOL JEM 2100 TEM operating at 200kV and TEM/ STEM FEI TECNAI F20 operating at 200 keV.

The TEM consists of a cylindrical tube about 2 meters long completely under vacuum (Fig.18).

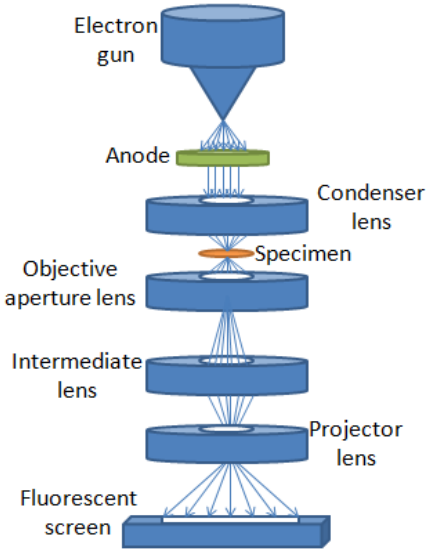

Fig. 18 TEM scheme

In contrast with the light microscope the electron microscope visualises objective using a thin beam of rapidly moving electrons that interfere with the specimen placed in the tube. The electrons are emitted by the cathode at the top of the tube and then accelerated by the anode. then they pass through a small aperture which forms the beam into the vacuum tube. The vacuum is fundamental. otherwise molecules of gases. such as those in air. absorb electrons. The part of the microscope that generate the electron beam is called electron gun; the beam is maintained along the tube by electromagnetic lenses. The electromagnetic field emitted by the coils focuses the beam at the centre of the tube. Electrons hit the specimen and they could be adsorbed. scattered or passed trough the sample. because different region of the specimen interact in different ways with the electrons. In the end of the tube the electrons are collected on fluorescent photographic film.

The beam that reaches the film consist of the different amount of electron which passed through particular region of the specimen. These differences are responsible of the contrast in the film. The original image produced by the electrons microscope is always black and white and it is not possible to see directly with the eyes[69].

Some disadvantages of the TEM use:

- Low sampling volume and rather slow process of obtaining information;
- High capital and running cost;
- Special training required for the operation of the equipment;
- Difficult sample preparation. Possibility of electron beam damage;.

- Samples which are not stable in vacuum are difficult to study;
- Magnetic samples require special care;
- Non-conducting samples require gold or carbon coating;
- Difficulty in the interpretation of images. In usual mode of operation information is integrated along the beam direction.

Advantages:

- Real (Image) and reciprocal space (diffraction pattern) information can be obtained from same region of sample;
- Chemical information via EDX (with additional attachments);
- High resolution imaging possible;
- Possible to obtain amplitude and phase contrast images. Many different kinds of phase contrast images can be obtained.

Preparation of the sample

A drop of the suspension was allowed to evaporate on a holey carbon film supported by a 300 mesh copper TEM grid. Samples were subjected to bright field diffraction contrast imaging experiments. Mean particle sizes and particle size distributions were determined by measuring the size of over 300 particles from different areas using the software Image J.

Support characterisation

The supports were characterised by SEM. surface area analyses with BET theory. The first two techniques were described above.

4.5 Catalyst performance

The model reaction studied was the catalytic formic acid decomposition. The decomposition of HCOOH in aqueous solution is performed in batch condition in a two neck 100 ml round bottom flask with a reflux condenser and a magnetic stirrer (Fig.19). 10 ml of a 0.5 M HCOOH solution was placed into the reactor under vigorous stirring. The screening temperature used was 50°C. Once reached the desired temperature. the

reaction was initiated by adding the catalyst; the temperature was monitored and controlled by a thermocouple immersed in a oil bath.

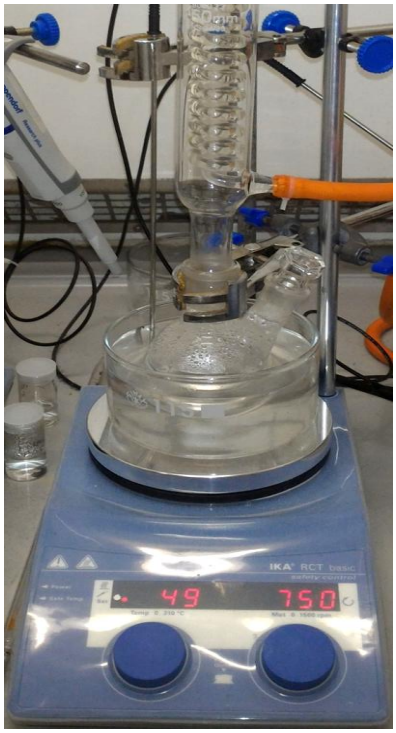

Fig. 19 Set up of the performed reaction

In order to monitor the reaction. samples are withdrawn regularly and analysed by high-performance liquid chromatography (HPLC. Agilent 1220 Infinity LC) using a column MetaCarb 87H 250 x 4.6 mm. Varian. at 60 ºC with a refractive index (RI) detector. HPLC gradient grade water was used as the mobile phase. at a flow rate of 0.4 mL min^{-1} (Fig.20). Typically the reaction is carried on for 4h.

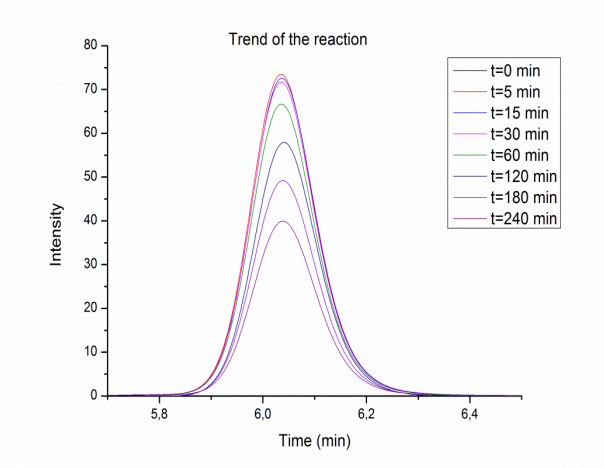

Fig. 20 Trend of the reaction followed by HPLC

A scheme of the HPLC instrument is reported in Fig.21.

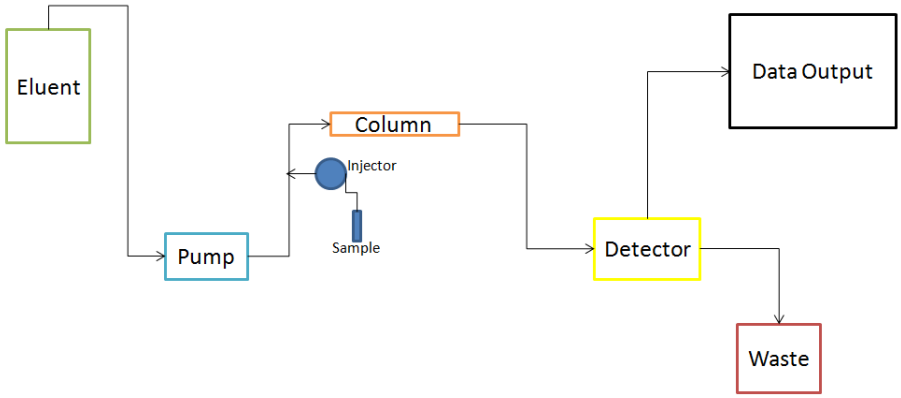

Fig. 21 Scheme of HPLC

The HPLC (High Performance Liquid Chromatography) is based on the partitioning of solutes between two phases: one phase (the mobile phase) is in constant movement relative to the other one (the stationary phase). The basis of separation is that different kinds of molecules on average spend different amount of time in the stationary phase. Due to the large number of partitioning steps, chromatography has enormous resolving power and can separate mixtures of components with very similar physical properties. When a good separation of a binary sample happens this will in the ideal case result in the elution of two Gaussian-shaped concentration peaks. The stationary-phase particles should have a small particle diameter, uniform geometry and small-size distribution, and should be homogeneously packed, and any extra column volume should be minimized[70]. The column used in this work it is a common column for organic acid. The column was calibrated using the external standard method. The standard used was a solution of succinic acid 0.2M.

The concentration of HCOOH is easily calculated from the areas obtained from HPLC. the formula used was:

$$[FA] = R_f \frac{Area\ FA}{Area\ SA}\ [SA]$$

Where:

- [FA] is the HCOOH concentration
- [SA] is the noted succinic acid concentration
- R_f is the retention factor calculated from the calibration
- Area FA and SA are the peaks area respectively of HCOOH and succinic acid

In this case R_f is 1.6. In the follow picture is reported the calibration line (Fig.22).

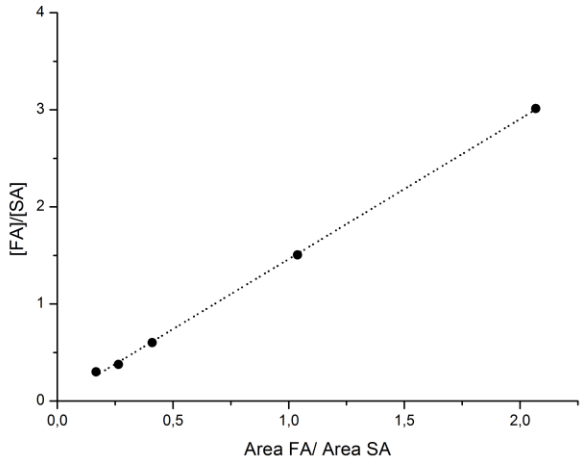

Fig. 22 Calibration line

Preparation of the sample

After withdrawing the sample. it was placed under centrifugation to separate the catalyst. Before injecting in the HPLC 0.1 mL of the solution obtained with 0.1 mL of $C_4H_6O_4$ were diluted in 9.8 mL of distilled water.

Chapter 5: Results and discussion

5.1 Optimisation of the synthesis of Pd catalyst

Interesting studies were carried out on formic acid decomposition, because it would be an efficient hydrogen storage media. In this work we focus our the studies to find out if the reaction is structure sensitive, thus we spent time to analyse the effect of the synthesis step on the preformed catalysts such as how vary the particles size and shape, how the capping agent (PVA) and the reducing agent ($NaBH_4$) influence the active sites and the effect of different supports on the active metal.

The aim of the first part of the work was to synthesise supported monometallic palladium nanoparticles using the sol immobilization method. The sol-method or colloidal method is widely used in catalysts preparation because, as previously reported, it allows to tune particle size, particle size distribution and to analyze the nanoparticles before immobilization, therefore to elucidate the role of metal nanoparticle and nature of support for a catalytic reaction. In our case, Pd nanoparticles were synthesised by reduction of the metal precursor (K_2PdCl_4) in deionised water using polyvinyl alcohol as stabiliser and sodium borohydride as reducing agent. A scheme of the used procedure is represented in Fig. 23.

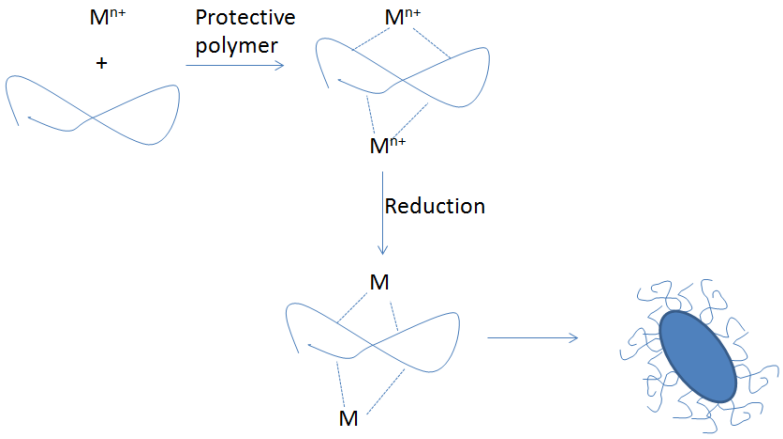

Fig. 23 Scheme of colloid method

The metallic nanoparticles are formed by reduction of metal, in this case of palladium, reduced by $NaBH_4$. The sodium borohydride produces hydrogen and gives electron available for the reduction in solution of the free cations. The result is the formation of palladium nanoparticles (eq.17):

$$4PdCl_4^{2-}{}_{(aq)} + 8e^- \rightarrow 4Pd_{(s)} + 16Cl^- \quad \text{eq.17}$$

In aqueous solution the reducing agent oxides as in the following pathways:

$$NaBH_4 + H_2O \rightarrow NaBO_2 + 4H_2 \quad \text{(eq.18)}$$

$$NaBH_4 + 8OH^- \rightarrow NaBO_2 + 6H_2O + 8e^- \quad \text{(eq.19)}$$

$NaBH_4$ undergoes self-hydrolysis (hydrolysis without catalyst) in aqueous solution (eq.18), nevertheless the generation of hydrogen is very slow and shortly afterwards the ambient of reaction becomes basic, thus the reaction route will be the one described in eq. 19[20].

The next step in catalysts preparation is the immobilization of the nanoparticles on a solid support. The support is dipped in the sol and the metal particles are adsorbed from the solution. The adsorption is influenced by the pH of the solution[42]. In our case sulfuric acid is added, because it improves the electrostatic interaction between the surface of the support (carbon and titania) and the metal colloid, for example in case of titania P25 the point zero charge was found at pH_{pzc}= 6.1[71], thus below this value increasing the acidity it possible to obtain a higher degree of positive charge improving the interaction. Characterisation of colloids as well as of supported nanoparticles was carried out.

Moreover, unsupported and supported metal nanoparticles were tested in the reaction of formic acid decomposition for the production of hydrogen for understanding the role of metal and support in terms of activity and stability.

5.1.1 **Synthesis of preformed Pd sol**

During the preparation of nanoparticles the concentration of the reagents and the ratio between stabilizer and metal covers a fundamental rule, influencing the size and shape of the particles. For these reasons, some tests were carried out varying the polyvinyl alcohol (PVA) and sodium borohydride content. PVA (Fig.24) is chosen as stabilizer for the synthesis of palladium nanoparticles. This polymer stabilizes the nanoparticles due to steric effect. In fact it has been reported that PVA creates a layer around Pd nanoparticles which enforces the stability of the colloids preventing aggregation.

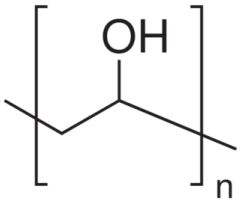

Fig. 24 Polyvynil alcohol

The stabilizer influences the nanoparticles formation and growth, the immobilization and as a consequence the activity of the catalyst. Varying the PVA content during the preparation of the catalyst, can influence the size of the particles and as a consequence the activity of the catalyst. The weight ratio between PVA and palladium was modified as shown in Table 1 from 0 to 1.2. In this Table, reaction conditions are reported together with Dynamic Light Scattering (DLS) analysis results of the obtained nanosuspensions (Intensity). The Polidispersive Index (PDI) is also reported in the table since it shows how large the Gaussian curve is; the higher the PDI value, the broader the curve.

Table 8 Characteristics of Pd sols prepared using different PVA/Pd weight ratio obtained by DLS analysis

Sample	PVA/Pd weight ratio	n_{NaBH4}/n_{pd} molar ratio	Addition	d_m and relative percentage by DLS	PDI
Pd-a	0	5	Graduated pipette	56 (6.8%); 300 (93.2%)	0.51
Pd-b	0.05	5	Graduated pipette	175 (100%)	0.72
Pd-c	0.1	5	Graduated pipette	415 (96.4%);5343(3.6%)	0.45
Pd-d	0.2	5	Graduated pipette	8 (100%)	1
Pd-e	0.3	5	Graduated pipette	15 (27.9%); 64 (10.9%); 246 (61.2%)	0.98
Pd-f	0.65	5	Graduated pipette	328 (100%)	0.25
Pd-g	1.2	5	Graduated pipette	52 (7%); 181 (93%)	0.31

At first, palladium nanoparticles were synthesized without any PVA (Pd-a). However, the obtained results were not satisfactory and the obtained sample was too much polydisperse and big in size.

It is known that particle size distribution can strongly affects the activity of the catalyst. Indeed, when the sol diameter is with high degree of polydispersity and nanoparticles agglomerate, the nanoparticles dimension is too high for a good application in catalysis. Supporting colloidal nanoparticles with the presence of aggregates could bring to large metallic particles on the surface. As a sequence the number of corner and edge sites will decrease, therefore can decrease the catalytic activity if the reaction is structure-sensitive.

Increasing the PVA/Pd weight ratio, the hydrodynamic diameter changed: it decreased from 0 to 0.2-0.3 and then it grown again. This trend could be explained due to a first positive effect of the steric stabilizer, leading to sol stabilization, then to particles collapse due to the excess of PVA that result in Pd agglomeration. Nevertheless, a higher amount of PVA significantly decreases the PDI of the suspension. This trend is more evident comparing DLS data in terms of volume, which can reveal more efficiently the smaller fraction present in the sols. Fig.25; 26 and 27 report the results obtained for suspensions Pd-a, Pd-e and Pd-g and evidence the difference in polydispersity and sol hydrodynamic diameters.

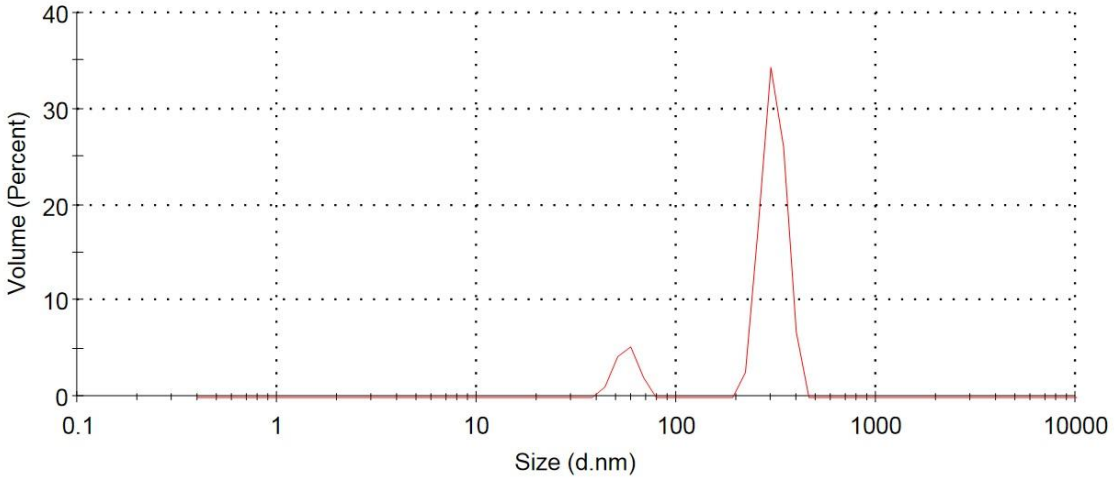

Fig. 25 DLS of colloid Pd-a (PVA/Pd=0 and $NaBH_4$/Pd=5)

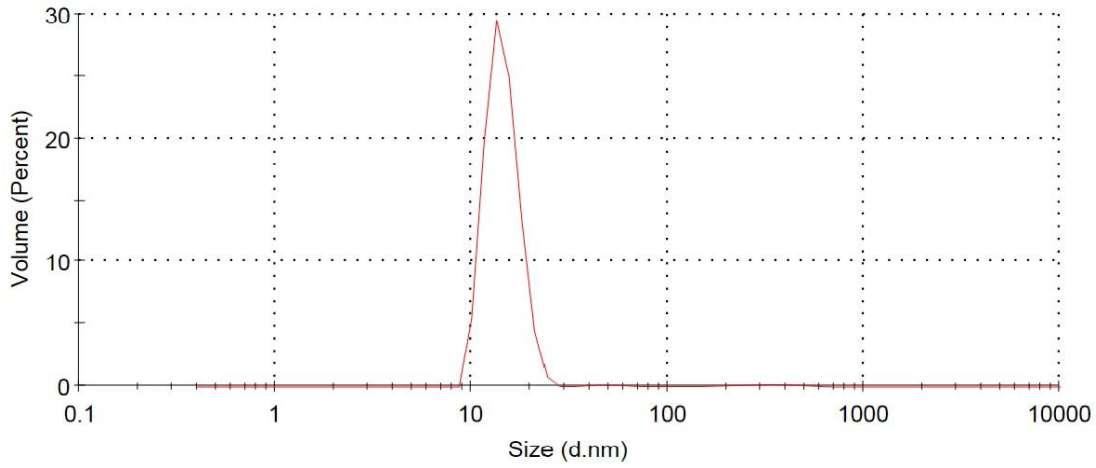

Fig. 26 DLS of colloid Pd-e (PVA/Pd=0.3 and $NaBH_4$/Pd=5)

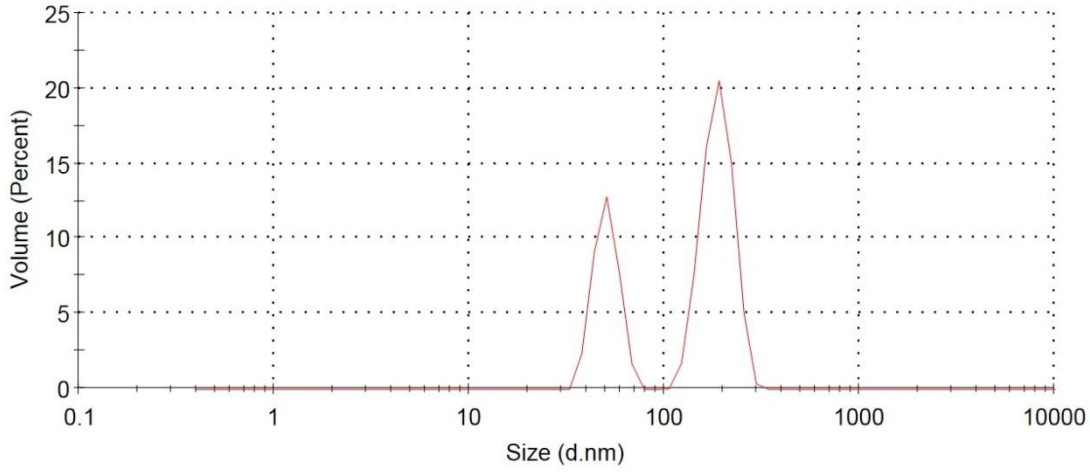

Fig. 27 DLS of colloid Pd-g (PVA/Pd=1.2 and $NaBH_4$/Pd=5)

For Pd-e curve appears only one peak, which means that the numbers of aggregations is small. Besides the sol nanoparticles size by DLS is 14.6 nm with a narrow distribution.

Keeping constant the weight ratio PVA vs Pd (PVA/Pd=0.65 as screening value) the $NaBH_4$/Pd molar ratio has been increased from 5 to 10 to verify the possibility to change nanoparticles dimensions (Table 9) by increasing the amount of reducing agent in the preparation. From these results, the different amounts of $NaBH_4$ does not seem to significantly influence the size of the sol nanoparticles at the studied range, in fact the hydrodynamic diameters result 328 nm for Pd-f and 341 nm in Pd-h (the value recorded consist of all the surrounding environment, so also of the PVA around the nanoparticles). Indeed, DLS tests show similar hydrodynamic diameter and PDI

(Fig.28; 29). Thus this parameter can be considered optimised refer to the sol particles size. These sol were supported first on carbon and then on titania.

Table 9 Characteristics of Pd sols prepared using different NaBH4/Pd ratio obtained by DLS analysis

Sample	PVA/M weight ratio	n_{NaBH4}/n_M molar ratio	Addition	d_m (nm) and relative percentage by DLS	PDI
Pd-f	0.65	5	Graduated pipette	328 (100%)	0.25
Pd-h	0.65	10	Graduated pipette	74 (5.5%); 341 (94.5%)	0.26

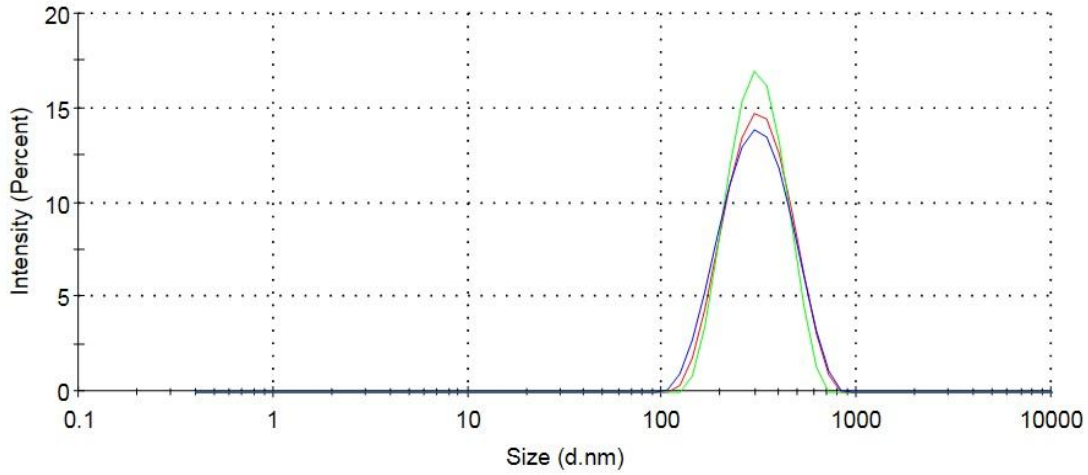

Fig. 28 DLS of colloid Pd-f (PVA/Pd=0.65 and $NaBH_4$/Pd=5)

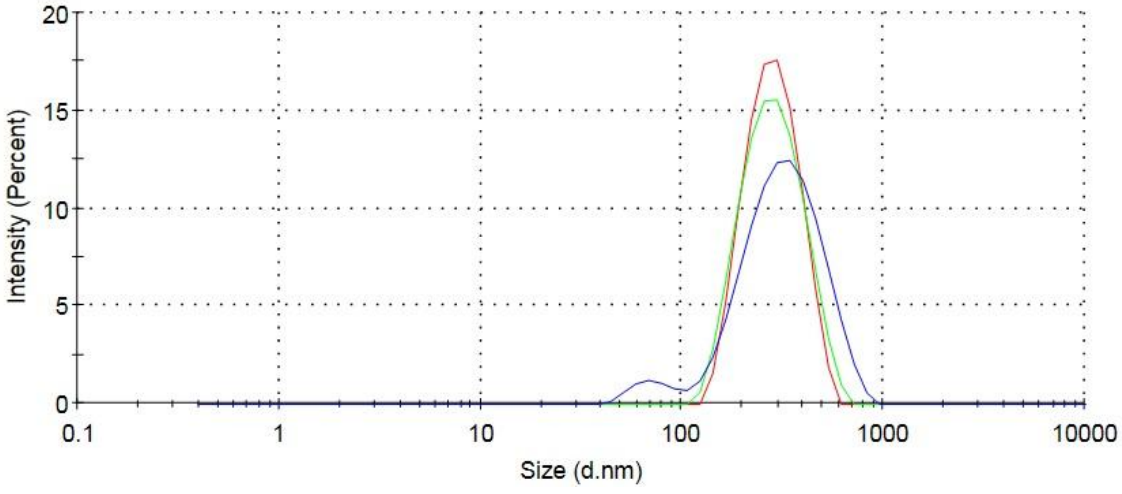

Fig. 29 DLS of colloid Pd-h (PVA/Pd=0.65 and $NaBH_4$/Pd=10)

5.1.2 **Preparation of the supported catalysts**

Ten distinct immobilized catalysts were prepared from the sol system studied before. The support material used were either Carbon Charcoal, Wood, Fisher Scientific (Surface Area =64m^2/g) or Titania-P25, Aeroxide (Surface Area =50m^2/g). Immobilisation of the sol is accomplished by adding the support (acidified at pH 1 by sulfuric acid) after 30 min of sol-generation under vigorous stirring conditions. The total metal loading was kept at 1%wt. After 1h the slurry was filtered and washed thoroughly with distilled water and dried at 120°C for 16h. In Table 10 are reported all the catalysts synthesised from the respectively sol (i.e. Pd/C-a points out a C-supported sample synthesised from sol Pd-a); data refer to the composition were measured by SEM-EDX and of the surface areas were collected by N_2 physisorption apparatus and multi-point BET analysis method; sample were pre-treated under vacuum.

Table 10 Structural parameters and chemical composition of Pd supported on C or on TiO_2-p25

Sample	Pd (wt%) by EDX	Surface area (m^2/g)
Pd/C-a	1	42
Pd/C-b	1	24
Pd/C-c	1	46
Pd/C-d	1	33
Pd/C-e	1	50
Pd/C-f	1	32
Pd/C-g	1	31
Pd/C-h	1	29
Pd/TiO_2-f	1	50
Pd/TiO_2-h	1	67

5.1.3 **Characterisation of Pd/C and Pd/TiO_2 catalysts**

Prepared catalysts were characterised by TEM. Some representative images are presented below. Nanoparticles showed a spherical morphology with a mean particle size ranging from 3nm to 5nm depending on the sample composition, (Table 11).

Table 11 Average diameters of metal NPs estimated from TEM analysis

Sample	d-TEM (nm)
Pd/C-a	n.d
Pd/C-e	4.8±2
Pd/C-f	3.0±0.9
Pd/C-g	3.1±1.1
Pd/C-h	3.2±0.99
Pd/TiO_2-f	5±2
Pd/TiO_2-h	3.1±0.99

A magnification on the sample without PVA (Pd/C-a) shows that the palladium nanoparticles tend to form aggregation (Fig.30) of many small nanoparticles. This result is in agreement with the DLS analysis on the colloid system, where the value of the hydrodynamic diameter resulted a large value. If the particles are not covered by the stabilizer the particles can grow and they will start to agglomerate and in some cases to agglomerate. It is possible to highlight small particles (2-8 nm) which tends to agglomerate in larger nanoparticles more than 1µm, in particular placed on the edge of surface of the catalyst. Images taken in the other areas of the carbon support it was evident the particles were reasonably well dispersed. Due to the difficulty to distinguish individual NPs, it wasn't possible to calculate precisely the particle size distribution.

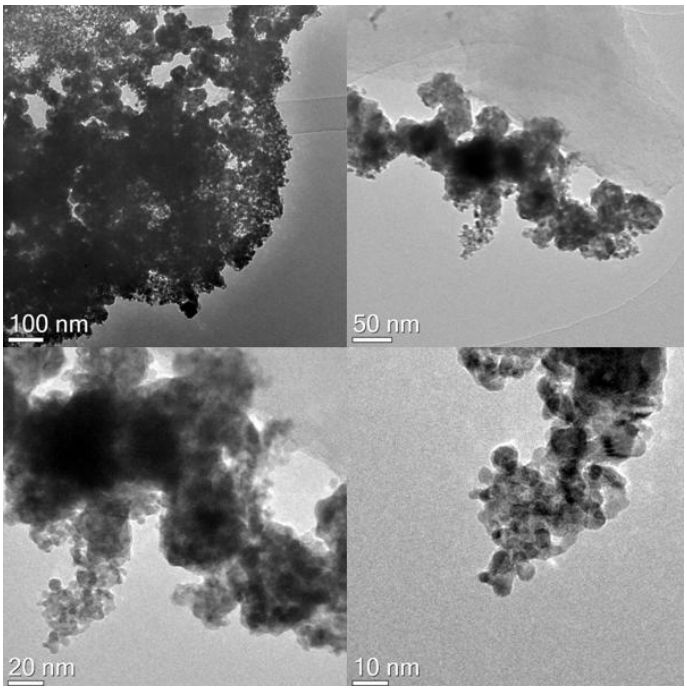

Fig. 30 TEM images of the Pd/C-a

Whereas with a larger weight ratio of PVA/Pd the TEM analysis permitted to identify the nanoparticles in order to calculate the mean particle diameter. In Fig.31 is represented the catalyst Pd/C-e. As displayed the supported catalyst with a weight ratio PVA/Pd of 0.3 is characterised from a broad distribution of particles. Fifty percent of the particles counted are in a range between 4 and 5 nm (Fig.32). Also in this case the sample is characterised by the presence of small nanoparticles between 1.5nm and 10nm and they are well dispersed on the carbon, although they prefer to accumulate on the borders. In some points there is a small presence of big agglomerated particles.

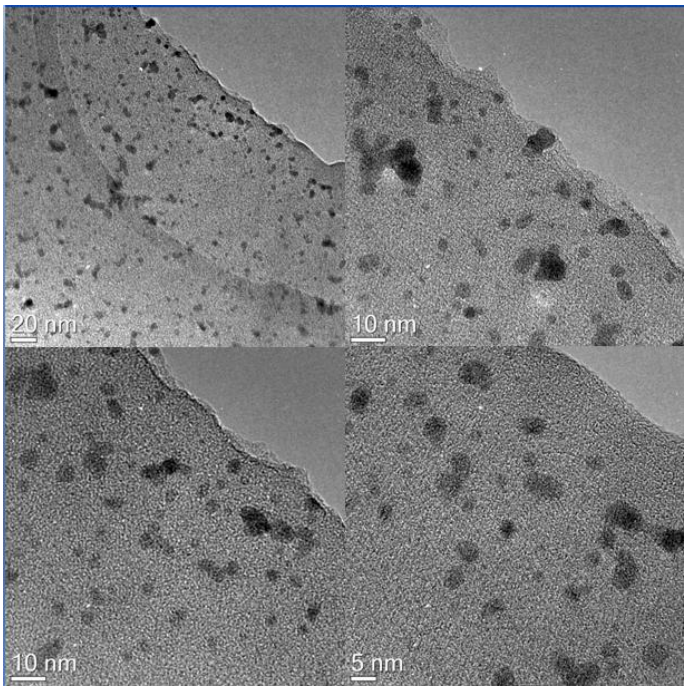

Fig. 31 TEM image of the Pd/C-e

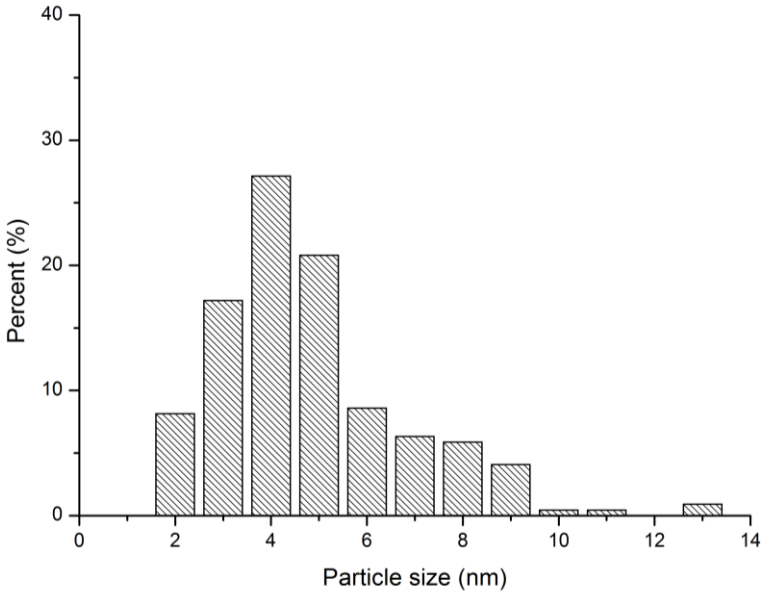

Fig. 32 Particle size distribution of Pd/C-e

The sample Pd/C-f with a PVA/Pd of 0.65 weight ratio and $NaBH_4$/Pd of 5 molar ratio was characterized by TEM, as showed in the representative image below (Fig.33). Increasing the amount of PVA resulted in an decrease of mean particle size. The mean particle size is 3±0.9nm (Fig.34). The TEM analysis evidences some areas of agglomeration in the support border.

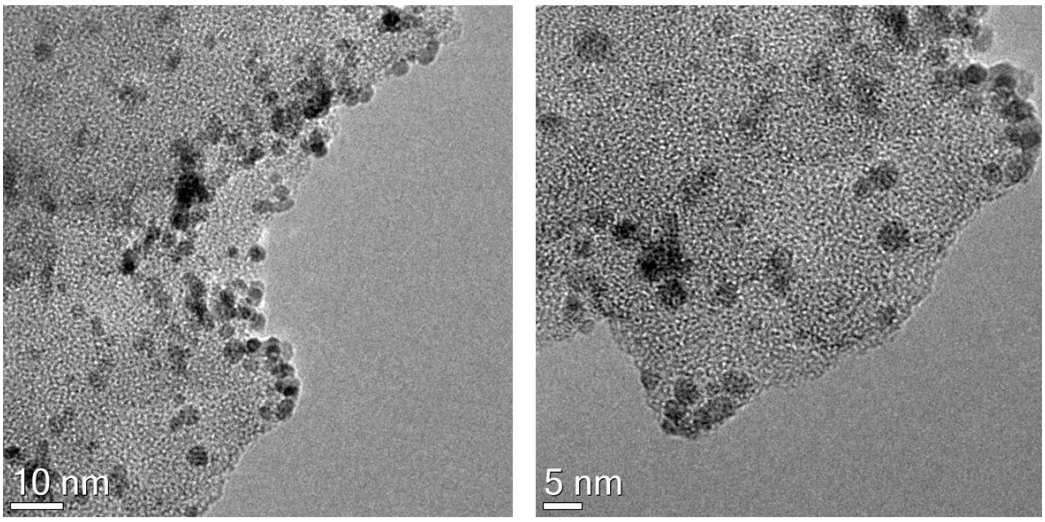

Fig. 33 TEM image of Pd/C-f

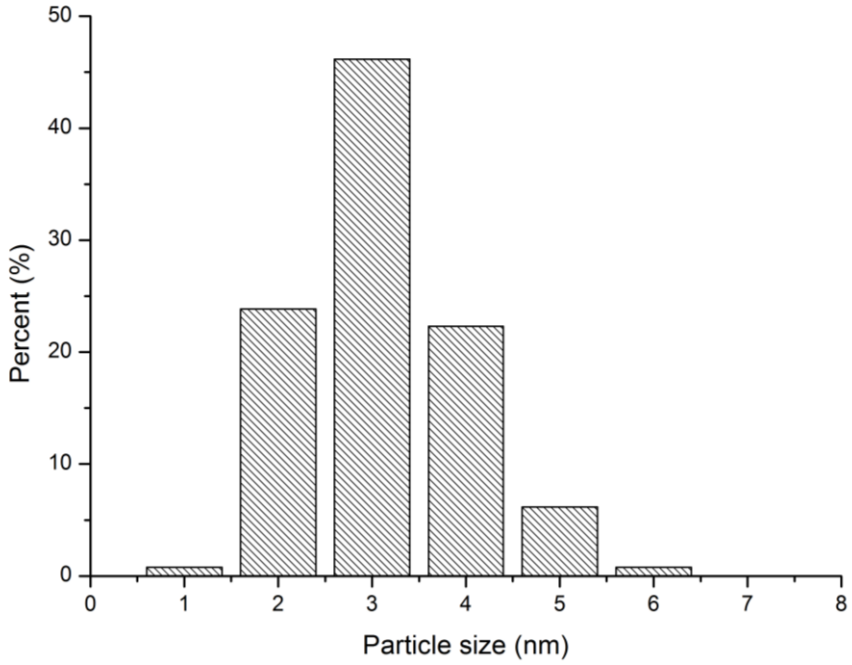

Fig. 34 Particle size distribution of Pd/C-f

Also the sample Pd/C-g with a PVA/Pd weight ratio of 1.2, as shown in the picture below (Fig.35) was characterized by TEM. The mean is 3.1±1.1nm (Fig.36). On the border of the catalyst there is the presence of larger particles.

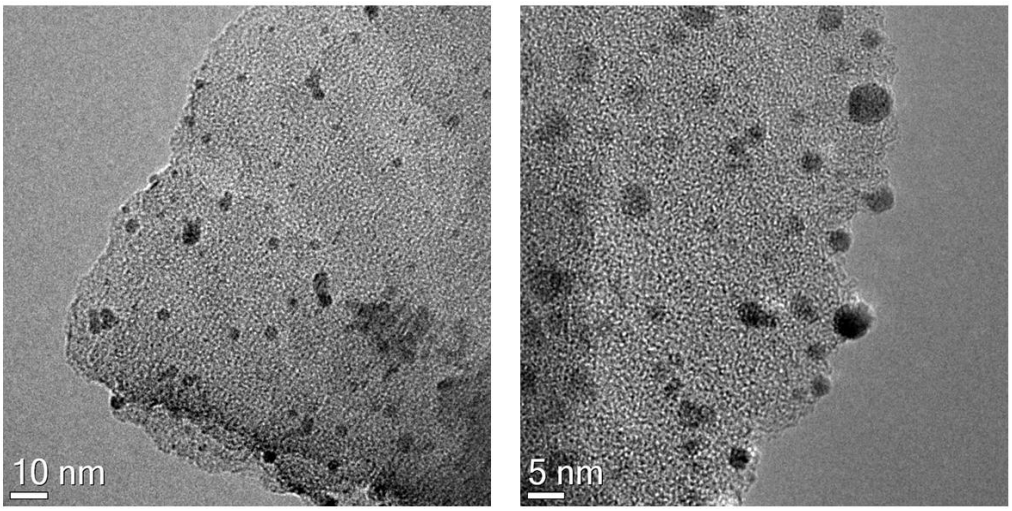

Fig. 35 TEM images of Pd/C-g

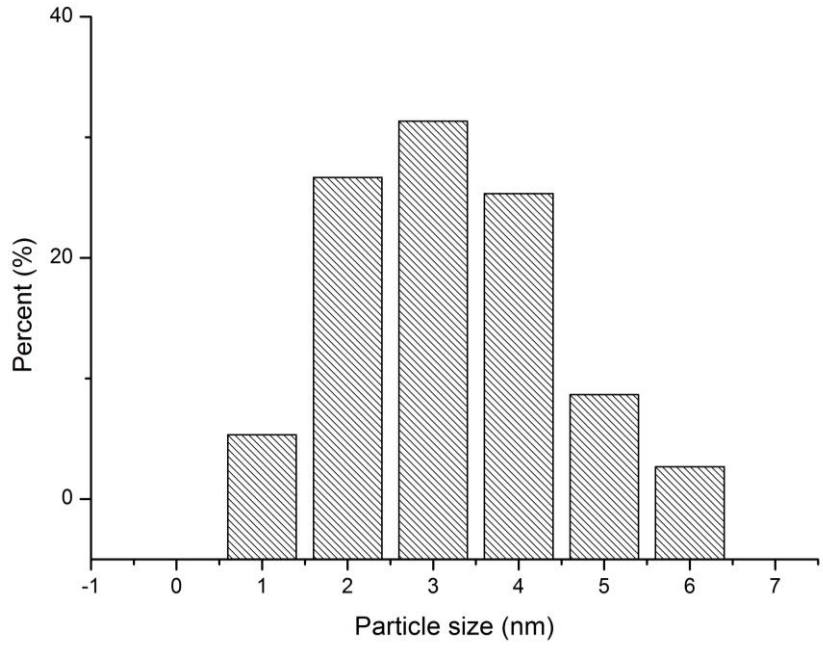

Fig. 36 Particle size distribution of Pd/C-g

The catalyst Pd/C-h with a PVA/Pd of 0.65 and a content of $NaBH_4$/Pd of 10 is showed in the picture Fig.37. The average diameter is 3.2±1.76nm (Fig.38). The size distribution is very narrow, almost the 75% of the NPs have a diameter between 2-3 nm.

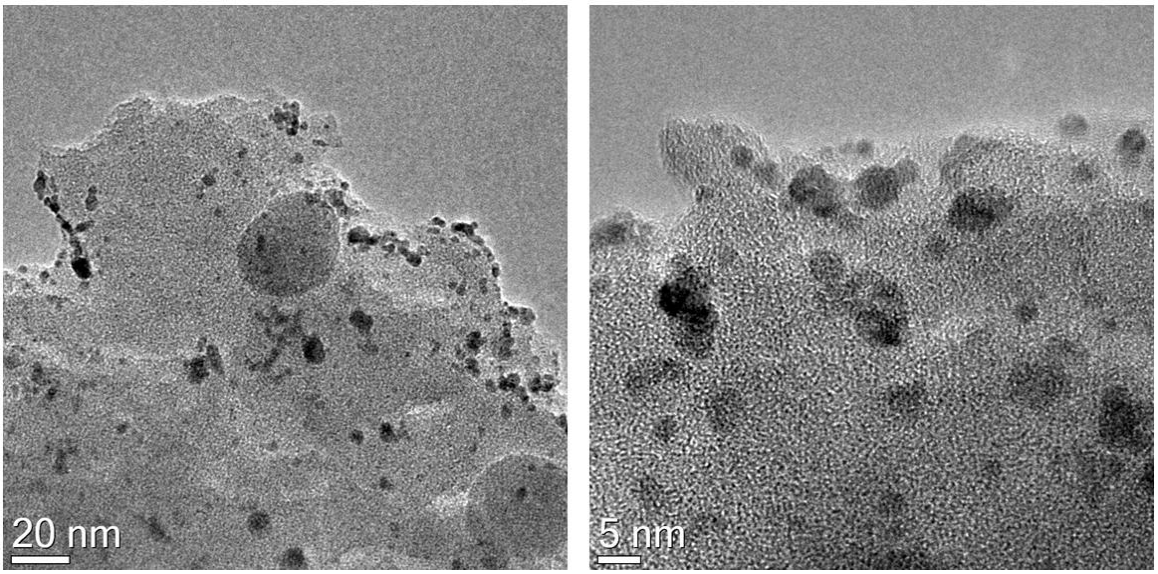

Fig. 37 TEM images of Pd/C-h

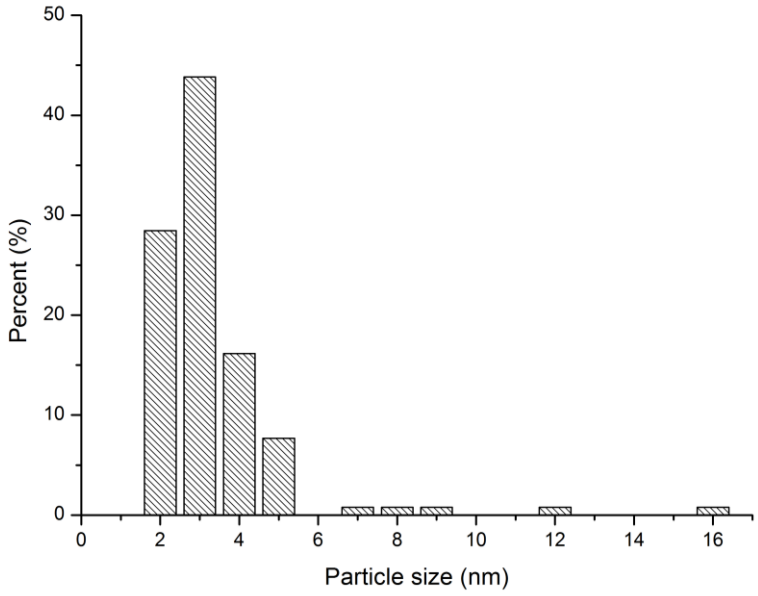

Fig. 38 Particle size distribution of Pd/C-h

The catalyst Pd/TiO_2-f with a PVA/Pd of 0.65 and a content of $NaBH_4$/Pd of 5 it is showed in the snapshots below (Fig.39). The particles dimension is broad in a range among 2-7 nm, but there are also particles around 9-11 nm. The mean is 5±2nm (Fig.40). The particles are well dispersed on the support, the biggest agglomerated particle found had a dimension of 30 nm.

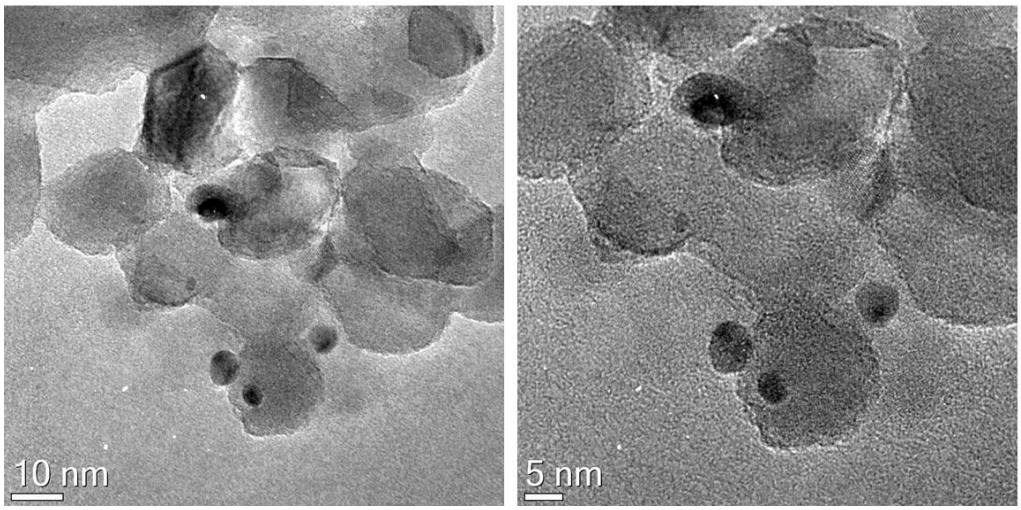

Fig. 39 TEM images of Pd/TiO_2-f

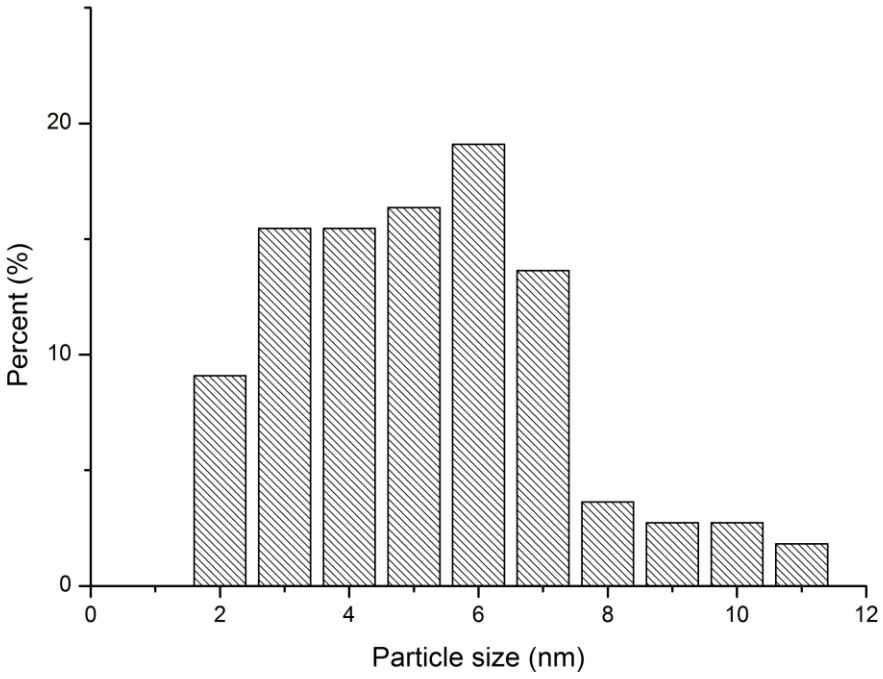

Fig. 40 Particle size distribution of Pd/TiO_2-f

The catalyst Pd/TiO_2-h with a PVA/Pd of 0.65 and a content of $NaBH_4$/Pd of 10 is showed in the images below (Fig.41). The mean is 3.1±0.99nm (Fig.42). The particles size distribution is narrow and the values are among 2-6 nm. In this sample there is not the phenomena of agglomeration and the palladium molecules are well dispersed on the support.

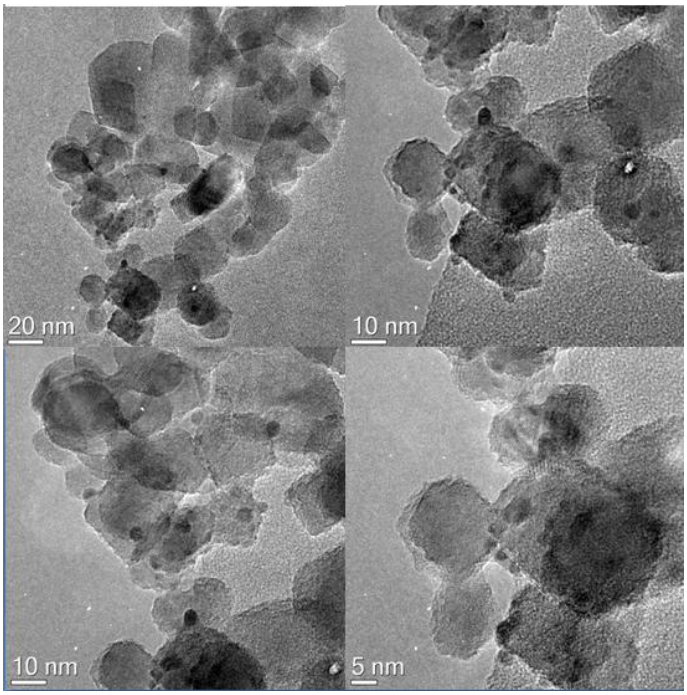

Fig. 41 TEM images of Pd/TiO_2-h

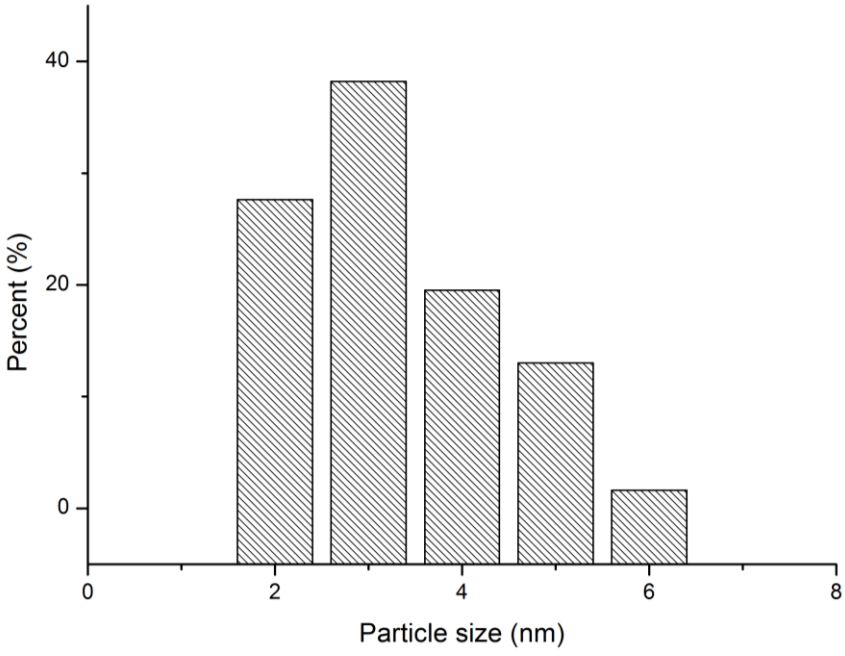

Fig. 42 Particles size distribution of Pd/TiO_2-h

XPS measurements (Table 12) were carried out to calculate the Pd^{II}/Pd° atomic ratio on the surface of the samples and the Pd content on the surface of the catalysts.

Table 12 Characterisation of the Pd content of the catalysts surface by XPS analysis

Catalyst	PVA/Pd weight ratio	$NaBH_4$/Pd molar ratio	$Pd_{surface}$ At%	Pd^{II}/Pd^0	$\%Pd^0$
Pd/C-a	0	5	2.2	1.3	44
Pd/C-b	0.05	5	2.8	0.4	72
Pd/C-c	0.1	5	3.6	0.3	64
Pd/C-d	0.2	5	7.2	1.6	38
Pd/C-e	0.3	5	7.8	1.6	39
Pd/C-f	0.65	5	3.7	0.6	62
Pd/C-g	1.2	5	2.4	2.4	30
Pd/C-h	0.65	10	4.1	0.5	65
Pd/TiO_2-f	0.65	5	0.3	1.6	39
Pd/TiO_2-h	0.65	10	1.1	0.7	55

It is particularly interesting to analyse the XPS spectra of the samples both with a different content of PVA and $NaBH_4$. Before analysing the spectra a deconvolution process has been done to can calculate the atomic ratio of Pd^{II}/Pd^0 as ratio of the peaks area.

From XPS analysis was evidenced that varying the PVA/Pd weight ratio from 0 to 1.2 the content of PdO in the catalysts and the Pd surface content change:

- in the catalysts the amount of Pd in the surface increases until a PVA/Pd weight ratio of 0.3, instead from 0.3 to 1.2 decreases again.
- In the sample the Pd in the zero oxidation state is higher, when the PVA/Pd weight ratio is small.

To explain the values reported for different $NaBH_4$/Pd molar ratio, in Fig.43a are reported the XPS profiles of the sample Pd/C-f ($NaBH_4$/Pd=5) and Pd/C-h ($NaBH_4$/Pd=10), in Fig43b are reported the XPS profiles of the sample Pd/TiO_2-f ($NaBH_4$/Pd=5) and Pd/TiO_2 -h ($NaBH_4$/Pd=10). As a matter of common knowledge the peaks at 335.5 eV and 340.8 eV correspond to $Pd3d_{5/2}$ and $Pd3d_{3/2}$ assigned to Pd^0. While the peaks at 337.6 eV and 342.9 eV correspond to Pd^{II} [27]. The $Pd^{II}/Pd°$ atomic ratios are reported in Table 12, the Pd° content increases adding more sodium borohydride, for the catalysts supported on titania this is more evident. Since the

catalysts analysed during the preparation are dried in oven at 110°C, the presence of PdO can be justified with the high affinity of Pd nanoparticles to partially oxidised.

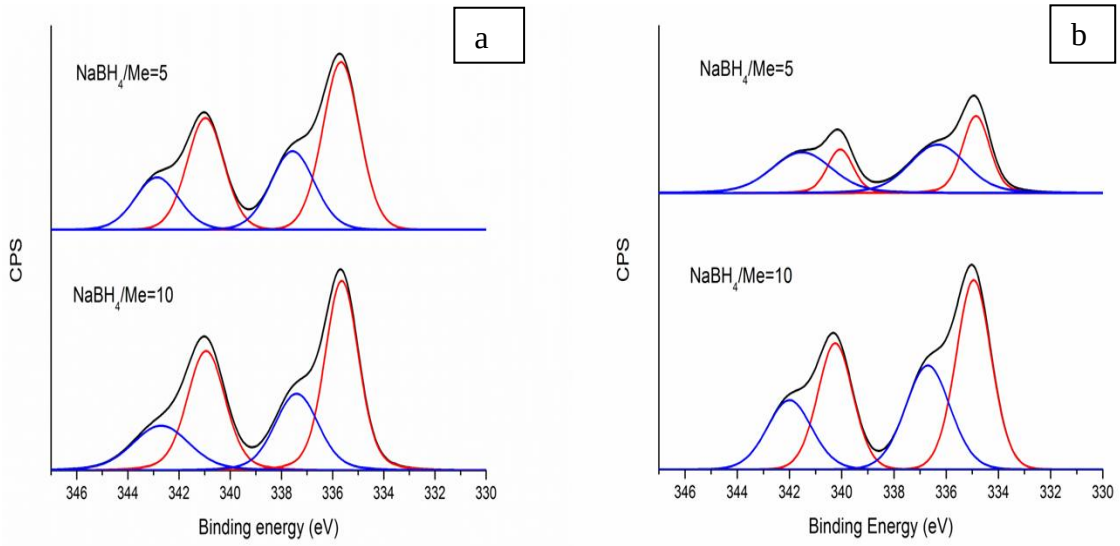

Fig. 43 XPS spectra: a) spectra for Pd/C-f and Pd/C-h; b) spectra for Pd/TiO_2-f and Pd/TiO_2-h

5.1.4 **Catalytic tests**

The prepared catalysts were tested in a probe reaction, the catalytic decomposition of formic acid to H_2 and CO_2 at mild reactions conditions. Indeed, formic acid has attracted attention as a liquid fuel for use in hydrogen fuel cells because it has high hydrogen content and it can be handled safely. FA decomposition can take place via two parallel pathways involving dehydrogenation (eq.15) or dehydration reactions (eq.16), which are linked by the water gas shift (WGS) reaction (eq.20). Nevertheless, in this preliminary screening work just formic acid conversion was monitored.

Dehydrogenation:

$$HCOOH \rightarrow H_2 + CO_2 \quad \Delta G = -48.4 \text{ kJ/mol} \quad \text{eq.15}$$

Dehydration:

$$HCOOH \rightarrow H_2O + CO \quad \Delta G = -28.5 \text{ kJ/mol} \quad \text{eq.16}$$

Water gas shift reaction:

$$H_2O + CO \leftrightarrow H_2 + CO_2 \quad \Delta H° = -41.1 \text{ kJ/mol} \quad \text{eq.20}$$

The reaction was performed in batch condition at 50°C.

Effect of Pd sol preparation (PVA/Pd ratio).

The catalyst are tested on formic acid decomposition (Fig.44). 10mL of 0.5M HCOOH was placed into the reactor, in batch conditions, with a stirring rate of 750rpm. The screening temperature used was 50°C. All reactions have been performed for 4h in a round bottom flask with a reflux condenser.

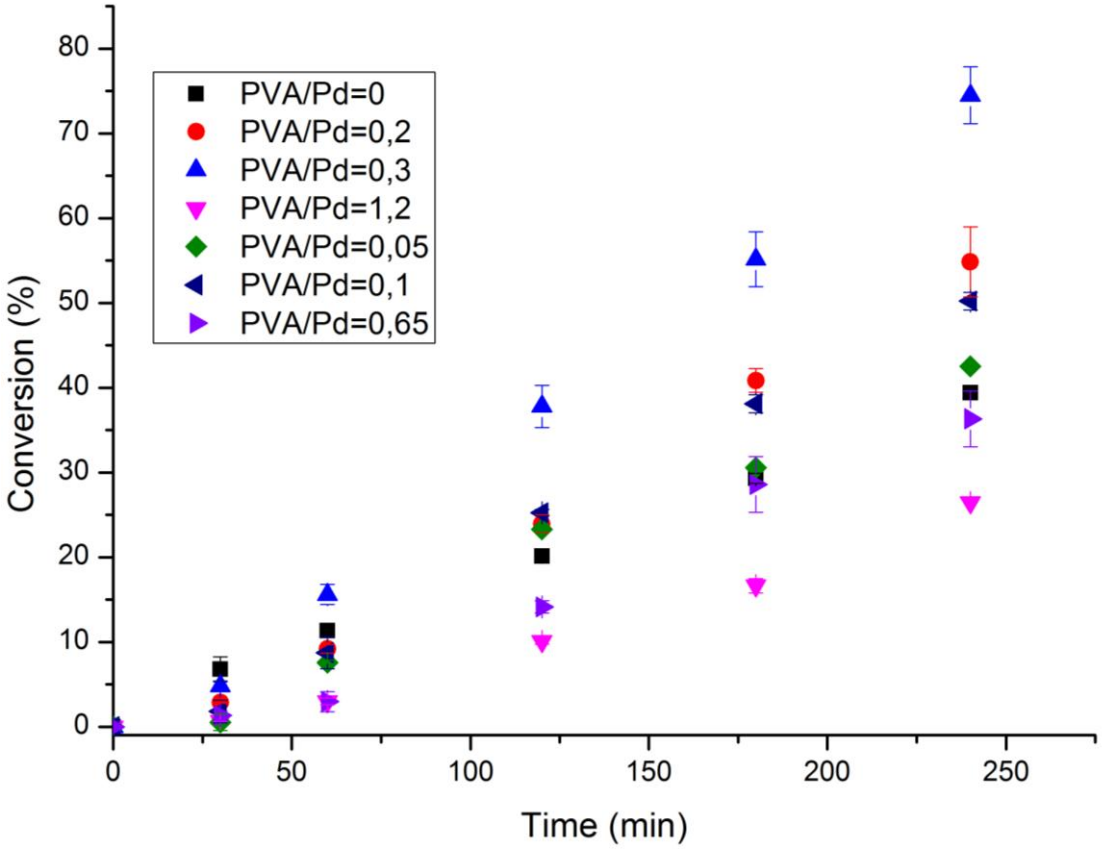

Fig. 44 Test on formic acid decomposition after 4h using different PVA/Pd ratio

The kinetics tests provide information on the catalytic performance of the catalysts and display different trends on the catalytic activity based on the PVA content used for Pd sol synthesis, the best catalytic performance was obtained with the catalyst Pd/C-e (PVA/Pd weight ratio =0.3) as showed in Fig.44 above. Besides plotting the conversion achieved with the different catalytic systems and the palladium surface content versus the PVA/Pd weight ratio it is possible to observe the typical vulcano trend (Fig.45). This graph highlights that the highest formic acid conversion corresponds to the largest Pd content on the surface (the values are reported in Table 12 and are evaluated by XPS analysis on the catalysts).

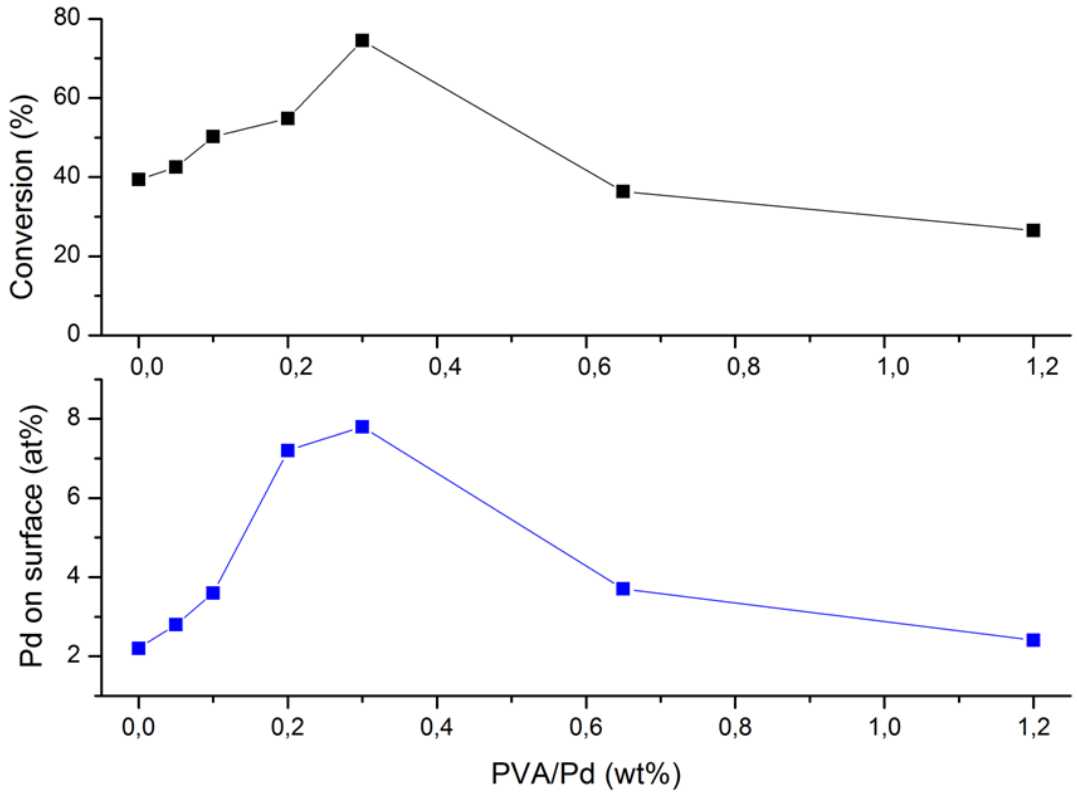

Fig. 45 Effect of Pd sol preparation in the catalytic decomposition of formic acid relative to conversion and Pd content on surface obtained by XPS analysis (as a function PVA/Pd weight ratio)

In order to explain the effect of PVA on the prepared sol it is reasonable to take account the mean Pd particle size and the PVA coverage too. Different TEM images reported in the previous paragraph show zones where the metal particles are small and well disperse, but in some area agglomerations appear. They are branched and probably they caused from the particles sintering.

Since the PVA is important for the controlling the growth and stabilisation of the particles and coverage of active sites, consequently it influences the activity of the catalyst: a larger presence of small nanoparticles enforces the catalytic potential. In this work the optimum distribution of particles size seems to be in a range of 4-5 nm. Small nanoparticles provide a higher surface area that can enhance the catalytic activity, because the fraction of low coordinated atoms grows by decreasing the particle size of Pd[72]. Although it is easy to understand that small nanoparticles are more catalytically active, it is harder to explain why smaller particles catalyses worst the formic acid decomposition. One hypothesis could be that the PVA forms a thicker layer around the particles, thus the availability of the active sites decrease and that when the PVA

content is too much the system could be destabilised. Besides there could be a geometric effect, thus the particles size can affect the binding of the substrate, as demonstrated in the CO oxidation[73].

Effect of Pd sol preparation (NaBH4/Pd molar ratio).

By increasing the $NaBH_4$/Pd molar ratio from 5 to 10, keeping constant PVA/Pd=0.65 weight ratio, the conversion increases for both supported catalysts on C and TiO_2, due to the following reasons: changes in the atomic ratio Pd^{II}/ Pd^0 (Fig.46) and mean particle size. Since that we observed in paragraph before, where DLS results are reported, verifying that there is not a big difference in the sol particles size, to explain these results we can refer to XPS analysis (Fig.43); while the sample immobilised on titania, the Pd^{II}/ Pd° atomic ratio decreases when increasing the amount of $NaBH_4$, explaining the increase of conversion, for carbon the decreasing of this ratio is less evident.

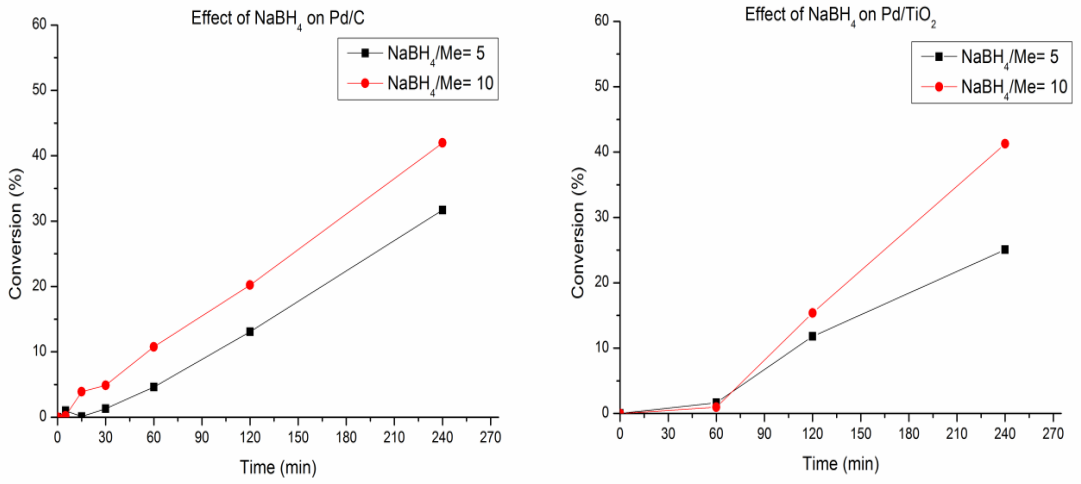

Fig. 46 Effect of Pd sol preparation in the catalytic decomposition of formic acid (as a function of $NaBH_4$/Pd molar ratio)

Pd metallic content (Table 12) seems to explain this variation in conversion since, when increasing the $NaBH_4$/Pd molar ratio, for both on Pd/carbon and Pd/titania catalysts the metal surface was found to be more reduced.

Effect of support (carbon or TiO_2)

The support can have a big influence in the catalytic activity, due to metal-support interaction. Two different supports were used in this work: carbon and titania. The supports were characterised by SEM (Fig.47), and the surface area analysed with BET theory.

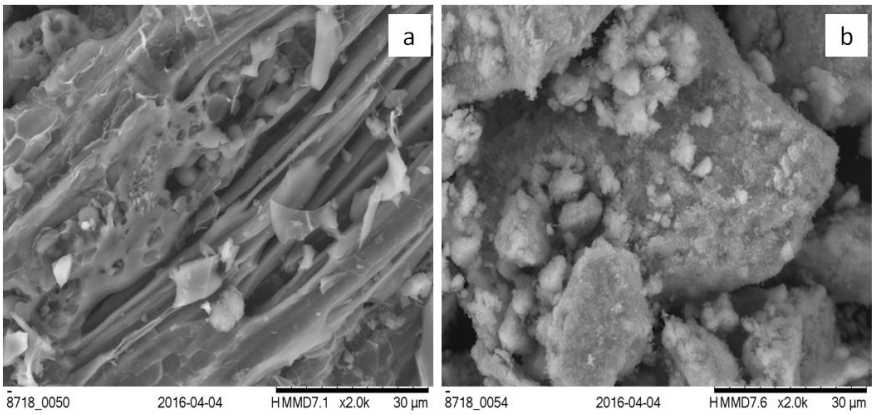

Fig. 47 a) SEM on carbon; b)SEM on titania

In the Table 13 below are showed the BET values:

Table 13 Surface area analysis on the supports

Support	Surface Area (m^2/g)
Carbon	64
Titania-P25	63

Titania P-25 is made of 18% anatase and 82% rutile, the value reported in the literature are around 55 m^2/g[74,75]. The data obtained is acceptable, considering the error range of the instrument. The two supports show a similar surface area. When metal nanoparticles are supported on carbon it shows a better performance in the formic acid decomposition (Fig.48). The supported catalysts compared arise from the sol Pd-f. Based on TEM images it is possible to observe that the particles are more spherical onto carbon than TiO_2, in fact typically particles on TiO_2 are hemispherical due to wetting effect of the metal nanoparticle onto metal oxide. Therefore the active surface area will be less influencing the catalytic activity negatively.

Besides the role of the support results fundamental to stabilise the particles, according to this the unsupported catalyst was tested on the reaction and after 2h the sol was found to collapse on the magnetic stirrer.

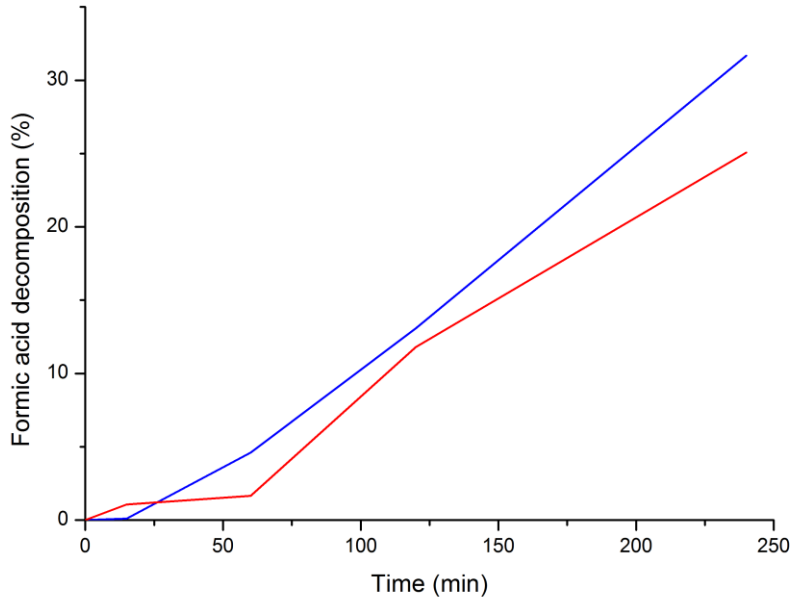

Fig. 48 Effect of the support on formic acid decomposition: - the red line represents the FA conversion obtained with Pd-TiO_2-f; - the blue line represents the FA conversion obtained with Pd-C-f

5.1.5 **Effect of Pd loading on Pd/C catalysts**

In order to study the effect of Pd loading on the reaction, we have prepared five catalysts with different content of palladium (from 0.2 to 1.2) that were tested keeping constant the substrate/metal molar ratio around 2000. The characterisation data of the prepared samples are reported in Table 14. The theoretical amount of active metal for the different catalysts was confirmed experimentally by EDX analyses.

Table 14 Surface area and EDX analysis

Loading Pd/C	Surface Area m^2/g	EDX
0.2wt%-Pd/C-e	71	0.2
0.5wt%-Pd/C-e	60	0.48
0.7wt%-Pd/C-e	71	0.68
1wt%-Pd/C-e	50	1
1.2wt%-Pd/C-e	35	1.25

The conversion of formic acid does not show any large fluctuation at low loading. For a Pd loading of 1 wt.%, the catalytic activity presents a peak, before decreasing again at 1.2 wt% (Fig.49).

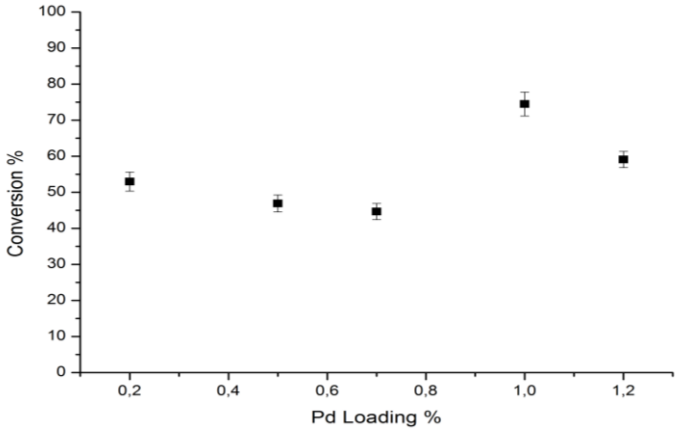

Fig. 49 Trend of formic acid conversion after 4h with different loading of Pd

After 4 hours, the higher TOF is reached for the Pd loading of 1wt. %. The values are reported in Table 15:

Table 15 TOF calculated for the mole of substrate obtained

Loading	TOF (h^{-1})
0.2	278
0.5	272
0.7	239
1	366
1.2	326

This effect might be attributed to the dispersion of the catalyst on the support. The Fig.50 shows some frames obtained from EDX mapping of the catalysts.

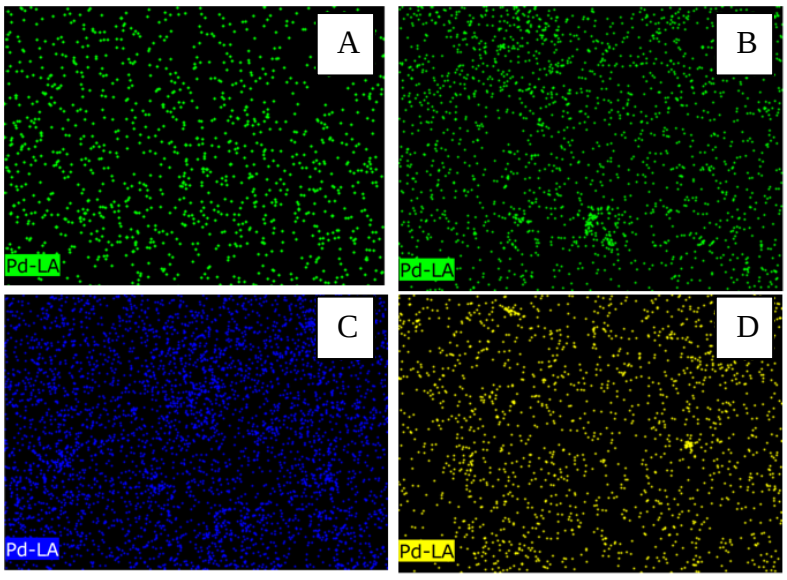

Fig. 50 EDX mapping: A) loading 0.2wt%;B) loading 0.7wt%; C) loading 1wt%; D) loading1.2wt%

It is evident from the images that the best dispersion is achieved in the sample with 1% of loading.

The nanoparticles dimension of three representative samples are calculated from TEM analysis. The catalysts chosen are those with the lowest and highest loading, and the one with 1wt. % of Pd. A summary of the average diameters are recorded in Table 16.

In the previous paragraph is reported the TEM characterisation for 1wt%-Pd/C-e (Fig.31).

Table 16 Average diameters of Pd NPs estimated from TEM analysis

Sample	d-TEM (nm)
0.2wt%-Pd/C-e	3.9±2.3
1wt%-Pd/C-e	4.8±2
1.2wt%-Pd/C-e	3.8±1.1

The catalyst with the smallest loading (Fig.51) is characterised by small nanoparticles among 2-6 nm, although some larger particles are presented. The histogram of the diameter distribution is reported in Fig.52.

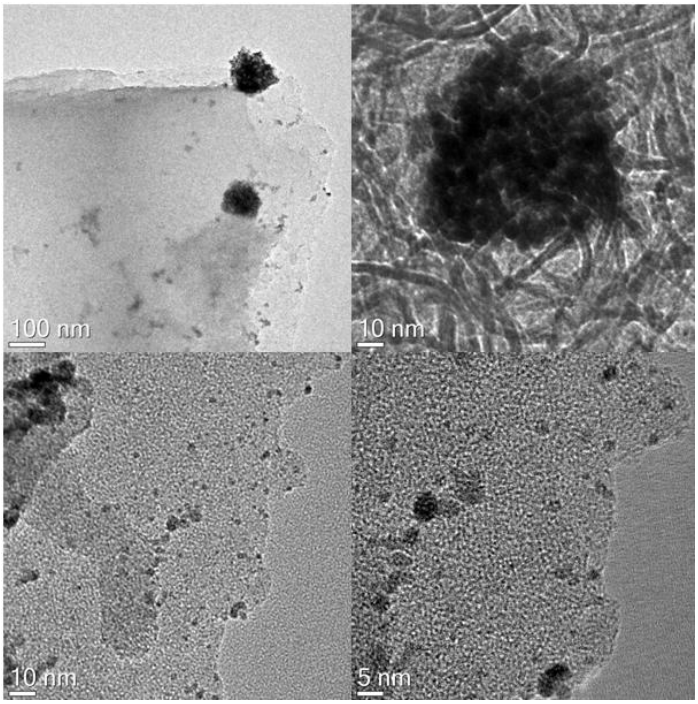

Fig. 51 TEM of 0.2wt%-Pd/C-e

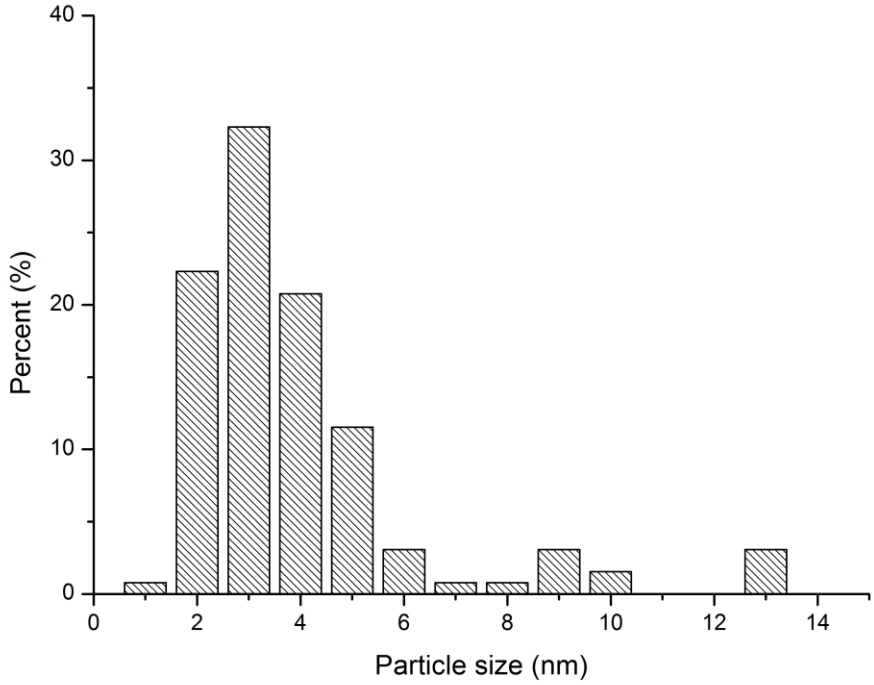

Fig. 52 Particles size distribution 0.2wt%-Pd/C-e

The sample with the higher content of palladium (Fig.53) is characterised by a narrower particles size distribution showed in the histogram below(Fig.54), but the presence of big agglomerations that could explain its lower activity compared to the 1wt%-Pd-e.

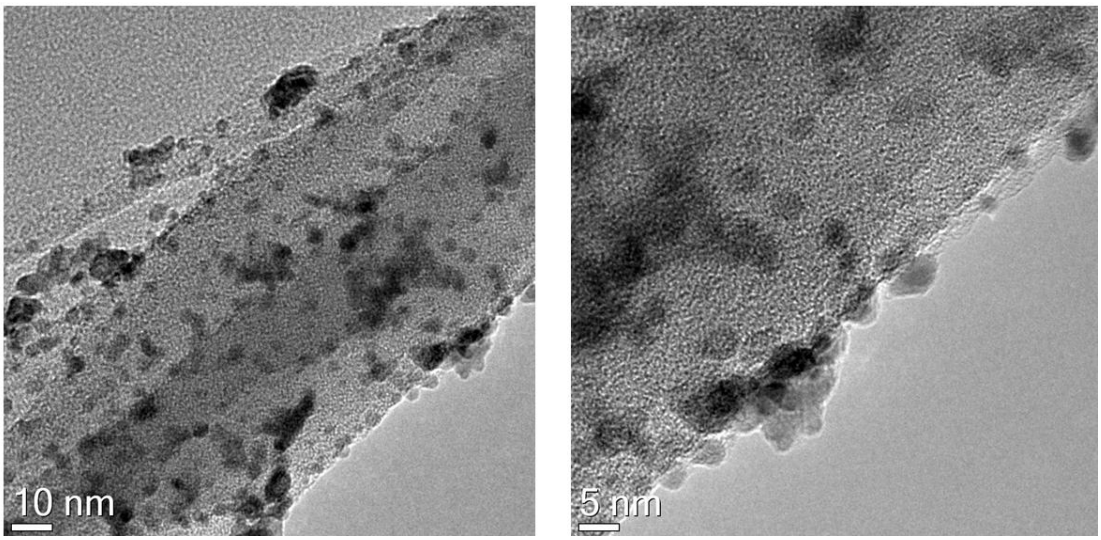

Fig. 53 TEM images of 1.2wt%Pd/C-e

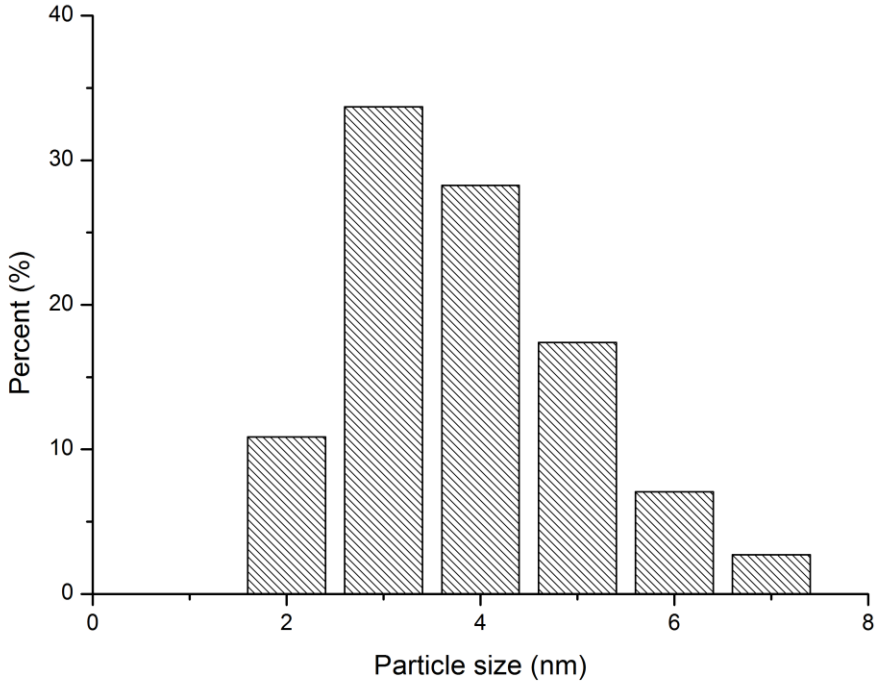

Fig. 54 Particles size distribution 1.2wt%-Pd/C-e

Although there is not a large difference in the particles size changing the loading we can explain that the catalytic activity increases from 0.2 to 1 wt%, because at the higher loading the Pd particles are slightly bigger and the interparticle distance on the support is lower, this gives a higher probability of substrate/metal interaction by dehydrogenation on these particles[76]. According to this from XPS analysis it was evidenced a similar percentage of Pd^0 (around 39%) in the different sample, but a big difference in the amount of palladium on the surface (Table 17) and the value for 1wt%-Pd/C-e was 7.9 at%.

Table 17 Characterisation of the Pd content of the catalysts surface by XPS analysis

Loading Pd/C	%Pd^0	Pd^{II}/Pd^0	At% Pd
0.2-Pd/C-e	43	1.4	1.9
0.5-Pd/C-e	35	1.9	4.6
0.7-Pd/C-e	36	1.8	4.8
1-Pd/C-e	39	1.6	7.9
1.2-Pd/C-e	39	1.6	6.9

To clarify definitively how the loading affected the model reaction would be interesting continuing the studies on the topic using DRIFT analysis to know how HCOOH interact with the palladium surface.

5.1.6 Pd/C catalyst stability and reusability

A thorough study was carried out by using the Pd-e sol prepared with PVA/Pd weight ratio of 0.3 and $NaBH_4$/Pd molar ratio of 5, because the Pd/C-e catalyst synthesized with this sol showed the best catalytic performance for the formic acid decomposition. After the characterisation, with the techniques described in the previous chapter we focused to understand better the following parameters: the mechanism of the reaction, the gas volume produced during the process and the reusability. Finally a comparison with a commercial catalyst Pd/C 5wt% from Sigma Aldrich was carried out.

Reusability tests and characterisation of the used catalyst

A reusability test was carried out by filtrating the catalyst at ambient temperature and atmospheric pressure without further washing and using it for a new reaction under the same reaction conditions. The recycle tests were 5. The graph (Fig.55) shows the results of this study.

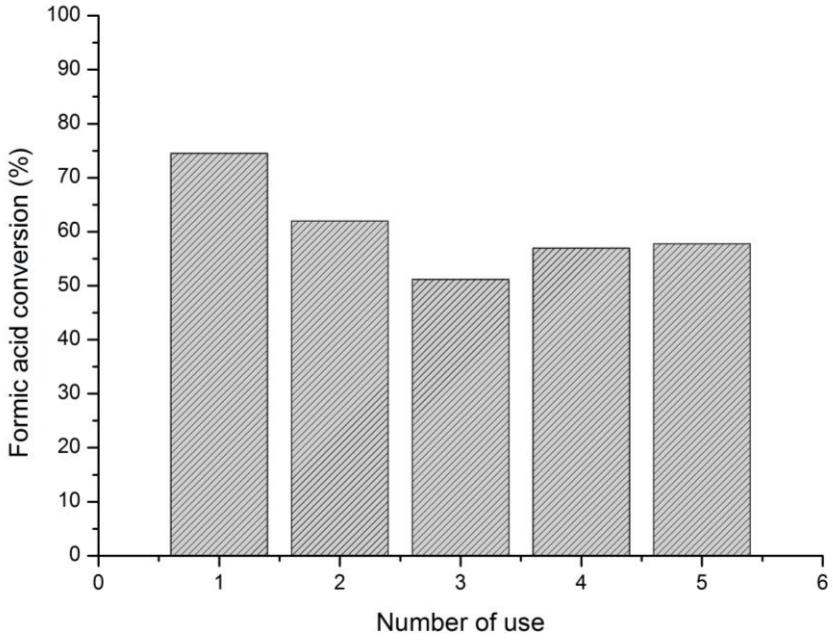

Fig. 55 Kinetic test for the recycle of the catalyst Pd/C-e

Initially the catalyst loses activity. The conversion passes from 74% to 51% at the third run. After the third cycle a stabilisation appears to be happened and the analysis revealed that the Pd/C catalyst preserved 69% of its activity in its fifth use. This kind of trend could have different explanation:

1) a prior deactivation could come from the sintering of the nanoparticles during the first run due to screening temperature used of 50°C[77] ;

2) initially during the reaction some leaching could affect the activity of the catalyst and the activity drops down, other studies as ICP-AES method should be available to confirm this hypothesis;

3) some sites active could adsorb poisonous species in the first recycles, but the activity of Pd/C could be partially recovered by washing and drying, because of the desorption of poisonous species such as CO from the surface[27].

To answer to these questions, characterisation of the catalyst was carried out. The morphology of the fresh and the reused catalysts was characterised by TEM as shown in Fig.56 and Fig.57. From the fresh to the first used there isn't a significant change of the Pd nanocatalysts dimension, in the fresh the particles size was 4.8±2 nm, in the catalyst after the first use the particle size becomes 5.1±2.2 nm, nevertheless there are more areas where the particles are sintered. This affords the first hypotheses.

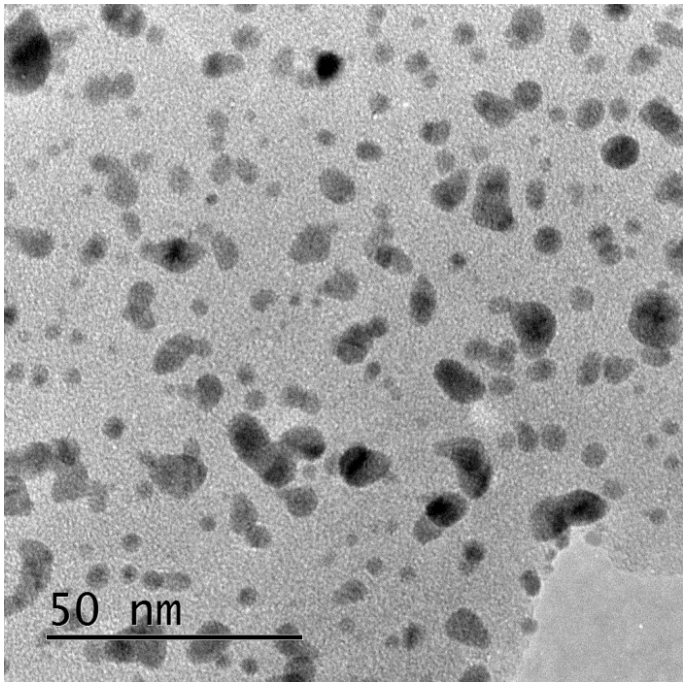

Fig. 56 TEM for the fresh catalyst

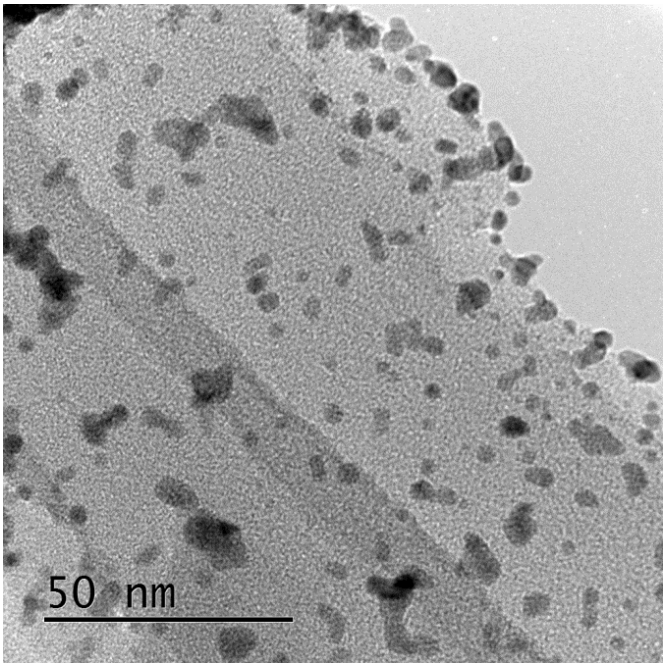

Fig. 57 TEM for the spent catalyst after two uses

The characterisation was made also on the catalyst after five runs: the catalyst was investigated by TEM and XPS.

In Fig. 58 is reported the XPS spectra of Pd3d shows two pairs of peaks: the one at 335.4 eV and 341 eV corresponding to $Pd3d_{5/2}$ and $Pd3d_{3/2}$, respectively were attribute to Pd° whereas those at 337.4 eV and 342.7 eV associated with Pd^{II} in palladium oxide[27].

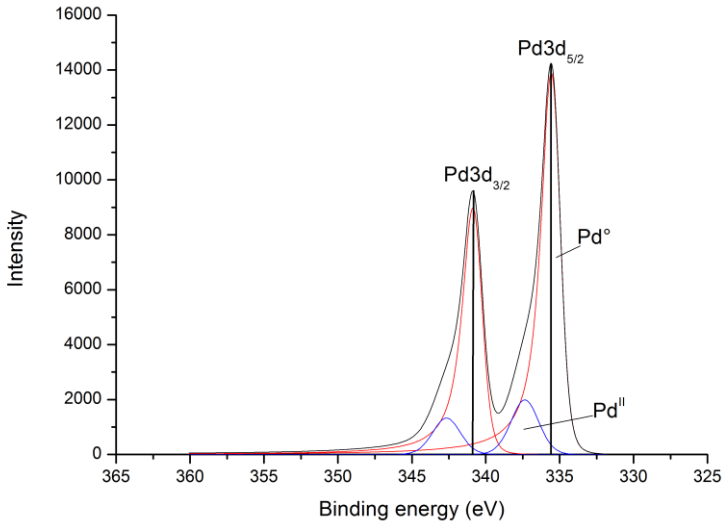

Fig. 58 XPS spectra for the catalyst after the fifth run

The $Pd^{II}/Pd°$ atomic ratio is higher for the newly Pd-e than for the renewed Pd/C catalyst, as reported in Table 18.

Table 18 $Pd^{II}/Pd°$ ratio obtained from XPS

Catalyst	Pd° (%)	$Pd^{II}/Pd°$
Pd-e new	39	1.59
Pd-e (fifth recycle)	88	0.13

The reduction of $Pd^{II}/Pd°$ ratio can be attributed to the ability of formic acid to reduce PdO due to the formation of H_2.

Representative images of the spent catalyst after five runs are reported below in Fig.59 with the analysis of the NPs size distribution in the histogram of Fig.60. The mean particle size of the fresh catalyst was 4.8nm, in the catalyst after 5 run, the dimensions of the metal molecules are increased and the distribution is spread: 50% of the particles are in range among 6nm and 11nm. Sintering phenomena is visible in the snapshots, in particular in the frame scaled at 20nm.

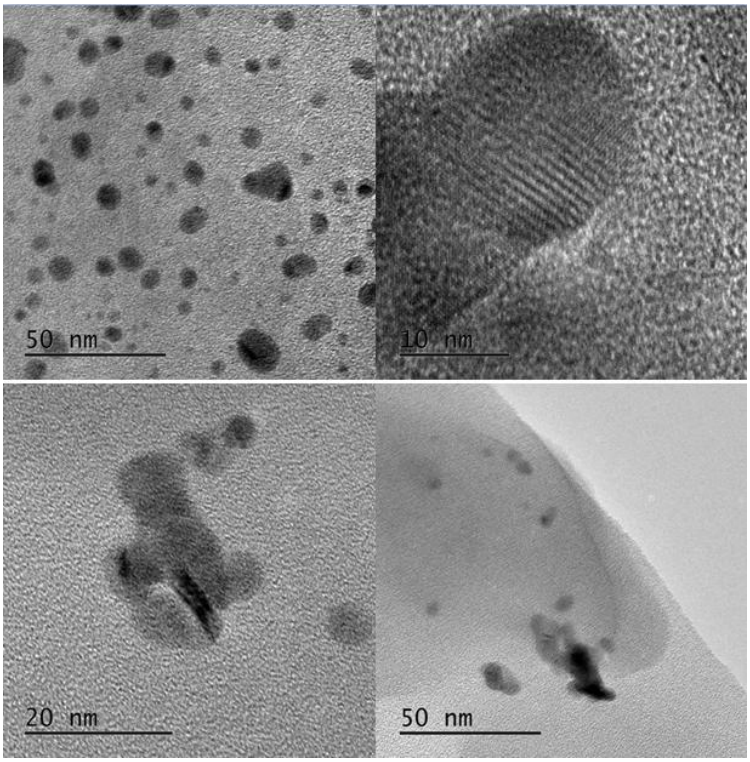

Fig. 59 TEM for the catalyst after the fifth run

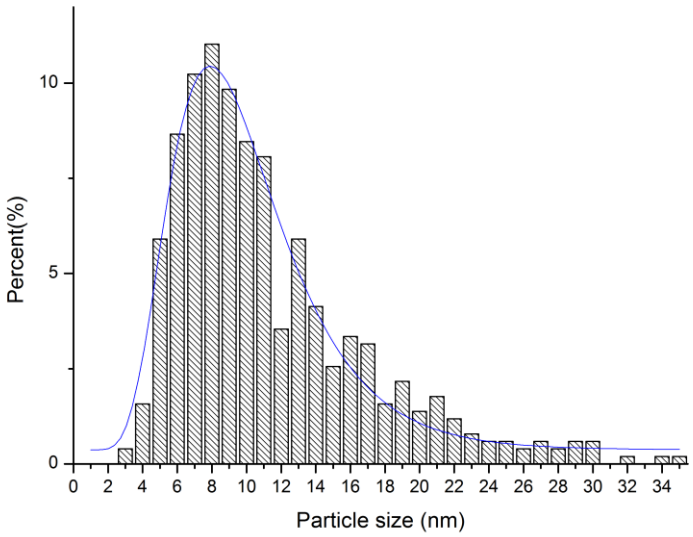

Fig. 60Particles size distribution for the catalyst after the fifth run

To figure out if formic acid is poisoning the catalyst, during the reaction a known concentration of formic acid was added and it was found that there isn't a significant deactivation of the catalyst which means that the behaviour of the catalyst is caused by other parameters (Fig.61).

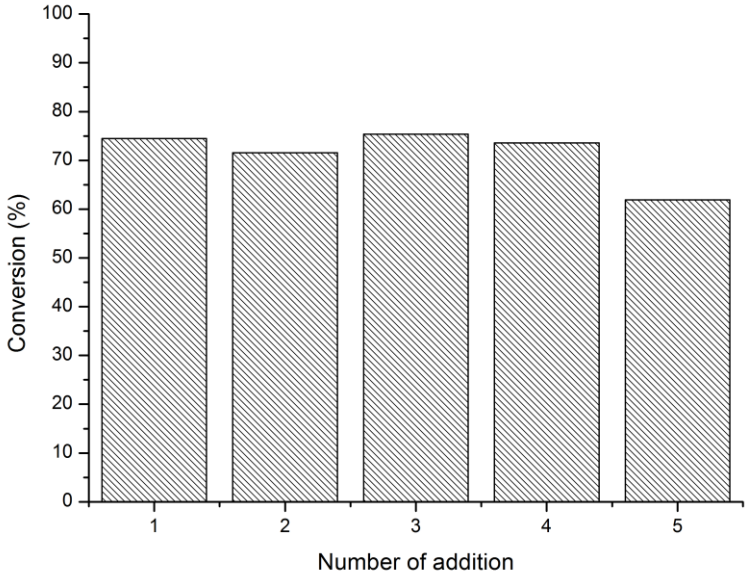

Fig. 61 Formic acid conversion obtained adding on line a known fresh amount of HCOOH into the reactor

Since the activity of the spent catalyst can be partially recovered by washing and drying, the most possible reasons of the loss of activity could be due to the sintering.

5.1.7 **Insight into the reaction mechanism**

The mechanism of the reaction was studied using the KIE (Kinetic Isotope Effect) theory[78]. The experiments were carried out using HCOOD, DCOOH and DCOOD. The performed reactions were conducted using the usual conditions: 10mL of 0.5M formic acid was placed into the reactor, in batch conditions, with a stirring rate of 750rpm at 50°C. All reactions have been performed for 4h in a round bottom flask with a reflux condenser, keeping a substrate molar ratio around 2000. Since it is assumed that the formic acid decomposition has a zero order reaction[2], which means that there are steps involving intermediates present at saturation coverage, the possible pathways are:

- H-C bond dissociation: it is kinetically relevant when the KIE values for HCOOD is close to unity but larger value for DCOOH;
- O-H bond dissociation: in case of KIE values close to 1 for DCOOH but nor for HCOOD;
- H_2 recombination and desorption in case of KIE values of approximately 1 for both HCOOD and DCOOH[78].

As shown in Table 19, HCOOD gave the closest KIE values to unity while, both DCOOH and DCOOD present larger values.

Table 19 KIE factor

Substrate	r_H/r_D
HCOOD	1.2
DCOOH	2.9
DCOOD	5.7

These results show that the reaction is kinetically limited by HCOOH dissociation. As presented in Mechanism 1, this is the most probable pathway for the formic acid decomposition.

Mechanism 1

$$HCOOH \leftrightarrow HCOO^* + H^* \qquad \text{(eq. 21)}$$

$$HCOO^* \rightarrow CO_2 + H^* \qquad \text{(eq. 22)}$$

$$H^* + H^* \rightarrow H_2 \qquad \text{(eq.23)}$$

The mechanism comprises formation of formates (eq. 21) which decompose to CO_2 and H_2 (eq.22, eq.23), for the cleavage of the bond C-H/D. The free H-atoms adsorbed after the O-H dissociation recombines with the H-atoms formed after the formate decomposition[29].

5.1.8 **Products of reaction**

The gas volume evolved from HCOOH solution containing the Pd/C is shown in Fig.62. To collect enough amount of gas 20 mL of HCOOH 2M are placed in round bottom flask at 50°C with Pd/C-e always keeping a substrate metal molar ratio around 2000.

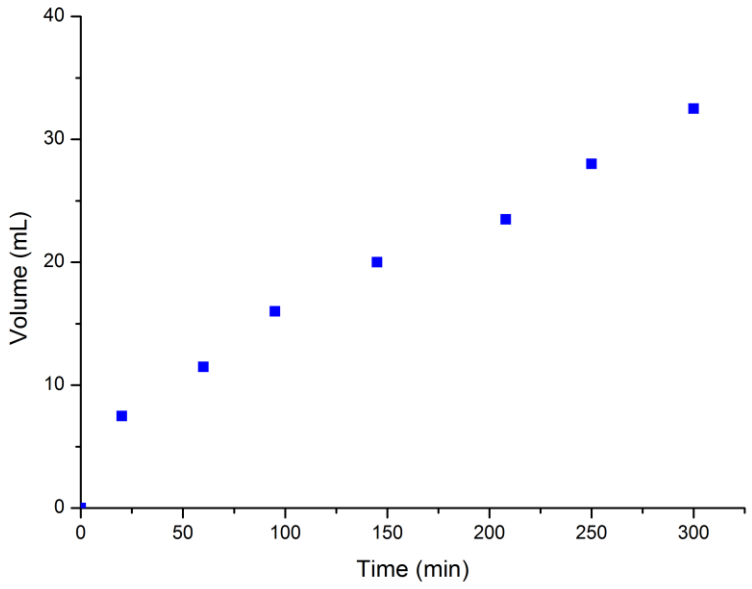

Fig.62 Gas volume evolution from HCOOH aqueous solution after 5h

After 4h 28 mL of gas was collected, theoretically this corresponds to 10^{-3} mol of gas, which an half should be of hydrogen and one of CO_2, if there aren't other byproducts. Further investigation into the products evolved should be done to clarify the selectivity of the reaction.

5.1.9 Comparison between home-made Pd/C catalyst and Sigma Aldrich commercial sample

The commercial catalyst Pd/C 5wt.%, by Sigma Aldrich was found to have really good catalytic performance towards the reaction. Complete conversion in 2 hours at 30°C cab be achieved with this catalyst. Instead, Pd-e need 6 hours to obtain similar conversion levels at 50°C. Therefore, the commercial one was used as a model to compare the activity of the prepared catalysts in formic acid decomposition. Pd/C 5w%t. was studied by many techniques, after testing it on the reaction.

Characterisation of commercial catalyst

X-ray diffraction pattern of the fresh catalyst is displayed in Fig.63. It shows the characteristic diffraction peaks of Pd at 2θ values 40.1º, 46.7º and 68.1º corresponding to the (111), (200) and (220) characteristic planes of face-centered cubic structure of Pd. From the full width half maximum of the peaks, using Scherer equation, the particles size is calculated, from the diffraction peak of the Pd (111), which was found to be 9.8 nm. The broad diffraction peak between 20º and 30º is related to the carbon support, in particular, the peak at 2θ of 26.6º was the peak of the (002) facet of the activated carbon[25,79,77]. This result shows that, when exposed to air, the palladium particles spontaneously oxidises. In Fig.63 the XPS spectra of the Pd3d was analysed.

The ratio Pd^{II} /Pd° was 0.92.

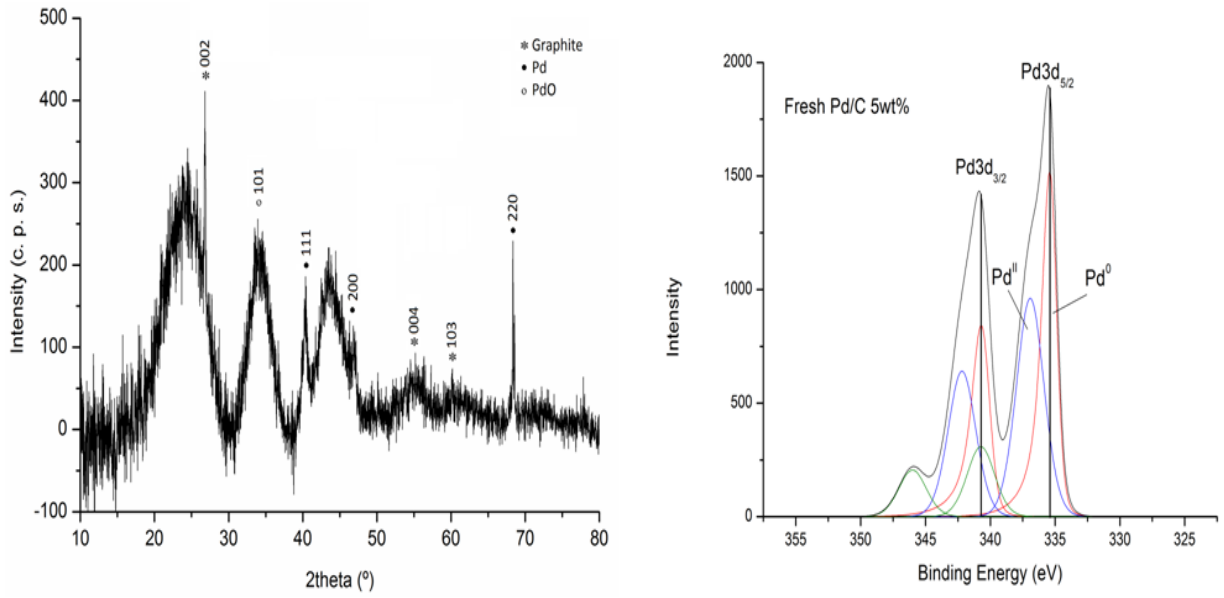

Fig. 63 X-ray diffraction pattern and XPS spectra of the fresh catalyst

The particle size and morphology was also examined by TEM. The measurement of the particles size distribution (Fig.64) indicated that more than 75% of the particle size was in the range of 3-4 nm.

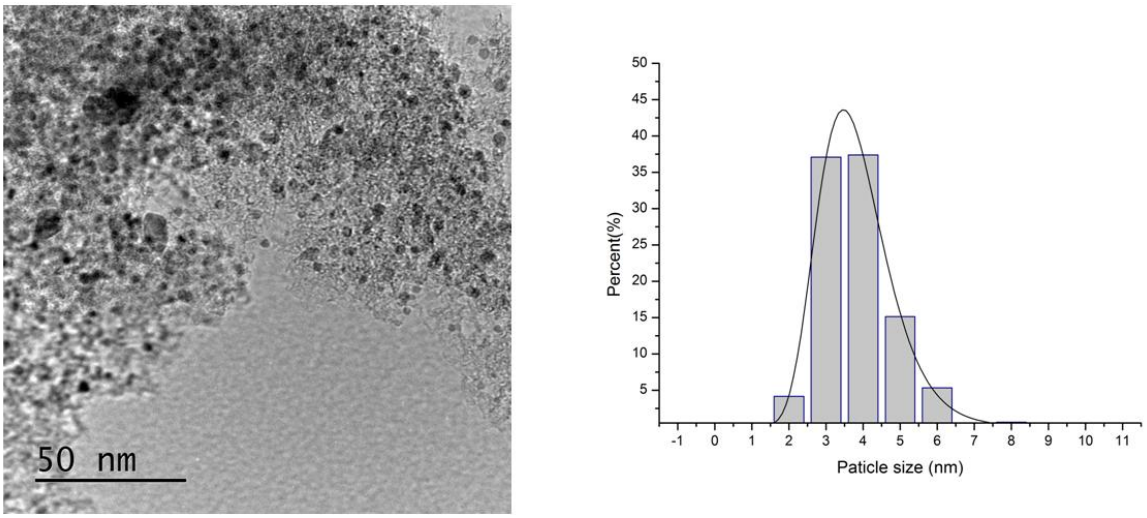

Fig. 64TEM picture of the commercial catalyst and his particles size distribution

The composition of these particles consisted of Pd, as evidence by the corresponding SEM-EDX analysis focusing on the particles. It confirmed the existence of Pd being approximately 5.2 the percentage of Pd, Fig.65 .

The surface area (by BET theory) of the Pd/C catalyst obtained was 934 m^2/g.

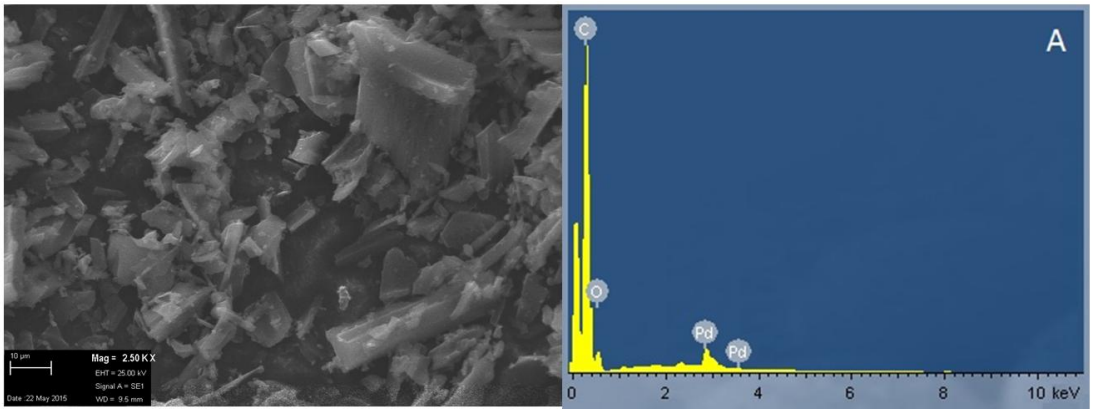

Fig. 65 SEM-EDX analysis for 5wt% Pd/C

There are many differences between the commercial catalyst and the homemade one such as: the average diameter of the particles is smaller, the surface area is larger and also the initial Pd° content varies. It is noteworthy that the physical and chemical

properties influence the activity of a catalyst, so it is expected that the commercial sample shows a different performance towards the reaction.

Comparison of catalytic activity

Both the catalyst are tested on formic acid decomposition using the usual conditions: 10mL of 0.5M HCOOH was placed into the reactor, in batch conditions, with a stirring rate of 750rpm. The screening temperature used was 30°C. All reactions have been performed for 2h in a round bottom flask with a reflux condenser.

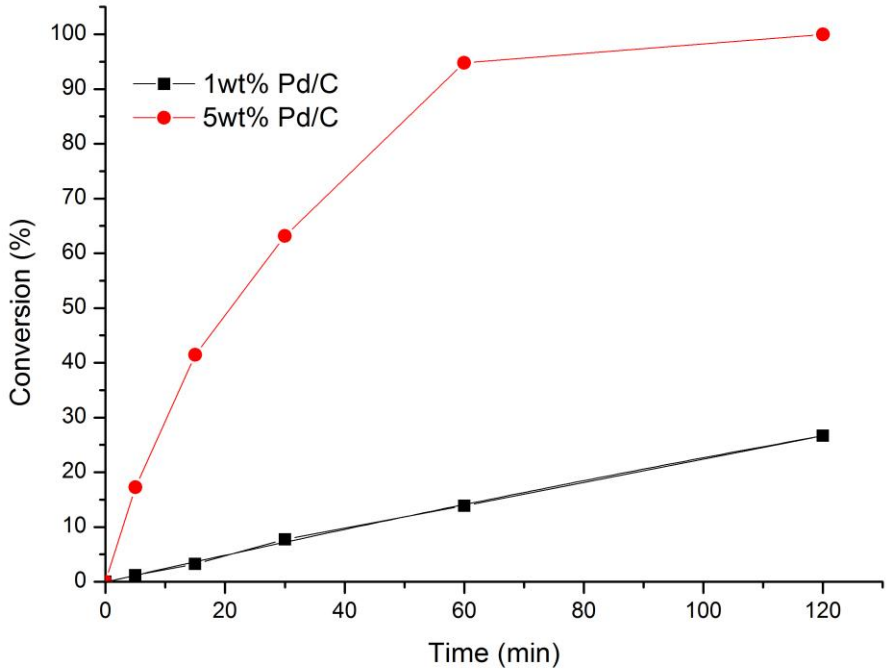

Fig. 66 Comparison between home-made Pd-e sample and commercial sample (5wt% Pd/C) in the FA decomposition. Reaction temperature 30°C.

The results obtained show a large difference in terms of activity (Fig.66). This can be associated to many factors:

- Particle size distribution is narrower in the commercial catalyst and the mean value of the nanoparticles size is 3.8nm smaller than the metal particles of the homemade catalyst (4.8nm). In the prepared one there are small particles size mixed with some larger, maybe caused by aggregation phenomena. Since the active sites are generated from small

nanoparticles as the literature recorded[31,32,72], a narrow distribution could enhance catalytic activity.

- The interaction between metal and support can not be ignored. On the surface of the commercial catalyst it is evidenced an atomic percentage of palladium of 1.6%, whose the palladium in the zero oxidation state was the 52% and on the surface of the homemade catalyst is resulted a content of 7.9%, whose the 39% of Pd^0 by XPS analysis previous reported. However the BET analysis show a large difference in the area value of the catalyst, due to the different supports used. They are both carbon, but the activated carbon provides a surface area larger than a non activated one, thus it facilitates a higher dispersion of the metal improving the catalytic performance.

A remarkable difference appears in the recycle of the catalyst too.

The commercial catalyst loses activity during the recycle (Fig.67). The recycles are made drying and washing the catalyst every cycle, as before. Analysis revealed that the 5wt% Pd/C catalyst preserved 72% of its activity in its fifth use.

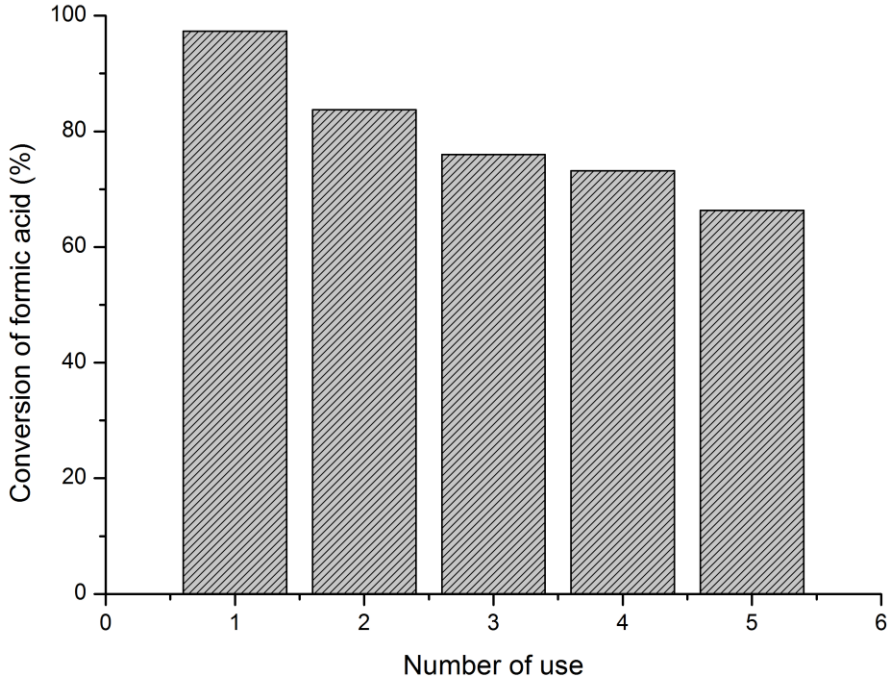

Fig. 67 Kinetic test for the recycle of the catalyst

From XPS analysis is evident, such as for the catalyst 1wt% Pd/C,that the $Pd^{II}/Pd°$ atomic ratio decreases from 0.92 to 0.18, this can be related to reduction by the formic acid, (Fig.68).

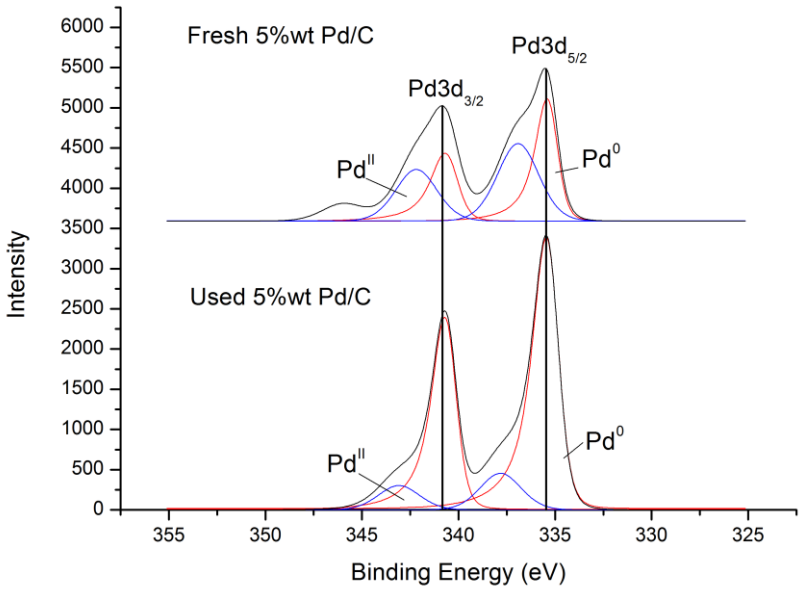

Fig. 68 XPS spectra for the fresh and the used commercial catalyst

The TEM analysis display the sintering phenomena on the surface, which can help to explain the deactivation of the catalyst. Fig.69 shows the palladium NPs.

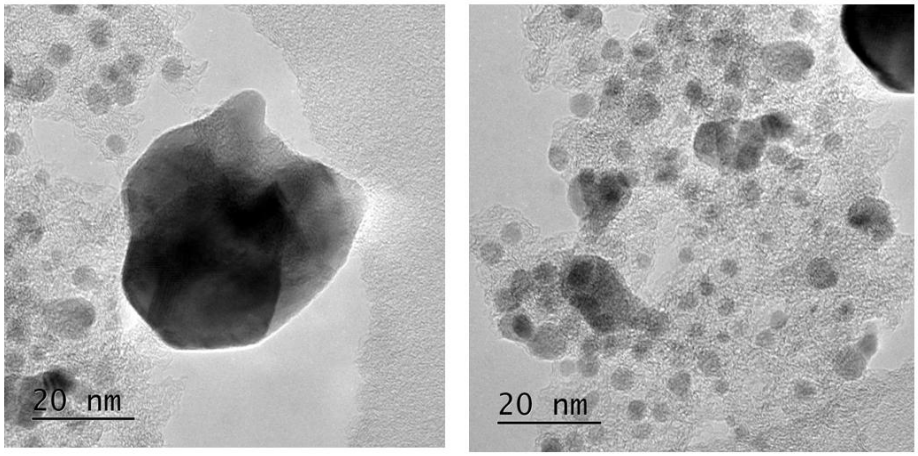

Fig. 69 TEM on the used commercial catalyst

5.2 Catalytic performance of Au_xPd_y/TiO2 for formic acid decomposition

A comparison between the catalytic activity of monometallic Pd, Au, and bimetallic Au_xPd_y has been studied. These catalysts had different affinity towards the formic acid decomposition. The palladium nanocatalyst had the best performance. All the catalysts were prepared using the synthesis procedure optimised for the palladium sol. The support used was titania, instead of carbon.

5.2.1 Synthesis of bimetallic catalyst

Catalyst with different molar ratio of Au:Pd were prepared. They are recorded in Table 20.

Table 20 Composition of monometallic and bimetallic suspensions

Sample	%mol [Pd^{2+}]	%mol [Au^{3+}]	PVA/M weight ratio	$NaBH_4$/M molar ratio
Pd-i	100	-	0.3	10
Au_1Pd_3	75	25	0.3	10
Au_1Pd_1	50	50	0.3	10
Au_3Pd_1	25	75	0.3	10
Au	-	100	0.3	10

The catalysts were made by sol-immobilisation technique by co-reducing the two metal precursors. When $NaBH_4$ is added to the solution there is a change in the colour of the solution: the solutions of palladium and Au_xPd_y (where x and y refer to the Au:Pd molar ratio in the material) assume the typical dark-brown sol, whereas the gold sol becomes red. After the immobilisation on titania for 1h, the slurries were washed with distilled water, filtered and dried for 16h at 110°C. The solutions after filtering were always colourless. For bimetallic sol, the preparation consists in the simultaneous reduction of $PdCl_4^{2-}$ and $AuCl_4^-$. It is noteworthy that this brings to the alloy formation for certain Au_xPd_y molar ratio.[53]

5.2.2 Characterisation of (Au_xPd_y)/ TiO_2 catalysts

Characterisation of the sol

DLS analysis

The colloid suspension of monometallic and bimetallic catalysts were characterised by DLS technique to know the hydrodynamic diameter. Besides it is useful to measure the PDI, that permits to understand how much the value is far from the average value, i.e. how much the suspension is homogeneous. In Table 21 are reported the average diameters based on intensity and volume with the relatively percent peaks and the PDI.

Table 21 Hydrodynamic diameter and PDI evaluated by DLS analysis

Suspension	Intensity $d_{average}$ (nm)	Volume $d_{average}$ (nm)	PDI
Pd-i	16(27.9%); 64 (10.9%); 246 (61.2%)	15 (97.9%); 66 (0.6%); 359 (1.5%)	0.98
Au_1Pd_3	10 (12.1%); 145 (86.4%); 5285 (1%)	6 (99.3%); 80 (0.1%); 186 (0.2%)	0.54
Au_1Pd_1	189 (94.6%); 9 (5.4%)	8 (98.8%); 224 (2.2%)	0.42
Au_3Pd_1	12(88%);761(12%)	9 (99.9%); 889 (0.1%)	0.27
Au	6 (40.2%); 63 (59.8%)	6	1

In Fig.70 there are DLS profiles of the sample based on volume distribution. The curves appear monomodal and similar among them. This enforces that also for the bimetallic system the aggregates can be ignored, because they have a scant presence.

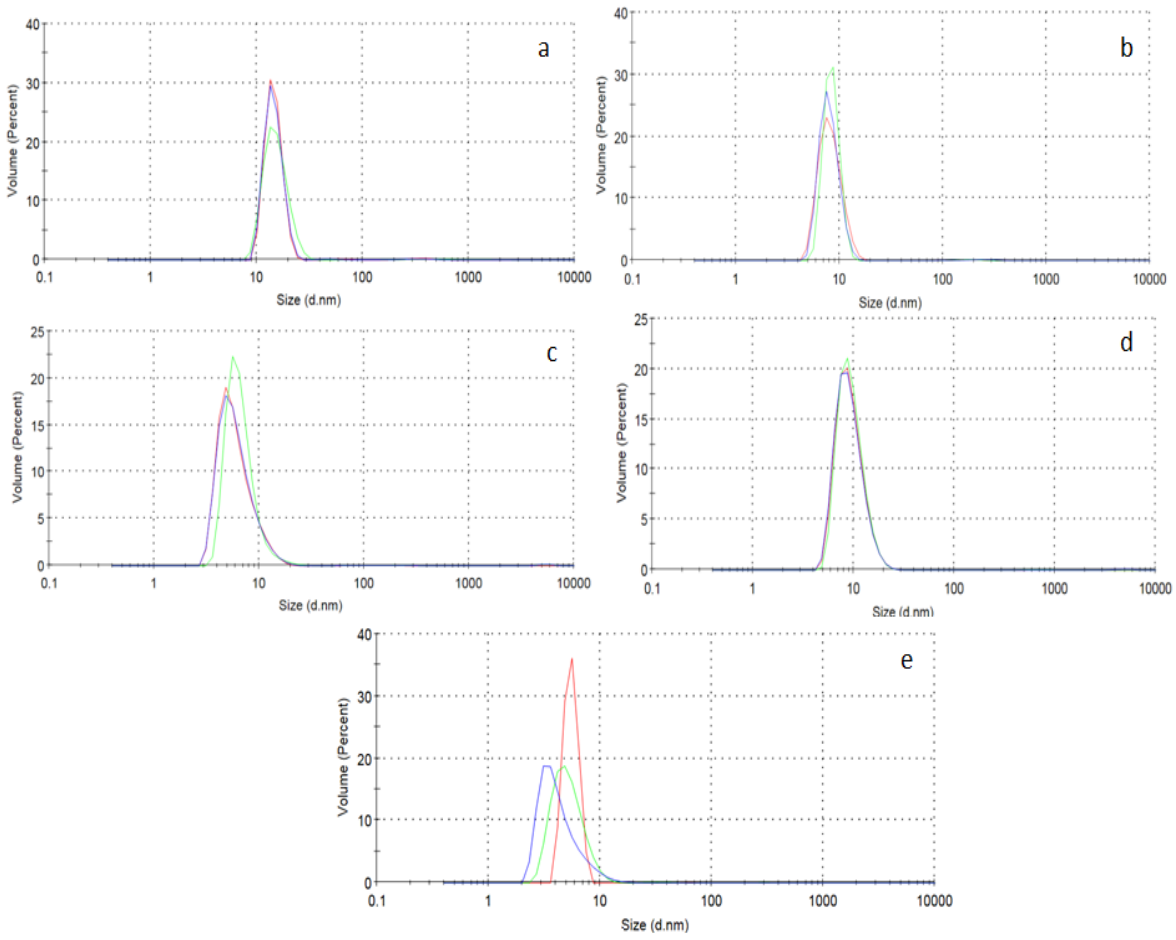

Fig. 70 DLS profiles for the catalyst a)Pd colloid; b) Au_1Pd_3; c) Au_1Pd_1 colloid; d) Au_3Pd_1 colloid; e)Au colloid

UV-visible spectroscopy analyses

UV-vis spectra (200-900 nm) of the monometallic and bimetallic catalysts were recorded in H_2O. This technique allows to follow the reductions of the metals. For monometallic sol different behaviours can be observed, in the case of Au sol, Fig.71a the plasmon resonance band is placed at 505nm[61]. When the $AuCl_4^-$ anion becomes Au^0 the peaks at λ_{max}= 220nm disappears and the plasmon resonance peak appear. The peak at value less than 517nm means that the particles size is lower than 9nm[80] confirming the measures of the DLS. In case of Pd, Fig.71b, the peak of the metal precursor at 235nm[24] disappears after the reduction. Pd^0 sols don't have a plasmon band, as reported in literature[81].

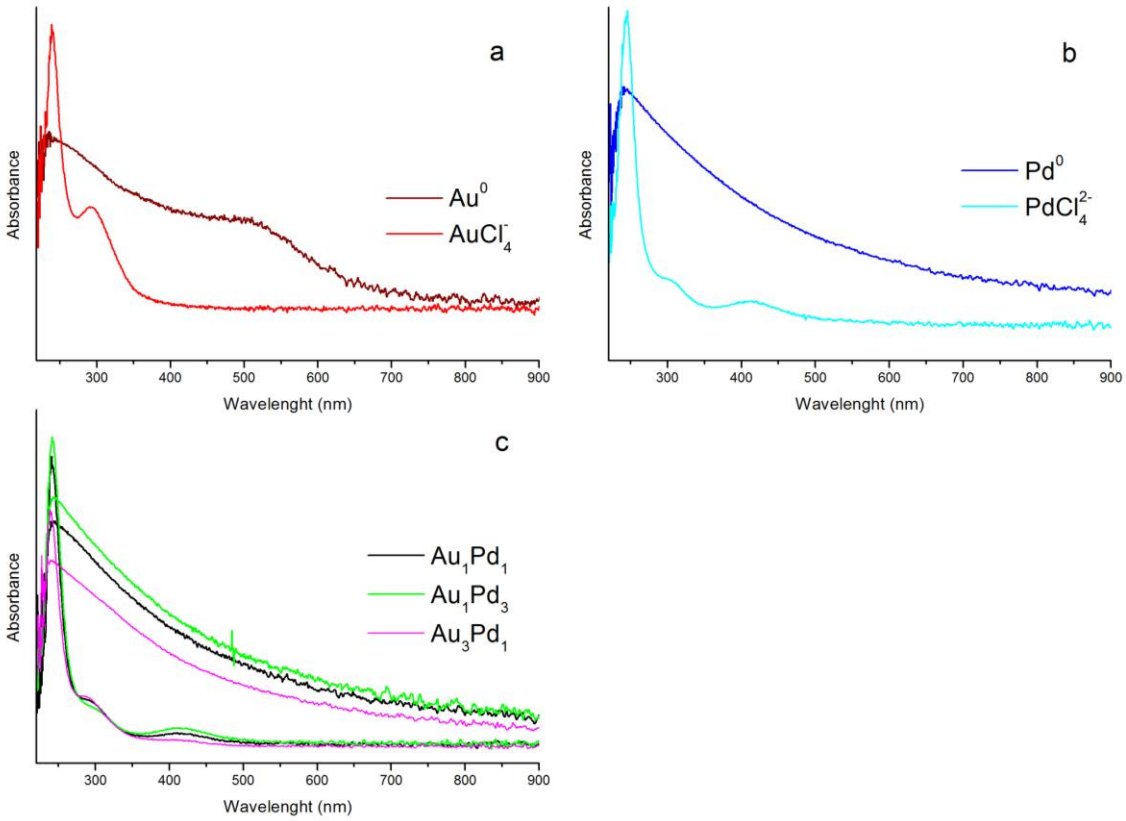

Fig. 71 UV-visible spectra:a)reduction of gold; b) reduction of palladium; c) reduction of the alloy gold palladium

Bimetallic Au_xPd_y systems are made of small and stable colloidal nanoparticles. The different absorbance of the brownish dispersions is due to composition and the Pd content (Fig.71c).

For the bimetallic alloy particles the spectra show the disappearance of the gold surface plasmon band. This event is widespread among the bimetallic sol if one of the metals lacks the plasmon band. An example it is verified in the formation of Ag-Pd nanoparticles, where the plasmon resonance band of Ag disappears[32], or in the formation of Ag-Rh nanoparticles[82]. For the bimetallic alloy palladium gold many works investigated this phenomena such as Deki *et al.*[83] demonstrated that when the nanoparticles of Au-Pd were dispersed on polymer thin film matrix based on the amount of Pd the plasmon peak of gold disappear, due to the formation of the alloy; Dimitratos *et al.* [55] in the studies about the effect of bimetallic nanoparticles Au-Pd on the oxidation of glycerol obtained the same results.

Characterisation of the supported catalyst

BET surface area

A typical analysis of a catalyst is about the surface area. In Table 22 are collected the values of the areas for catalysts supported by titania and for the support, to compare the effect of the supported active phase with the support.

Table 22 Surface area by BET analysis

Sample	Surface Area m^2/g
Pd-i- TiO_2	51
Au_1Pd_1- TiO_2	45
Au_1Pd_3- TiO_2	51
Au_3Pd_1- TiO_2	50
Au- TiO_2	47
TiO_2	63

Comparing Au-TiO_2 with the Pd-TiO_2 there is not a huge difference in the surface area. The surface area of the support loses less than 25% that could be due to the coverage from PVA and to the large experimental error. Also the other catalysts have comparable areas, this could be because all the catalysts were prepared with the same amount of PVA.

SEM-EDX analysis

Every sample was characterised by SEM-EDX. All the catalysts appear similar. An example is shown below (Fig.72). The catalyst of the images is Au_1Pd_1- TiO_2. The frame presents the usual profile of the titania support, but with this resolution the particles of the active phase are not visible. Comparing the snapshot with the one recorded for the TiO_2-P25 the profile of the support is not changed after the deposition of the metal phase, it maintains physical characteristic similar in all the samples examined.

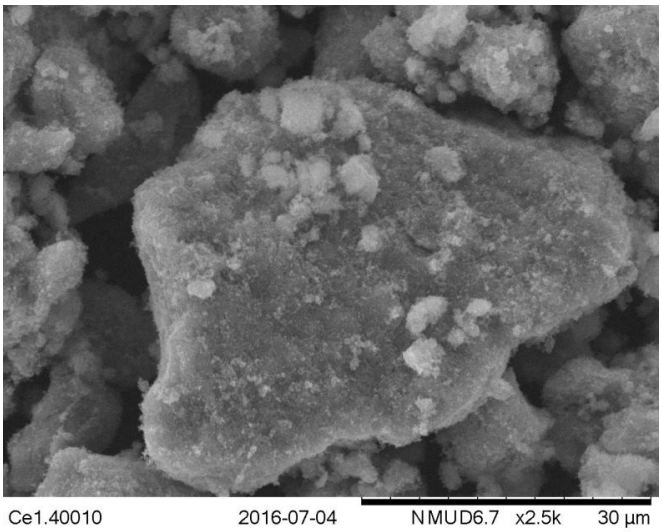

Fig. 72 SEM of Au_1Pd_1- TiO_2

With SEM-EDX semi-quantitative measures are available, thus the loading of the catalysts was checked. The sample were prepared with a metal content of 1 wt.%. The data (Table 23) verified the theoretical value.

Table 23 EDX analysis confirm the supposed loading for the monometallic and bimetallic catalysts

Sample	EDX Au %wt	EDX Pd %wt
Pd- TiO_2	-	0.96
Au_1Pd_1- TiO_2	0.4	0.7
Au_1Pd_3- TiO_2	0.13	0.8
Au_3Pd_1- TiO_2	0.7	0.3
Au- TiO_2	1	-

EDX-mapping (Fig.73) displays that the metal are well distributed on the support.

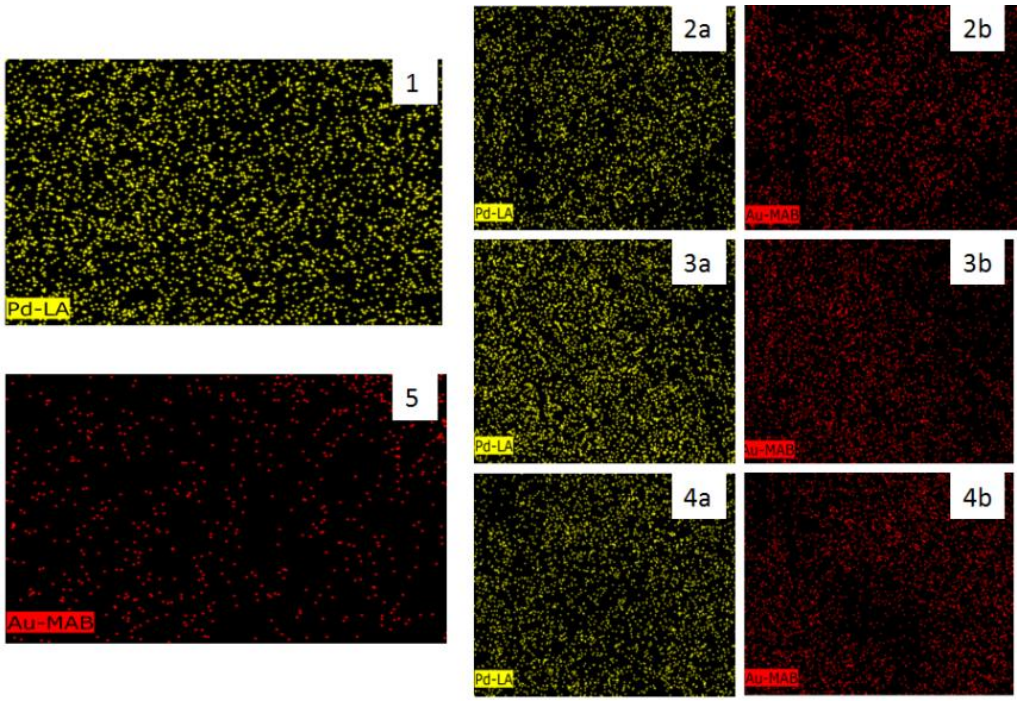

Fig. 73 EDX mapping 1)Pd-TiO_2; 2a)Pd of Au_1Pd_3-TiO_2 ,b) Au of Au_1Pd_3-TiO_2 3a) Pd of Au_1Pd_1-TiO_2 b) Au of Au_1Pd_1-TiO_2 4a) Pd of Au_3Pd_1-TiO_2 b) Au of Au_3Pd_1-TiO_2; 5)Au- TiO_2

XPS analysis

The textural characterisation of catalytic surfaces was carried out by means of XPS, so one can gain insights to the oxidation states of metal catalysts. In the previous chapter we described how to recognise the oxidation state of palladium; the same could be done for gold. As noted the binding energy of Au 4f species can reflect its oxidation state, the peak at 84 eV and 88 eV associated to $Au4f_{7/2}$ and $Au4f_{5/2}$ respectively are related to Au foil, any shifts in the gold catalysts are caused by many factors[40]. In this work the gold monometallic and bimetallic catalysts are supported on titania and the relative binding energy of $Au4f_{7/2}$ shifts at 83 eV as demonstrated by Radnik *et all.*[84], thus it is possible to say that all the gold in our catalysts is in the metallic state. In the bimetallic catalysts there is an overlapping of the peak $Au4d_{5/2}$ with the Pd3d doublet.

The Au(4f) and Au(4d)+Pd(3d) X-ray photoelectron spectra for the series of catalysts are shown in Fig.74, Fig.75.

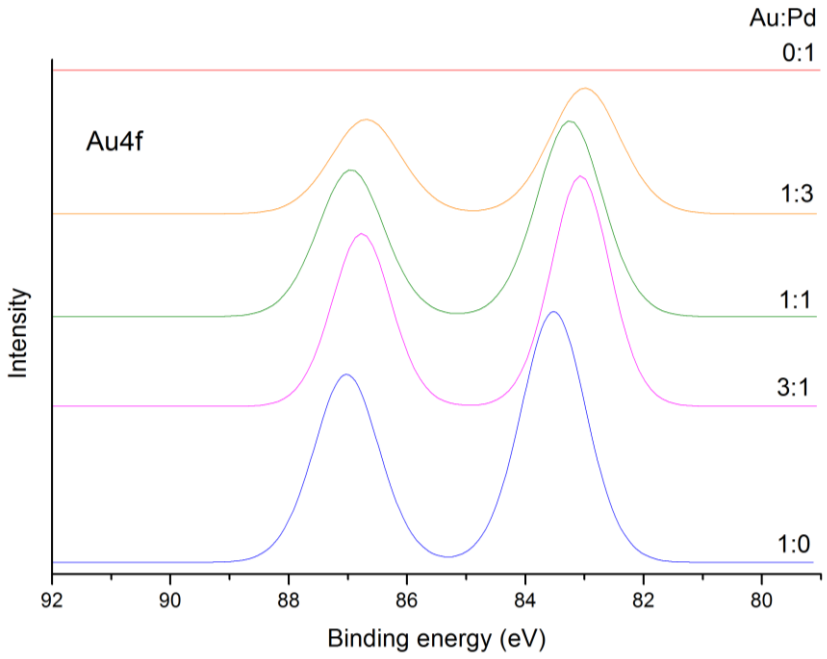

Fig. 74 Au(4f) spectra for the series of Au_xPd_y-TiO_2 catalysts; nominal Au:Pd molar ratios are as indicated

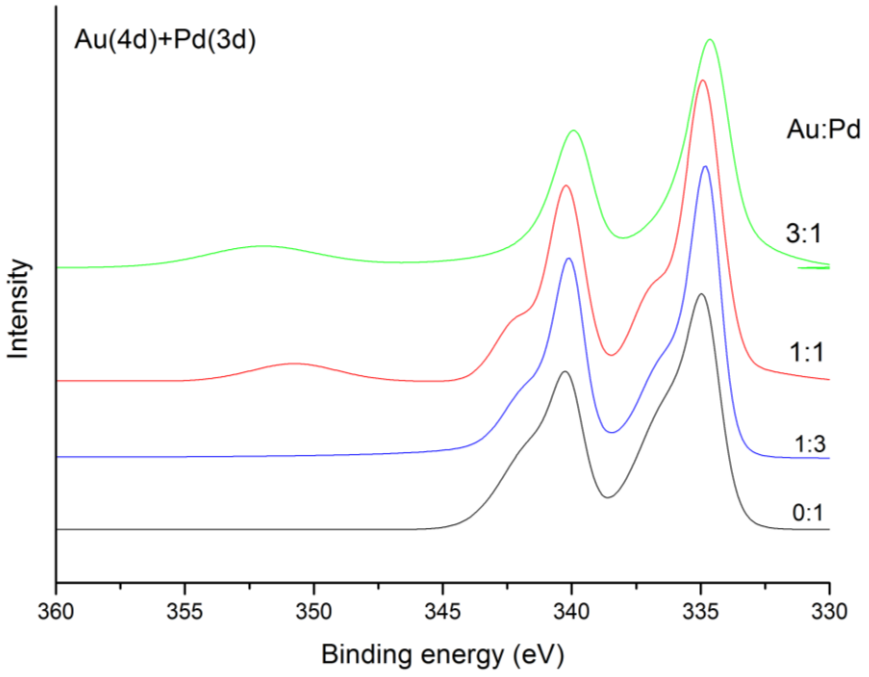

Fig. 75 Au(4d)+Pd(3d) spectra for the series of Au_xPd_y-TiO_2 catalysts; nominal Au:Pd molar ratios are as indicated

When ratio Pd/Au is <1 the Pd nanoparticles comprise predominantly Pd^0 species ($Pd(3d_{5/2})$ binding energy ca. 335 eV),but the presence of Pd^{II} species is indicated for higher Pd contents (Figure 75), with the highest concentration corresponding to the Pd-

only catalyst. Representative Pd^{II}/Pd^{0} atomic ratio calculated from XPS spectra for the catalysts is shown in Table 24 below.

Table 24Pd^{II}/Pd^{0} ratio from XPS analysis for monometallic and bimetallic catalysts

Sample	Pd^{II}/Pd^{0}
Pd- TiO_2	1.65
Au_1Pd_1- TiO_2	0.6
Au_1Pd_3- TiO_2	0.2
Au_3Pd_1- TiO_2	-
Au- TiO_2	-

TEM analysis

Monometallic and bimetallic catalysts were analysed by transmission electron microscopy. The particles size and their distribution were calculated for each sample. The characterisation is reported in the images below. The first sample examined is Pd-TiO_2 (Fig.76). In Fig.77 is shown the histogram of the particles size distribution. The mean size found is 3.61nm, the Pd NPs are smaller compared to the catalyst 1 wt% Pd-C.

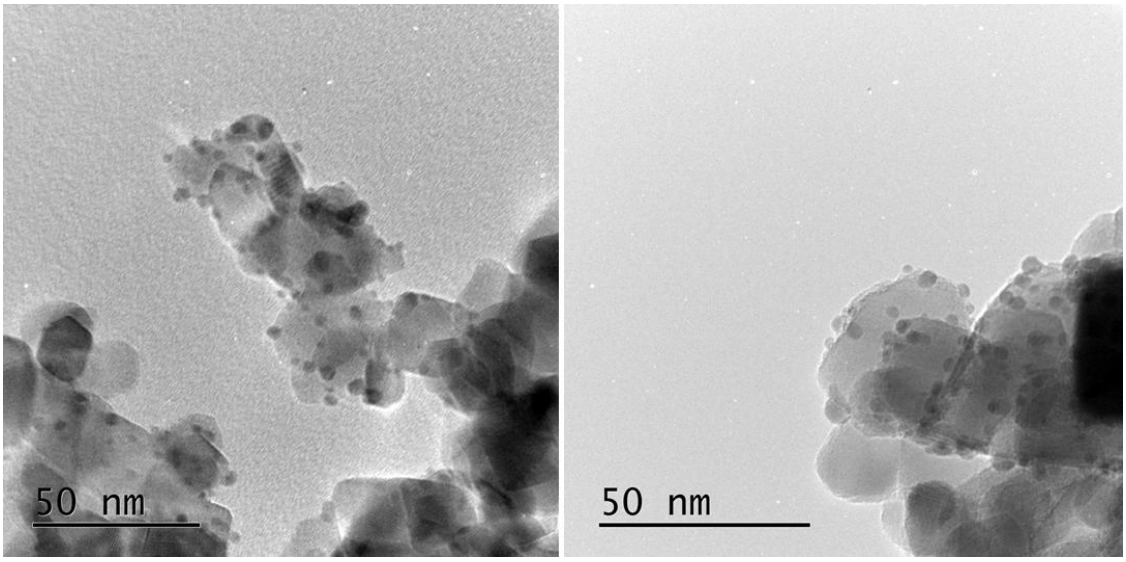

Fig. 76TEM of Pd-TiO_2

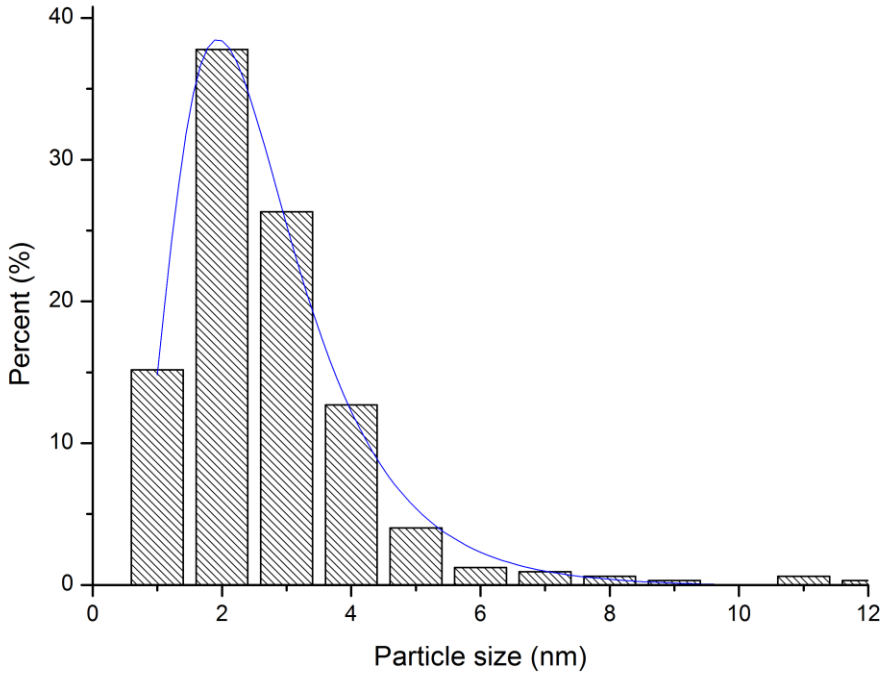

Fig. 77 Particles size distribution Pd-TiO_2

The TEM analysis on Au-TiO_2 are illustrated in Fig.78. Fig.79 shows the histogram of the particle size distribution. The mean size is 4nm, but more than 40% of nanoparticles have a dimension of 3nm.

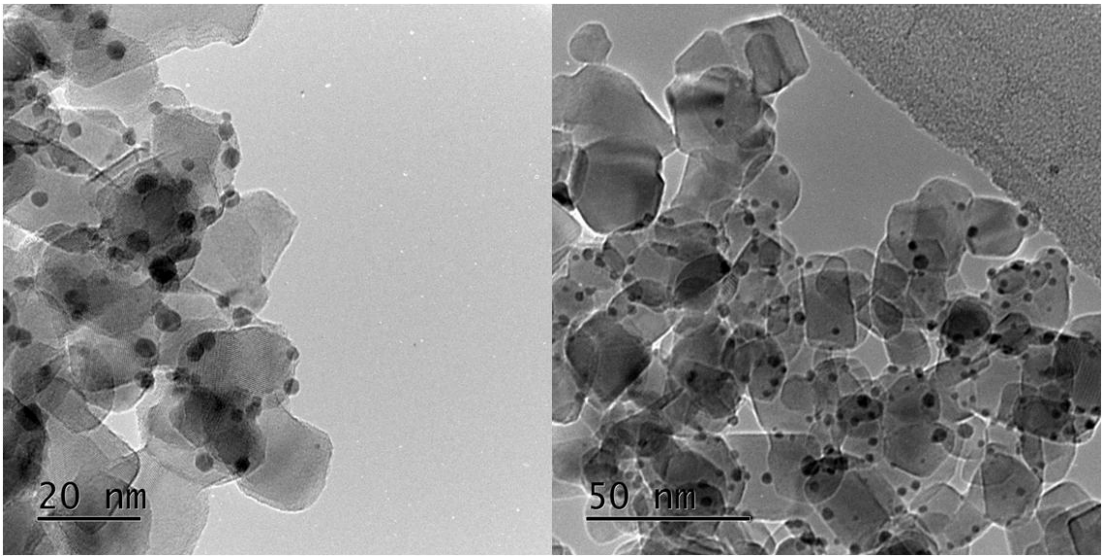

Fig. 78 TEM of Au-TiO_2

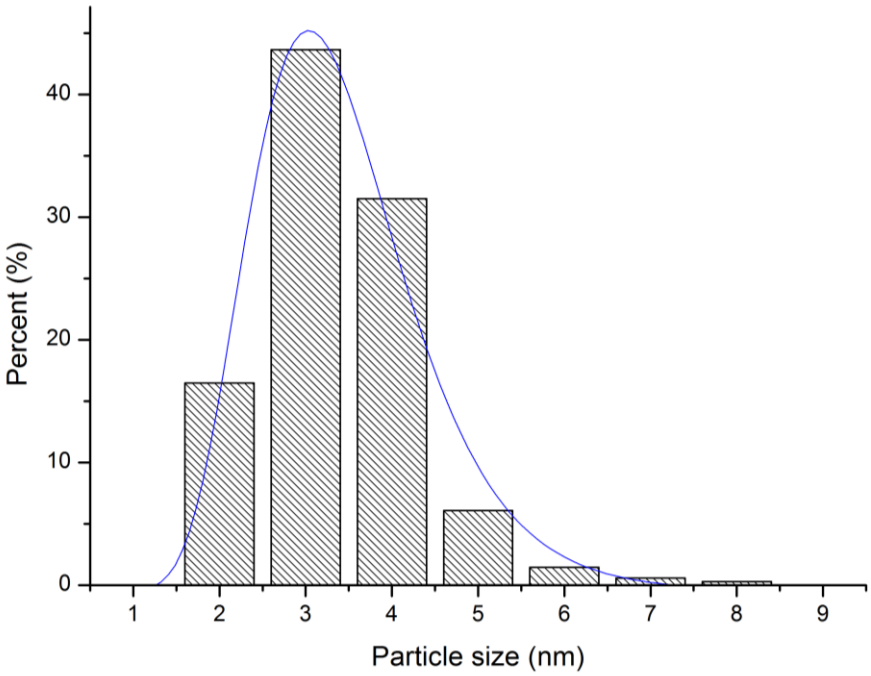

Fig. 79 Particles size distribution Au-TiO_2

Representative images of the 120°C dried Au_xPd_y particles immobilised on titania support are shown in Fig.80; Fig.82; Fig.84. Particles size distribution derived from TEM imaging studies are shown in Fig.81, Fig.83;Fig.85 for Au_1Pd_1, Au_1Pd_3, Au_3Pd_1 respectively.

The mean particles size of the catalysts are 3.4nm, 3.2nm and 3nm respectively.

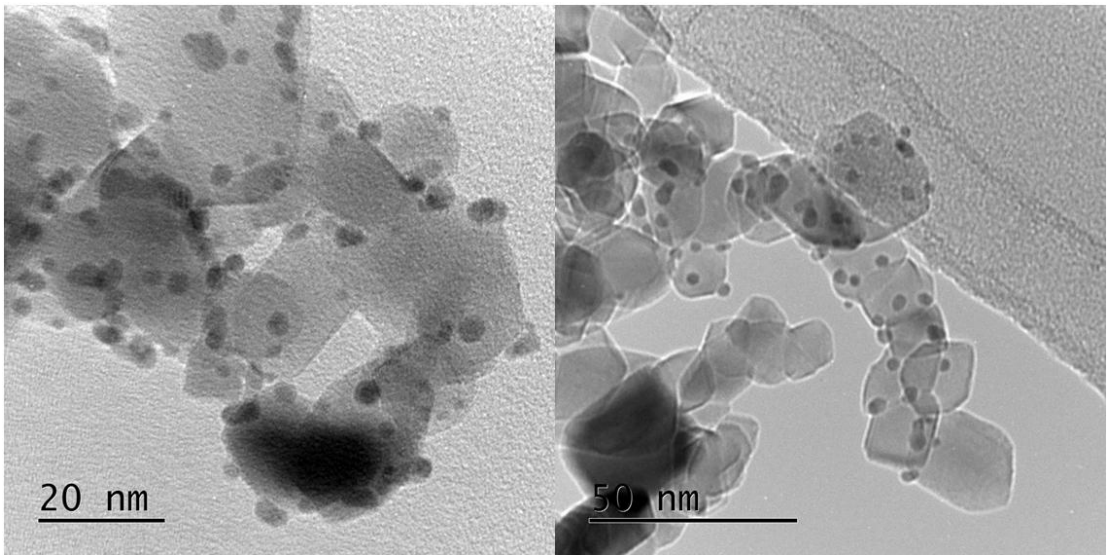

Fig. 80 TEM of Au_1Pd_1-TiO_2

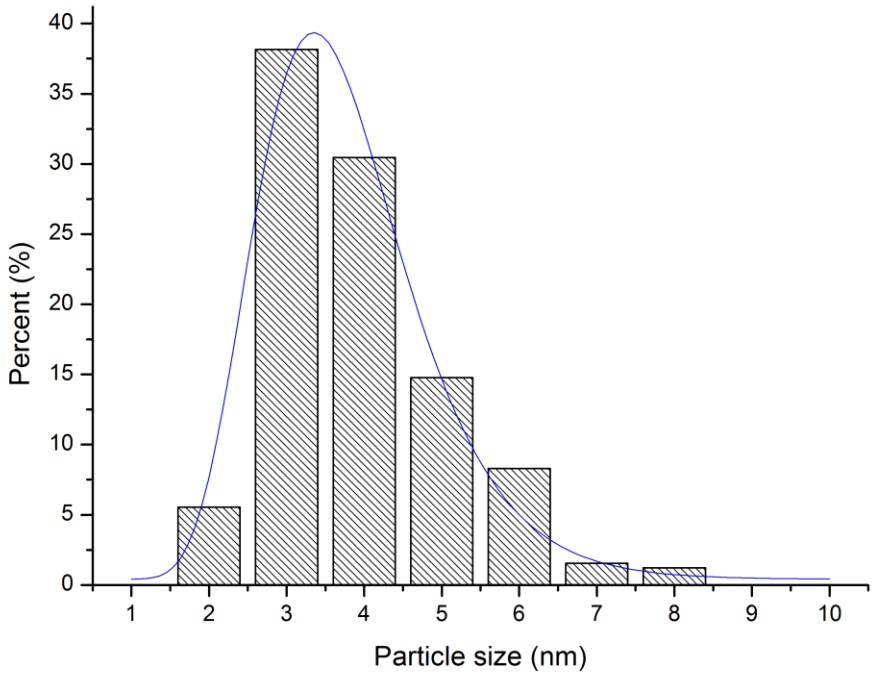

Fig. 81 Particles size dimension Au_1Pd_1-TiO_2

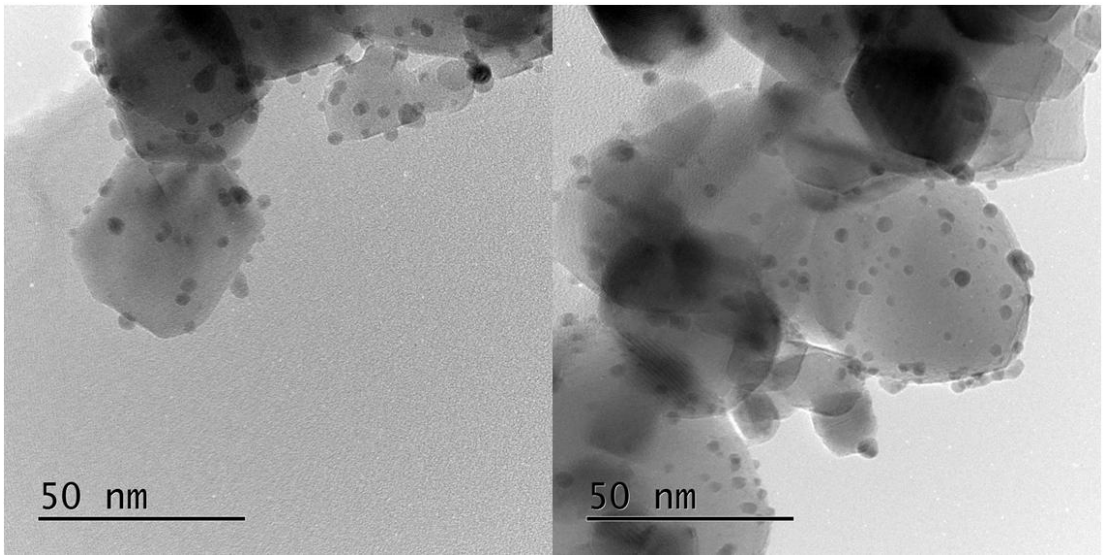

Fig. 82 TEM of Au_1Pd_3-TiO_2

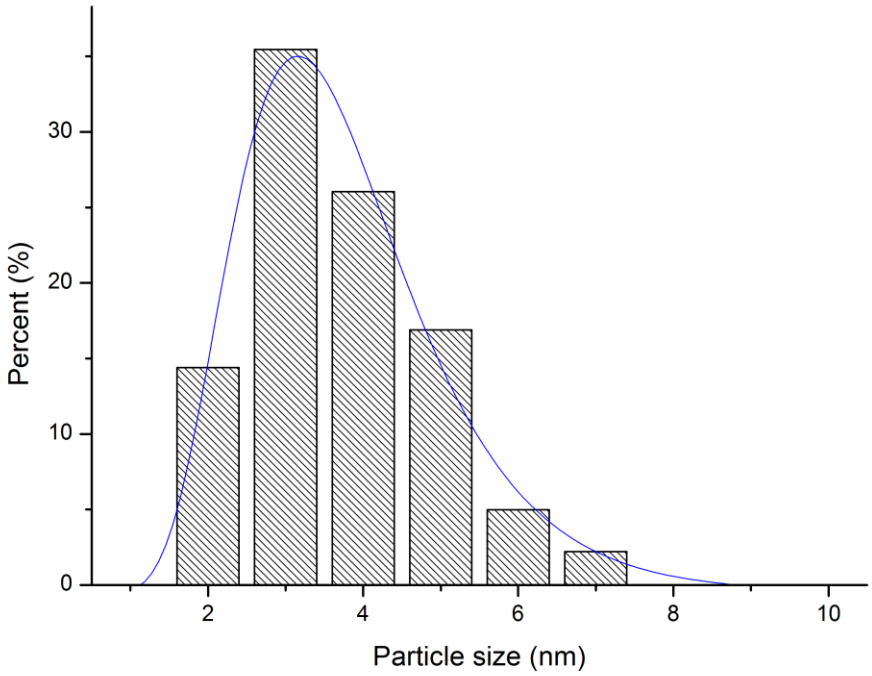

Fig. 83 Particles size dimension Au_1Pd_3-TiO_2

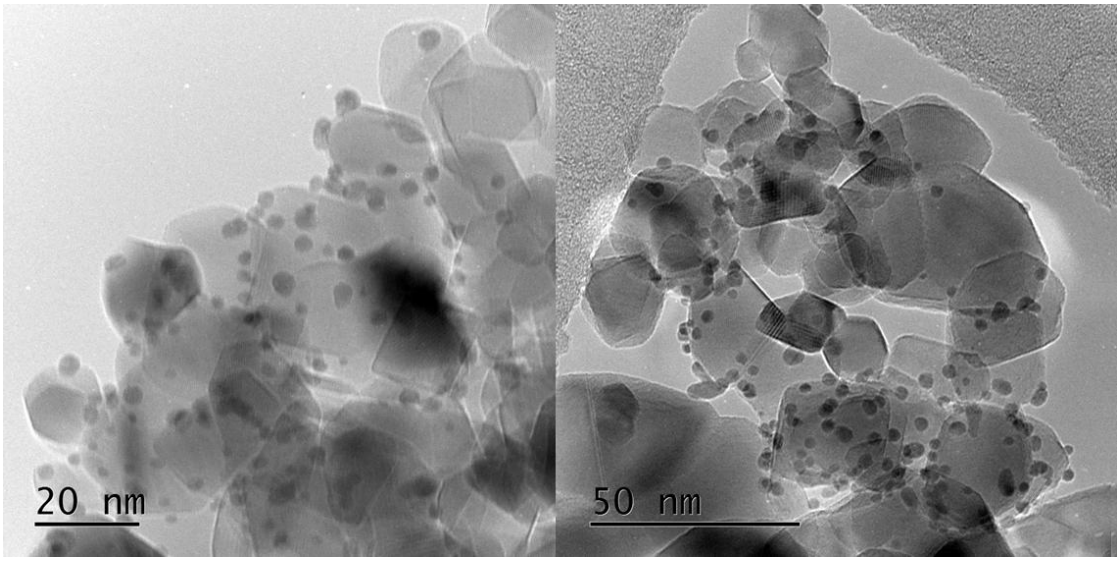

Fig. 84 TEM of Au_3Pd_1-TiO_2

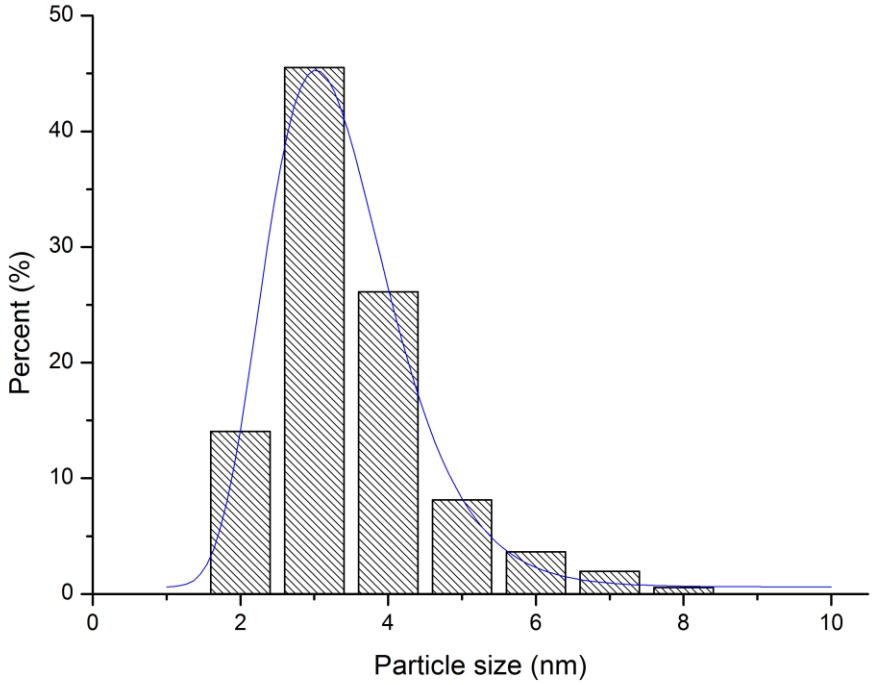

Fig. 85 Particles size dimension Au_3Pd_1-TiO_2

All the histograms indicate that titania-supported NPs have a narrow particles size distribution. The data derived from TEM imaging studies are summarised in Table 25.

Table 25 Summary of particle size data for monometallic and bimetallic catalysts

Sample	d_m-TEM/nm
Pd- TiO_2	3.6±1.9
Au_1Pd_1- TiO_2	3.4±1.1
Au_1Pd_3- TiO_2	3.2±1.2
Au_3Pd_1- TiO_2	3±1.0
Au- TiO_2	4±0.9

Indeed, TEM measurements indicate that the Pd-TiO_2 and Au-TiO_2 nanoparticles are larger as compared to Au_xPd_y-TiO_2, suggesting that the addition of the two metals decrease particles sizes in agreement with previous studies.

5.2.3 **Comparison among the performances of monometallic and bimetallic catalysts**

The catalytic activities of Au_xPd_y-TiO_2 NPs with different compositions, together with Au-TiO_2 and Pd- TiO_2 for the FA decomposition at 50°C are presented in Fig.86. We can see that Au is not active toward dehydrogenation of FA. Among all the bimetallic of Au_xPd_y-TiO_2 NPs investigated, Au_3Pd_1-TiO_2 exhibits the highest catalytic activity with the turnover frequency (TOF) value of 627h−1 at 50°C temperature after 5 min.

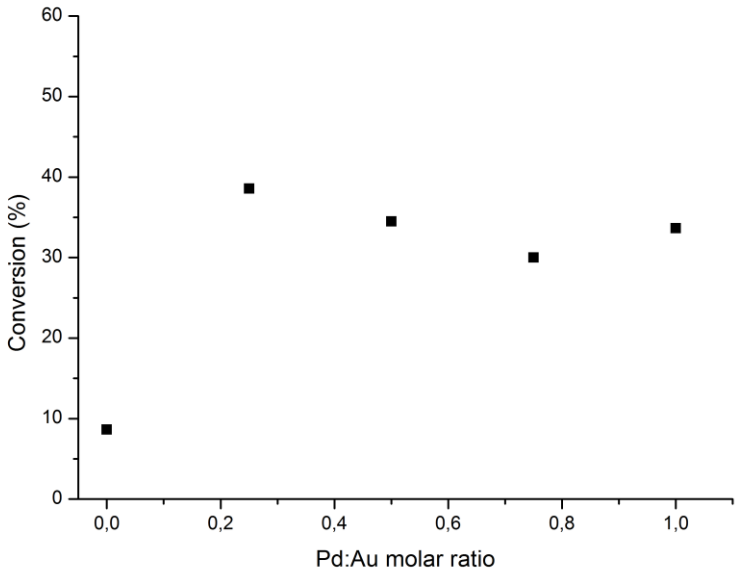

Fig. 86 Conversion of formic acid after 4h using catalysts with different molar ratio Pd:Au

As noted that the bimetallic systems can be more active towards the model reaction, X.Gu *et all.*[85] working on AuPd immobilized in the metalorganic frameworks MIL-101 and ethylenediamine(ED)-graftedMIL101 (ED-MIL-101) demonstrated that Au-Pd NPs with strong bimetallic synergistic effects have a much higher catalytic activity; in our studies Au_3Pd_1-TiO_2 exhibits the best performance, pointing out the strong molecular-scale synergy of Au-Pd alloy, due to the narrow particle size distribution of the AuPd NPs and the synergistic effect with titania. This interesting trend shows that with a minimum amount of Pd metal (Pd/Au molar ratio of 0.2), the Au small activity was increased by a factor of 4, which means that diluting Pd on Au had a positive effect, this is similar to other reactions such as in the synthesis of vinyl acetate[86].

Chapter 6: Conclusion

Catalytic decomposition of formic acid was carried out by using a range of different systems to understand the structure sensitivity of the reaction . The experiments were first of all performed with Pd supported on carbon analyzing its different preparation method to find the most active form towards the reaction. The palladium nanoparticles were synthesised by sol immobilisation technique, because this method allows to control the features of the colloidal catalysts before the immobilisation step, such as particle size and oxidation state. For the performed reaction, the 1wt% Pd/C-e prepared with a weight ratio of PVA/Pd=0.3 and a molar ratio of $NaBH_4$/Pd=5 was found to be more active than all the other Pd catalysts prepared. The pathway followed to synthesize monometallic palladium sols had provided the using poly(vinyl alcohol) as a stabilizing agent (PVA) and the $NaBH_4$ as reducing agent. The preformed sol were characterised by DLS and the supported catalyst by XPS, TEM, SEM-EDX. Different results in activity were found for the catalysts varying the PVA/Pd weight ratio and the $NaBH_4$/Pd molar ratio.

PVA plays an important role in the nanoparticles growth and coverage of the active sites, thus it influences the catalytic activity. Varying the PVA/Pd weight ratio from 0 to 1.2 gradually small particles are formed, in particular when the PVA/Pd weight ratio is 0.3 the nanoparticles size is 4.8 nm and the best reaction performance is showed (Fig.87), even if at major ratio smaller particles are synthesised. This effect could be explained by high coverage degree of the active sites reached adding too PVA, which destabilises the system. By XPS analysis besides it is showed that the larger Pd/C ratio in the surface it is reached when the PVA/Pd is of 0.3.

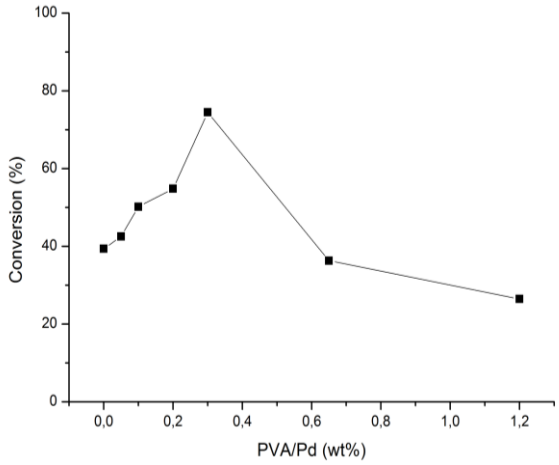

Fig. 87 Catalytic performances of the catalysts made varying the PVA/Pd weight ratio

The other parameter that could influence the preparation of the sol is the reducing agent: the preformed sol are made with the different $NaBH_4$/Pd molar ratio (from 5 to 10), keeping a screening ratio of PVA/Pd=0.65. The tests on the catalysts prepared demonstrated an improvement in the formic acid conversion when the ratio was higher both for catalysts immobilised on carbon and titania (Fig.88). The results obtained have conditioned the successive synthesis of the catalysts in particular when titania was used as supporting material, since on carbon the conversion is slightly higher.

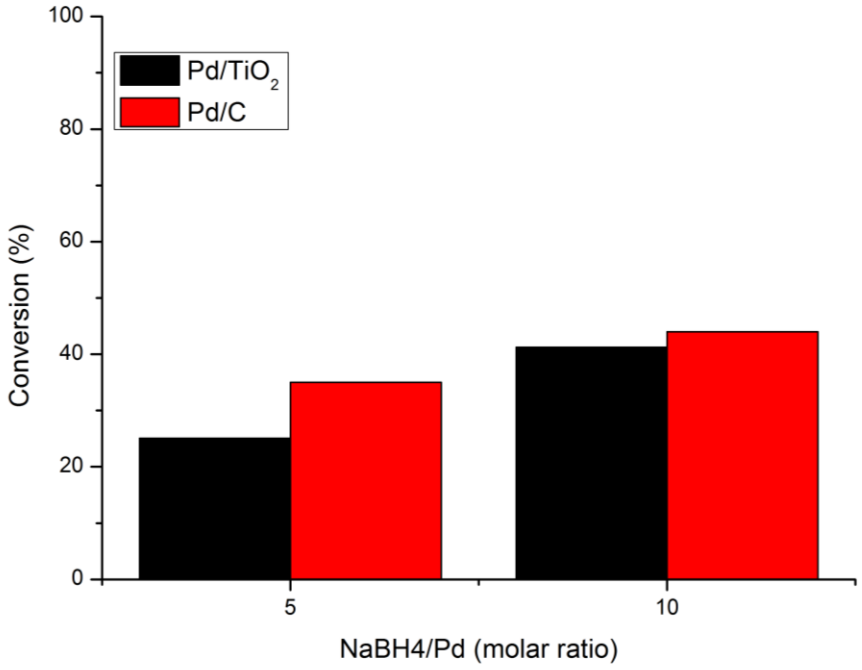

Fig. 88 Catalytic performance of the catalysts supported on carbon (red columns) and titania (black column) varying the $NaBH_4$/Pd molar ratio from 5 to 10

The DLS analysis haven't evidenced an effect of the $NaBH_4$ on the preformed sol as mentioned and also after the immobilisation step there is not a variation in the particles size as confirmed by TEM analysis. Thus for the catalysts supported on two types of materials the differences in activity it was attributed to the increase of Pd metallic content at larger ratio, measured by XPS.

These studies have made possible a comparison between the supports, finding that the interaction between metal and support lead to the best catalytic performance when the supporting material was carbon. One reason of this was found in the shape of the supported nanoparticles, because when supported on titania are hemispherical, decreasing the active surface area exposed and as consequences the catalytic activity. Other deeply studies on the interaction between particles and supports should be done in

the next investigations, also to see how it affects the selectivity and the yields in the products.

According with the results the successive catalysts were prepared with PVA/Pd weight ratio of 0.3 and a $NaBH_4$/Pd ratio of 5 if supported on carbon and of 10 if supported on titania.

Finally to observe the effect of the Pd content, the loading was varied from 0.2wt% to 1.2wt%. The 5 catalysts prepared were supported on carbon and substrate/metal molar ratio in the reaction was kept around 2000. Full conversion wasn't achieved with the whole series of catalysts, but the one with 1wt% of loading showed the highest activity towards the model reaction. The reason was attributed to the Pd atomic surface content. The XPS analysis showed that even if the amount of Pd in the zero oxidation state doesn't change, the amount of palladium on the surface support increases increasing the loading with a maximum for the 1wt% catalyst.

According with the experiments made it was possible to continue the investigations using the catalyst 1wt% Pd/C-e to explore other aspects. First all tests on the catalyst reusability were carried out showing that the homemade Pd/C-e loses only 31% of its activity after 5 uses, probably caused by the sintering phenomena since the particles size was found to increase from 4.8 nm to 5.1nm by TEM analysis. Then, in order to get insights about the rate determining step of the reaction mechanism kinetic isotope effects (KIE) was studied confirming the pathway described in previous work found in literature, where after the formation of formate the CO_2 and H_2 were evolved. Nevertheless other studies on the products reaction have to be done, without that we can only made hypothesis and also further studies to understand how palladium and HCOOH interact would be carried on by DRIFT technique using CO chemisorption.

The homemade catalysts was compared to a commercial one (5 wt% Pd/C) too, to observe the different catalytic behaviours towards the model reaction after the characterisation of the two systems. The commercial one is appeared to be better than the homemade Pd/C-e under every point of view. The TOF after 15 min for the commercial one is $3637h^{-1}$ against the $184h^{-1}$ of the prepared one. The commercial one is really interesting and more investigations on how it works will can help in the synthesis of a more efficient homemade catalyst.

Several monometallic and bimetallic catalysts were synthesized with gold and palladium nanoparticles on titania P25 and they were tested in the model reaction for 4h. The metal loading onto titania was kept to 1% wt because it was found to be the best

ratio for catalytic activity. The metal nanoparticles were synthesized by sol-immobilisation method optimised for the Pd nanoparticles, in the first part of the work, as we mentioned. The synthesized sols were analyzed with UV-VIS spectrophotometry to determine the effective alloying of the two metals before immobilisation and by DLS to have an idea of the particles hydrodynamic diameter. After immobilisation the loading of the sample was confirmed by EDX analysis and the catalysts were characterised by XPS and TEM. TEM measurements confirmed the presence of small nanoparticles in particular for the bimetallic systems Au_xPd_y- TiO_2.

Within monometallic gold and palladium catalysts the more active was the palladium catalyst, as reported in Fig. 89, in fact it achieved a higher conversion.

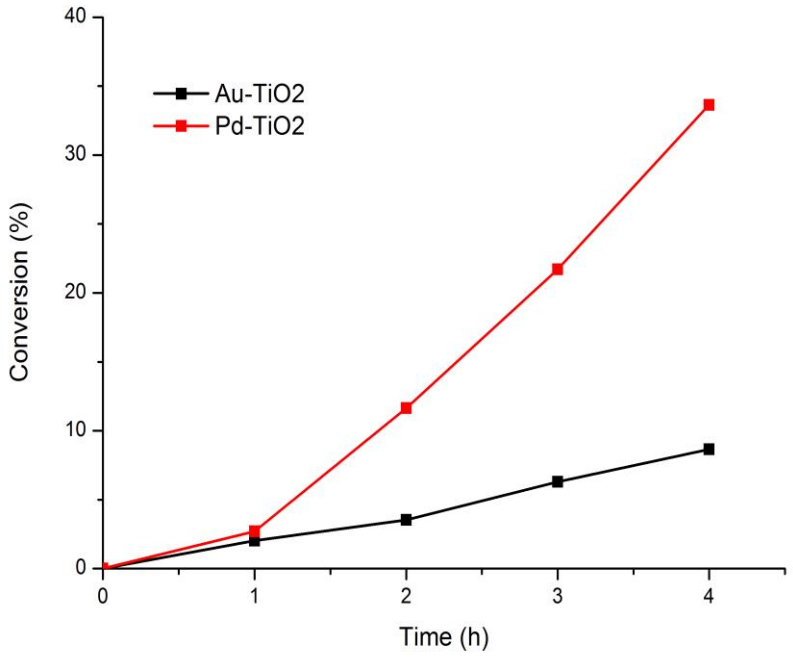

Fig. 89 Catalytic performances of Au-TiO_2 and Pd-TiO_2 catalysts

Bimetallic alloys were also tested to try to combine the good catalytic activity of palladium with the properties of gold (Fig.90). Different ratios were examined with a total metal loading of 1% w/w on titania and synthesized by sol methods.

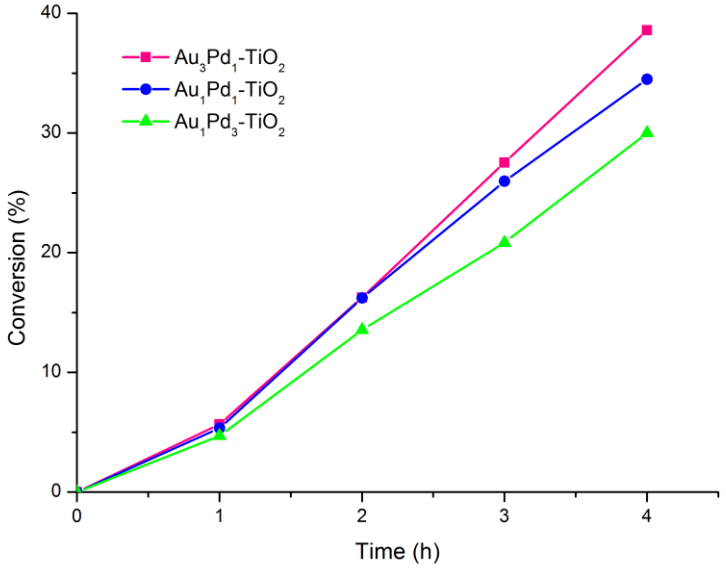

Fig. 90 Catalytic performances of the bimetallic Au_1Pd_3-TiO_2, Au_1Pd_1-TiO_2, Au_3Pd_1-TiO_2 catalysts

The conversion suggests that when a small amount of palladium is added to a catalyst principally composed of gold it increases in the activity. Instead for large amounts of palladium and small of gold the conversion values hasn't a positive effect. The Au_3Pd_1-TiO_2 catalyst increases the conversion value compared with the two monometallic catalysts. In Figure 91 is reported the catalytic activity trend of the different alloys in the performed reaction after 4h.

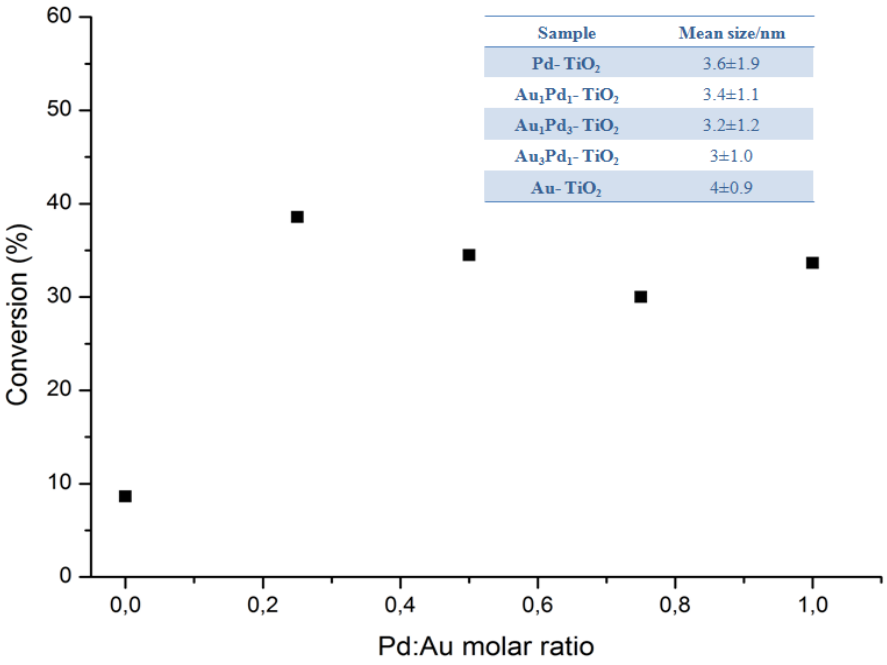

Sample	Mean size/nm
Pd- TiO_2	3.6±1.9
Au_1Pd_1- TiO_2	3.4±1.1
Au_1Pd_3- TiO_2	3.2±1.2
Au_3Pd_1- TiO_2	3±1.0
Au- TiO_2	4±0.9

Fig. 91 Trend of the catalytic performances of Au_xPd_y-TiO_2 catalysts and relative mean particles size by TEM analysis

In conclusion, palladium nanoparticles supported on carbon are promising catalysts for the reaction of formic acid decomposition. Nonetheless, further characterisation is necessary to define and quantify the products of reaction, to better characterise the synthesized catalysts and to explain the mechanism. Furthermore, alloying of Au and Pd metal with specific atomic ratio seems a good way to enhance the activity of the catalysts for the synergic effect of gold and palladium.

References

1. Park, S., Vohs, J. M. & Gorte, R. J. Direct oxidation of hydrocarbons in a solid-oxide fuel cell. *Nature* **404,** 265–267 (2000).
2. Jiang, H. L., Singh, S. K., Yan, J. M., Zhang, X. B. & Xu, Q. Liquid-Phase chemical hydrogen storage: Catalytic hydrogen generation under ambient conditions. *ChemSusChem* **3,** 541–549 (2010).
3. Jain, I. P. Hydrogen the fuel for 21st century. *Int. J. Hydrogen Energy* **34,** 7368–7378 (2009).
4. Ramachandran, R. A. M. & Menon K., R. AN OVERVIEW OF INDUSTRIAL USES OF HYDROGEN. *Int. J. Hydrogen Energy* **23,** 593–598 (1998).
5. Bang, Y. *et al.* Hydrogen production by steam reforming of liquefied natural gas (LNG) over mesoporous nickel e alumina xerogel catalysts prepared by a single-step carbon-templating sol e gel method. *Int. J. Hydrogen Energy* **37,** 11208–11217 (2012).
6. Oliveira, E. L. G., Grande, C. A. & Rodrigues, A. E. Methane steam reforming in large pore catalyst. *Chem. Eng. Sci.* **65,** 1539–1550 (2010).
7. Pasel, J., Samsun, R. C., Schmitt, D., Peters, R. & Stolten, D. Test of a water – gas-shift reactor on a 3 kW e -scale — design points for high- and low-temperature shift reaction ☪. *J. Power Sources* **152,** 189–195 (2008).
8. Corbo, P. & Migliardini, F. Hydrogen production by catalytic partial oxidation of methane and propane on Ni and Pt catalysts. *Int. J. Hydrogen Energy* **32,** 55–66 (2007).
9. Gao, J., Guo, J., Liang, D., Hou, Z. & Fei, J. Production of syngas via autothermal reforming of methane in a fluidized-bed reactor over the combined CeO 2 – ZrO 2 / SiO 2 supported Ni catalysts. *Int. J. Hydrogen Energy* **33,** 5493–5500 (2008).
10. Choudhary, V. R., Banerjee, S. & Rajput, A. M. Continuous Production of H 2 at Low Temperature from Methane Decomposition over Ni-Containing Catalyst Followed by Gasification by Steam of the Carbon on the Catalyst in Two Parallel Reactors Operated in Cyclic Manner. *J. Catal.* **198,** 136–141 (2001).
11. Li, C. & Suzuki, K. Bioresource Technology Process design and simulation of H 2 -rich gases production from biomass pyrolysis process. *Bioresour. Technol.* **101,** S86–S90 (2010).
12. Knutsen, G., Ka, T., Skja, K. & Lindblad, P. H 2 production from marine and freshwater species of green algae during sulfur deprivation and considerations for bioreactor design. *Int. J. Hydrogen Energy* **33,** 511–521 (2008).
13. Farrauto, R. J. New catalysts and reactor designs for the hydrogen economy. *Chem. Eng. J.* **238,** 172–177 (2014).
14. Zhang, L., Chae, S., Hendren, Z., Park, J. & Wiesner, M. R. Recent advances in proton

exchange membranes for fuel cell applications. *Chem. Eng. J.* **204-206,** 87–97 (2012).

15. Borup, R. *et al.* Scientific Aspects of Polymer Electrolyte Fuel Cell Durability and Degradation. *Chem. Rev.* **107,** 3904–3951 (2007).
16. Sharma, S. & Ghoshal, S. K. Hydrogen the future transportation fuel: From production to applications. *Renew. Sustain. Energy Rev.* **43,** 1151–1158 (2015).
17. Armor, J. N. Catalysis and the hydrogen economy. *Catal. Letters* **101,** 131–135 (2005).
18. Di Domenico, D. DEIDROGENAZIONE CATALITICA DI IDROCARBURI PER LA PRODUZIONE DI H2 'ON - BOARD'. (Univerity of Bologna, 2014).
19. Dalebrook, A. F., Gan, W., Grasemann, M., Moret, S. & Laurenczy, G. Hydrogen storage: beyond conventional methods. *Chem. Commun. (Camb).* **49,** 8735–51 (2013).
20. Yadav, M. & Xu, Q. Liquid-phase chemical hydrogen storage materials. *Energy Environ. Sci.* 9698–9725 (2012). doi:10.1039/c2ee22937d
21. Karahan, S., Zahmakıran, M. & Ozkar, S. Catalytic hydrolysis of hydrazine borane for chemical hydrogen storage : Highly efficient and fast hydrogen generation system at room temperature. *Int. J. Hydrogen Energy* **36,** 4958–4966 (2011).
22. Brack, P., Dann, S. E. & Wijayantha, K. G. U. *Heterogeneous and homogenous catalysts for hydrogen generation by hydrolysis of aqueous sodium solutions*. *Energy science & engineering* **3,** (2015).
23. Liu, X., Li, S., Liu, Y. & Cao, Y. Formic acid: A versatile renewable reagent for green and sustainable chemical synthesis. *Cuihua Xuebao/Chinese J. Catal.* **36,** 1461–1475 (2015).
24. Zhu, Q.-L., Tsumori, N. & Xu, Q. Sodium hydroxide-assisted growth of uniform Pd nanoparticles on nanoporous carbon MSC-30 for efficient and complete dehydrogenation of formic acid under ambient conditions. *Chem. Sci.* **5,** 195 (2014).
25. Sa, F. Catalytic decomposition of carbon-based liquid-phase chemical hydrogen storage materials for hydrogen generation under mild conditions. (2016). doi:10.1007/s13203-016-0159-9
26. Eley, D. D. & Luetic, P. The formic acid decomposition on palladium-gold alloys. *Trans. Faraday Soc.* **53,** 1483 (1957).
27. Wang, X. *et al.* Pd/C nanocatalyst with high turnover frequency for hydrogen generation from the formic acid-formate mixtures. *Int. J. Hydrogen Energy* **39,** 837–843 (2014).
28. Mori, K., Dojo, M. & Yamashita, H. Pd and Pd − Ag Nanoparticles within a Macroreticular Basic Resin : An Effi cient Catalyst for Hydrogen Production from Formic Acid Decomposition. *ACS Catal.* **3,** 1114–1119 (2013).
29. Liu, X., He, L. I. N., Liu, Y. & Cao, Y. Supported Gold Catalysis : From Small Molecule Activation to Green Chemical Synthesis. *Acc. Chem. Res.* **XXX,** (2013).
30. Bi, Q. *et al.* Efficient Subnanomeric Gold-Catalyzed Hydrogen Generation from Formic

Acid Decomposition under Ambient Conditions **. *J. Am. Chem. Soc.* **134,** 8926–8933 (2012).

31. Zhou, X. *et al.* High-quality hydrogen from the catalyzed decomposition of formic acid by Pd-Au/C and Pd-Ag/C. *Chem. Commun. (Camb).* 3540–3542 (2008). doi:10.1039/b803661f
32. Tedsree, K. *et al.* Hydrogen production from formic acid decomposition at room temperature using a Ag–Pd core–shell nanocatalyst. *Nat. Nanotechnol.* **6,** 302–307 (2011).
33. Dai, H. *et al.* AgPd nanoparticles supported on MIL-101 as high performance catalysts for catalytic dehydrogenation of formic acid. *J. Mater. Chem. A* **2,** 11060 (2014).
34. Semagina, N. & Kiwi-Minsker, L. Recent Advances in the Liquid-Phase Synthesis of Metal Nanostructures with Controlled Shape and Size for Catalysis. *Catal. Rev. Sci. Eng.* **51,** 147–217 (2009).
35. White, R. J., Luque, R., Budarin, V. L., Clark, J. H. & Macquarrie, D. J. Supported metal nanoparticles on porous materials . Methods and applications. *Chem. Soc. Rev.* **38,** 481–494 (2009).
36. Gurunathan, S., Han, J., Park, J. H. & Kim, J. A green chemistry approach for synthesizing biocompatible gold nanoparticles. **9,** 1–11 (2014).
37. Lemine, O. M. Microstructural characterisation of αlfa-Fe2O3 using , XRD line profiles analysis , FE-SEM and FT-IR. *Superlattices Microstruct.* **45,** 576–582 (2009).
38. Campelo, J. M., Luna, D., Luque, R., Marinas, J. M. & Romero, A. A. Sustainable Preparation of Supported Metal Nanoparticles and Their Applications in Catalysis. 18–45 (2009). doi:10.1002/cssc.200800227
39. Isfort, C. S. & Rochnia, M. Production and physico-chemical characterisation of nanoparticles. *Toxicol. Lett.* **186,** 148–151 (2009).
40. Villa, A. *et al.* Characterisation of gold catalysts. *Chem. Soc. Rev.* (2016). doi:10.1039/C5CS00350D
41. Daniel, M. C. & Astruc, D. Gold Nanoparticles: Assembly, Supramolecular Chemistry, Quantum-Size-Related Properties, and Applications Toward Biology, Catalysis, and Nanotechnology. *Chemical Reviews* **104,** 293–346 (2004).
42. Prati, L. & Villa, A. The Art of Manufacturing Gold Catalysts. *Catalysts* **2,** 24–37 (2012).
43. Bowker, M., Nuhu, A. & Soares, J. High activity supported gold catalysts by incipient wetness impregnation §. *Catal. Today* **122,** 245–247 (2007).
44. Zanella, R., Delannoy, L. & Louis, C. Mechanism of deposition of gold precursors onto TiO 2 during the preparation by cation adsorption and deposition – precipitation with NaOH and urea. *Appl. Catal. A Gen.* **291,** 62–72 (2005).

45. Villa, A., Wang, D., Veith, G. M., Vindigni, F. & Prati, L. Sol immobilization technique: a delicate balance between activity, selectivity and stability of gold catalysts. *Catal. Sci. Technol.* **3,** 3036–3041 (2013).
46. An, K., Alayoglu, S., Ewers, T. & Somorjai, G. A. Colloid chemistry of nanocatalysts : A molecular view. *J. Colloid Interface Sci.* **373,** 1–13 (2012).
47. Physical Stability of Disperse Systems. *Part. Sci.* **1,** 1–2 (2009).
48. Saldan, I., Semenyuk, Y. & Marchuk, I. Chemical synthesis and application of palladium nanoparticles. 2337–2354 (2015). doi:10.1007/s10853-014-8802-2
49. Haruta, M., Kobayashi, T., Sano, H. & Yamada, N. Novel Gold Catalysts for the oxidation of carbon monoxide at a temperature far below 0°C. *Chem. Lett.* 405–408 (1987).
50. Hutchings, G. J. Vapor Phase Hydrochlorination of Acetylene : Correlation of Catalytic Activity of Supported Metal Chloride Catalysts. *J. Catal.* **96,** 292–295 (1985).
51. Dimitratos, N., Kiely, J. & Hutchings, G. J. General Introduction to the Field of Environmental Catalysis : Green Catalysis with Supported Gold and Gold Bimetallic Nanoparticles.
52. Enache, D. I. *et al.* Solvent-Free Oxidation of Primary Alcohols to Aldehydes Using Au-Pd/ TiO2 Catalysts. *Science (80-.).* **362,** (2012).
53. Tiruvalam, R. C., Pritchard, J. C., Dimitratos, N., Hutchings, G. J. & Kiely, C. J. Aberration corrected analytical electron microscopy studies of sol-immobilized Au + Pd , Au { Pd } and Pd { Au } catalysts used for benzyl alcohol oxidation and hydrogen peroxide production. 63–86 (2011). doi:10.1039/c1fd00020a
54. Lopez-sanchez, J. A. *et al.* Applied Catalysis A : General Reactivity studies of Au – Pd supported nanoparticles for catalytic applications. *"Applied Catal. A, Gen.* **391,** 400–406 (2011).
55. Dimitratos, N. *et al.* Effect of particle size on monometallic and bimetallic (Au , Pd)/ C on the liquid phase oxidation of glycerol. *Catal. Letters* **108,** 147–153 (2006).
56. Edwards, J. K. *et al.* Direct synthesis of hydrogen peroxide from H 2 and O 2 using TiO 2 -supported Au – Pd catalysts. *Elsevier* **236,** 69–79 (2005).
57. Yu, H., Wang, X., Sun, H. & Huo, M. Photocatalytic degradation of malathion in aqueous solution using an Au – Pd – TiO 2 nanotube film. *J. Hazard. Mater.* **184,** 753–758 (2010).
58. Su, R. *et al.* Promotion of Phenol Photodecomposition over TiO 2 Using Au , Pd , and Au À Pd. *ACSNANO* **6,** 6284–6292 (2012).
59. Bowker, M. *et al.* Hydrogen production by photoreforming of biofuels using Au , Pd and Au – Pd / TiO 2 photocatalysts. *J. Catal.* **310,** 10–15 (2014).
60. Su, R. *et al.* Designer Titania-Supported Au À Pd Nanoparticles for E ffi cient

Photocatalytic Hydrogen Production. *ACSNANO* **8,** 3490–3497 (2014).

61. Lopez-sanchez, J. A. *et al.* Au – Pd supported nanocrystals prepared by a sol immobilisation technique as catalysts for selective chemical synthesis. **1944,** (2008).
62. Zhao, P., Li, N. & Astruc, D. State of the art in gold nanoparticle synthesis. *Coord. Chem. Rev.* **257,** 638–665 (2013).
63. Motion, B. Dynamic Light Scattering : An Introduction in 30 Minutes. 1–8
64. Faust, C. Ben. Modern chemical tecniques. *R. Soc. Chem.* 92–115 (1992).
65. S.Lowell; Joan E. Shields; Martin A. Thomas; Matthias Thommes. *Characterization of Porous Solids and Powders : Surface Area , Pore Size and Density*. (Kluwer Academic Publishers, 2004).
66. Egerton, R. F. *Physical principles of electron microscopy : an introduction to TEM, SEM, and AEM.* (2005).
67. G.E.Muilenberg; C.D.Wagner; W.M.Riggs;L.E.Davis;J.F.Moulder; *Handbook of generic x-ray photoelectron spectroscopy*. (Perkin-Elmer Corporation).
68. John F. Watts; John Wolstenholme. *An Introduction to Surface Analysis by XPS and AES*. (2003).
69. David B. Williams; C. Barry Carter. *Transmission Electron Microscopy: a textbook for material science*. (1996).
70. Fornstedt, T., Forssén, P. & Westerlund, D. in *Analytical Separation Science* 1–24 (2015).
71. Preocanin, T. & Kallay, N. Point of Zero Charge and Surface Charge Density of TiO 2 in Aqueous Electrolyte Solution as Obtained by Potentiometric Mass Titration *. *Croat. Chem. acta* **79,** 95–106 (2006).
72. Yudanov, I. V., Genest, A., Schauermann, S., Freund, H.-J. & Rosch, N. Size Dependence of the Adsorption Energy of CO on Metal Nanoparticles: A DFT Search for the Minimum Value. (2012).
73. Valden, M., Lay, X. & Goodman, D. W. Onset of Catalytic Activity of Gold Clusters on Titania with the Appearance of Nonmetallic Properties. *Science (80-.).* **281,** 1647–1650 (1998).
74. Suttiponparnit, K., Jiang, J., Sahu, M. & Suvachittanont, S. Role of Surface Area , Primary Particle Size , and Crystal Phase on Titanium Dioxide Nanoparticle Dispersion Properties. 1–8 (2011).
75. Ho, K. Y. & Yeung, K. L. Properties of TiO2 support and the performance of Au/TiO2 catalyst for CO oxidation reaction. *Gold Bull.* **40,** 15–30 (2007).
76. Bowker, M., Stone, P., Bennett, R. & Perkins, N. Formic acid adsorption and decomposition on TiO 2 (1 1 0) and on Pd / TiO 2 (1 1 0) model catalysts. *Surf. Sci.* **511,** 435–448 (2002).

77. Hu, C., Pulleri, J. K., Ting, S. W. & Chan, K. Y. Activity of Pd/C for hydrogen generation in aqueous formic acid solution. *Int. J. Hydrogen Energy* **39,** 381–390 (2014).
78. Ojeda, M. & Iglesia, E. Formic acid dehydrogenation on au-based catalysts at near-ambient temperatures. *Angew. Chemie - Int. Ed.* **48,** 4800–4803 (2009).
79. Onder, M., Sun, X. & Sun, S. Monodisperse gold – palladium alloy nanoparticles and their composition-controlled catalysis in formic acid dehydrogenation under mild conditions † ¨. *Nanoscale* 910–912 (2013). doi:10.1039/c2nr33637e
80. Link, S. & El-sayed, M. A. Size and temperature dependence of the plasmon absorption of colloidal gold nanoparticles. **1,** 4212–4217 (1999).
81. Somorjai, G. A. *Introduction to Surface Chemistry and Catalysis*. (Wiley, 1994).
82. Hirakawa, K. & Ãy, N. T. Ag / Rh Bimetallic Nanoparticles Formed by Self-assembly from Ag and Rh Monometallic Nanoparticles in Solution. **32,** 78–79 (2003).
83. Deki, S., Akamatsu, K., Hatakenaka, Y., Mizuhata, M. & Kajinami, A. Synthesis and characterisation of nano-sized gold-palladium bimetallic particles dispersed in polymer thin film matrix. **11,** 59–65 (1999).
84. Radnik, J., Mohr, C. & Claus, P. On the origin of binding energy shifts of core levels of supported gold nanoparticles and dependence of pretreatment and material synthesis. *Phys. Chem. Chem. Phys.* **5,** 172–177 (2003).
85. Gu, X., Lu, Z., Jiang, H., Akita, T. & Xu, Q. Synergistic Catalysis of Metal À Organic Framework-Immobilized. *J. Am. Chem. Soc.* **133,** 11822–11825 (2011).
86. Chen, M. S. *et al.* The nature of the active site for vinyl acetate synthesis over Pd – Au. *Catal. Today* **117,** 37–45 (2006).

Acknowledgment

The academic studies have been very hard, long, but they allowed me to grow up, they made me face challenges and make beautiful experiences., My internship at Cardiff University, for example; thus first of all I want to thank Dr. Nikolaos Dimitratos, Dr. Cheri Hammond and their groups for welcoming me in their labs and for helping me in the last part of this ride. I also want to thank also Prof.ssa Stefania Albonetti and the group in Bologna that support me from afar.
And thanks to the Erasmus+ Programme without it this experience would not have been possible.

There would be so many people whom say "Thank you!"
My lovely flatmates of Cardiff Saeda, Luca, Nick, Max, Margherita, Isa and Laura who made me laugh and left an infinity of memories which will keep with me forever.
My oldest academic friends Vanessa, Francesco, Tonno, Lazzo and Mola and my every day life friends.

Finally the most important people, my family: my mum, my dad and Elia, I was so lucky to have had you and my love Lorenzo who made these last two years amazing.